

# STARS

University of Central Florida  
STARS

---


Electronic Theses and Dissertations, 2004-2019

---

2013

## Cooperative Control And Advanced Management Of Distributed Generators In A Smart Grid

Ali Maknoungejad  
*University of Central Florida*

 Part of the [Electrical and Electronics Commons](#)  
Find similar works at: <https://stars.library.ucf.edu/etd>  
University of Central Florida Libraries <http://library.ucf.edu>

This Doctoral Dissertation (Open Access) is brought to you for free and open access by STARS. It has been accepted for inclusion in Electronic Theses and Dissertations, 2004-2019 by an authorized administrator of STARS. For more information, please contact [STARS@ucf.edu](mailto:STARS@ucf.edu).

---

### STARS Citation

Maknoungejad, Ali, "Cooperative Control And Advanced Management Of Distributed Generators In A Smart Grid" (2013). *Electronic Theses and Dissertations, 2004-2019*. 2556.  
<https://stars.library.ucf.edu/etd/2556>



COOPERATIVE CONTROL AND ADVANCED MANAGEMENT OF DISTRIBUTED  
GENERATORS IN A SMART GRID

by

ALI MAKNOUNINEJAD

B.S. Electrical Engineering, University of Tehran, 2001

M.S. Electrical Engineering, University of Central Florida, 2010

A dissertation submitted in partial fulfilment of the requirements  
for the degree of Doctor of Philosophy  
in the Department of Electrical Engineering and Computer Science  
in the College of Engineering and Computer Science  
at the University of Central Florida

Spring Term  
2013

Major Professor: Zhihua Qu

© 2013 Ali Maknoungejad

## ABSTRACT

Smart grid is more than just the smart meters. The future smart grids are expected to include a high penetration of distributed generations (DGs), most of which will consist of renewable energy sources, such as solar or wind energy. It is believed that the high penetration of DGs will result in the reduction of power losses, voltage profile improvement, meeting future load demand, and optimizing the use of non-conventional energy sources. However, more serious problems will arise if a decent control mechanism is not exploited. An improperly managed high PV penetration may cause voltage profile disturbance, conflict with conventional network protection devices, interfere with transformer tap changers, and as a result, cause network instability.

Indeed, it is feasible to organize DGs in a microgrid structure which will be connected to the main grid through a point of common coupling (PCC). Microgrids are natural innovation zones for the smart grid because of their scalability and flexibility. A proper organization and control of the interaction between the microgrid and the smartgrid is a challenge.

Cooperative control makes it possible to organize different agents in a networked system to act as a group and realize the designated objectives. Cooperative control has been already applied to the autonomous vehicles and this work investigates its application in controlling the DGs in a micro grid. The microgrid power objectives are set by a higher level control and the application of the cooperative control makes it possible for the DGs to utilize a low bandwidth communication network and realize the objectives.

Initially, the basics of the application of the DGs cooperative control are formulated. This includes organizing all the DGs of a microgrid to satisfy an active and a reactive power objective. Then, the cooperative control is further developed by the introduction of clustering DGs into several groups to satisfy multiple power objectives. Then, the cooperative distribution optimization is introduced

to optimally dispatch the reactive power of the DGs to realize a unified microgrid voltage profile and minimize the losses. This distributed optimization is a gradient based technique and it is shown that when the communication is down, it reduces to a form of droop. However, this gradient based droop exhibits a superior performance in the transient response, by eliminating the overshoots caused by the conventional droop.

Meanwhile, the interaction between each microgrid and the main grid can be formulated as a Stackelberg game. The main grid as the leader, by offering proper energy price to the micro grid, minimizes its cost and secures the power. This not only optimizes the economical interests of both sides, the microgrids and the main grid, but also yields an improved power flow and shaves the peak power. As such, a smartgrid may treat microgrids as individually dispatchable loads or generators.

To my mother, Azizeh, who like a candle, put her life to light the path of her children; and to my father, Yahya, who by his fate, gave strength to his children.

## ACKNOWLEDGMENTS

I take this opportunity to express my great appreciation towards Dr. Zhihua Qu for his invaluable and great advice and support. Without his advice and guidelines, I couldn't accomplish this work. Dr. Qu not only helped me in going through this research and accomplish the work, but even more importantly, showed me how to look from different perspectives into the same problem.

I also need to express my gratitude to Dr. Issa Batarseh, who not only helped me make my way into this program, but also by his friendly and supportive attitude, encouraged me to continue my work. I also need to express my sincere thanks to Dr. Nasser Kutkut, whose support and advice during the first two years of my program was very helpful and important to me. I would also like to thank the other members of my committee for reviewing my dissertation, providing feedback and advice and attending my defense: Dr. Saeed Lotfifard, Dr. Michael Haralambous and Dr. Thomas Wu.

I also need to express my great appreciation and gratitude to Dr. Daryoosh Vashayee, for his sincere and invaluable help in the process of my applying for a PhD position. Without his help and motivation, I could not have initiated the process for my PhD.

I also need to take this opportunity to express my sincere love and appreciation to my mother, without whose devotion, my achievements were impossible and my sister, Sohila, for her consistent encouragement, support and love.

This work is partially supported by the US Department of Energy, under the Solar Energy Grid Integration Systems (SEGIS) program.

# TABLE OF CONTENTS

|  |     |
|--|-----|
| LIST OF FIGURES . . . . .  | xi  |
| LIST OF TABLES . . . . .   | xiv |
| CHAPTER 1: INTRODUCTION . . . . .                                  | 1   |
| Review of the Existing Microgrid Inverter Controls . . . . .       | 8   |
| Current Source Inverters (CSI) . . . . .                           | 8   |
| Droop . . . . .  | 11  |
| Impedance Emulation . . . . .                                      | 13  |
| Statement of the Contribution . . . . .                            | 18  |
| CHAPTER 2: COOPERATIVE CONTROL OF DISTRIBUTED GENERATORS . . . . . | 21  |
| Power Objectives . . . . .   | 22  |
| Active Power . . . . .   | 22  |
| Reactive Power . . . . .   | 23  |
| Inverter Modeling . . . . .  | 27  |
| Cooperative Control Formulation . . . . .                          | 30  |



|   |        |
|---|--------|
| Communication Network . . . . .   | 30     |
| Cooperative Law . . . . .   | 33     |
| The effect of the Communication Frequency on the Convergence Rate . . . . .   | 35     |
| ZigBee Communication . . . . .  | 36     |
| Virtual Leaders Control . . . . .   | 38     |
| Active Power . . . . .  | 38     |
| Reactive Power . . . . .  | 38     |
| Closed Loop System Analysis . . . . .   | 40     |
| Cooperative Control Nash Equilibrium . . . . .                                | 45     |
| Simulation Results . . . . .  | 47     |
| Conclusion . . . . .  | 51     |
| <br>CHAPTER 3: COOPERATIVE DISTRIBUTED OPTIMIZATION . . . . .                 | <br>52 |
| Active Power Loss Analysis . . . . .  | 54     |
| Cooperative Control based on the Distributed Optimization . . . . .           | 55     |
| Realizing a Unified Voltage Profile as the Global Objective . . . . .         | 56     |
| Calculation of the Units Sub-Gradient:Agents with DG installed . . . . .      | 57     |
| Calculation of the Units Sub-Gradient:Agents without a DG Installed . . . . . | 59     |

|  |         |
|--|---------|
| Choosing the Gradient Gains . . . . .                                | 61      |
| Minimizing the Active Power Losses as the Global Objective . . . . . | 61      |
| Single Units Applying Optimization: Gradient based Droop . . . . .   | 62      |
| Analysis . . . . .   | 65      |
| Simulation Results . . . . .   | 70      |
| Simulations of the cooperative distributed optimization . . . . .    | 71      |
| Simulations of the Gradient based Droop . . . . .                    | 77      |
| Conclusion . . . . .   | 79      |
| <br>CHAPTER 4: MAIN GRID-MICROGRIDS INTERACTION MANAGEMENT . . . . . | <br>81  |
| Redefining Some Microgrid Variables . . . . .                        | 82      |
| Microgrid Optimization . . . . .                                     | 83      |
| Main Grid Optimization . . . . .                                     | 85      |
| Interaction between the Main Grid and the Microgrid . . . . .        | 86      |
| Game Solution . . . . .  | 90      |
| Simulations . . . . .  | 94      |
| Conclusion . . . . .   | 102     |
| <br>APPENDIX A: INTRODUCTION TO THE GAME THEORY . . . . .            | <br>104 |

APPENDIX B: SEARCH ALGORITHM FOR NASH EQUILIBRIUM . . . . . 107

APPENDIX C: DETAILS OF FINDING GAME SOLUTIONS FOR THE FIRST HOUR . 110

APPENDIX D: DISTRIBUTED OPTIMIZATION STABILITY ANALYSIS . . . . . 114

APPENDIX E: PUBLICATIONS FROM THE DOCTORAL RESEARCH . . . . . 120

LIST OF REFERENCES . . . . . 123

## LIST OF FIGURES

|      |   |    |
|------|---|----|
| 1.1  | US maps of the solar energy and the wind speed, courtesy of NREL . . . . .    | 1  |
| 1.2  | Homes getting equipped with solar panels . . . . .                            | 3  |
| 1.3  | Typical smart grid block diagram . . . . .                                    | 4  |
| 1.4  | A smart grid diagram based on IEEE 5-bus system . . . . .                     | 5  |
| 1.5  | A typical microgrid, consisting of DGs and loads . . . . .                    | 7  |
| 1.6  | Voltage disturbance caused by a typical radiation intermittency . . . . .     | 10 |
| 1.7  | Electrical equivalent circuit of a typical synchronous generator . . . . .    | 11 |
| 1.8  | frequency and voltage droop control characteristics. . . . .                  | 12 |
| 1.9  | Comparing the size of a large inductor and an actual micro inverter . . . . . | 14 |
| 1.10 | GEC simplified inverter model . . . . .                                       | 16 |
| 1.11 | GEC active power droop curve . . . . .  | 17 |
| 1.12 | Volt-VAR droop characteristics of GEC . . . . .                               | 18 |
| 2.1  | Different applications of the cooperative control . . . . .                   | 21 |
| 2.2  | Typical structure of a microgrid with distributed generators . . . . .        | 24 |
| 2.3  | Different choices of the critical point on a typical feeder . . . . .         | 26 |

|      |  |    |
|------|--|----|
| 2.4  | Typical structure of a PV based DG . . . . .                                   | 27 |
| 2.5  | Inverter model block diagram with PI control . . . . .                         | 29 |
| 2.6  | Sample graphs of the communication topology . . . . .                          | 32 |
| 2.7  | Graphs for time-varying communication topologies. . . . .                      | 33 |
| 2.8  | Z-domain to S-domain mapping . . . . .   | 35 |
| 2.9  | ZigBee communication network . . . . .   | 37 |
| 2.10 | Search for the active power flow fair utilization ratio . . . . .              | 38 |
| 2.11 | The system diagram of the case of study microgrid . . . . .                    | 48 |
| 2.12 | Point of common coupling (PCC) voltage . . . . .                               | 49 |
| 2.13 | Critical points voltages . . . . .   | 50 |
| 2.14 | Main grid-microgrid power flow . . . . .                                       | 50 |
| 3.1  | A typical ULTC and capacitor bank, installed in local power stations . . . . . | 52 |
| 3.2  | A simple, three node communication topology . . . . .                          | 60 |
| 3.3  | Saturation effect of the single unit optimization application . . . . .        | 63 |
| 3.4  | The system diagram of the case of study microgrid . . . . .                    | 70 |
| 3.5  | PV profile of DGs . . . . .  | 71 |
| 3.6  | Global cost function of the microgrid, $F_v$ . . . . .                         | 72 |

|      |  |     |
|------|--|-----|
| 3.7  | Main grid to the microgrid active power flow . . . . .           | 73  |
| 3.8  | Main grid reactive power flow to the microgrid . . . . .         | 74  |
| 3.9  | Microgrid active power loss . . . . .                            | 74  |
| 3.10 | Voltages of DG6 and point of common coupling . . . . .           | 75  |
| 3.11 | Comparing the microgrid active power loss . . . . .              | 76  |
| 3.12 | Comparing the microgrid global cost function . . . . .           | 77  |
| 3.13 | Voltage and $\alpha_q$ waveforms of $DG_1$ . . . . .             | 78  |
| 3.14 | Trajectory of $\alpha_{q_1}$ and $V_1$ . . . . .                 | 79  |
| 4.1  | A simplified game model . . . . .                                | 88  |
| 4.2  | Case of study smart grid . . . . .                               | 95  |
| 4.3  | PV profiles of DGs of the microgrid . . . . .                    | 96  |
| 4.4  | Load profiles of different feeders . . . . .                     | 97  |
| 4.5  | Main grid load profile . . . . .                                 | 97  |
| 4.6  | Conventional generation cost per unit . . . . .                  | 98  |
| 4.7  | The effect of the proposed game approach on power flow . . . . . | 101 |

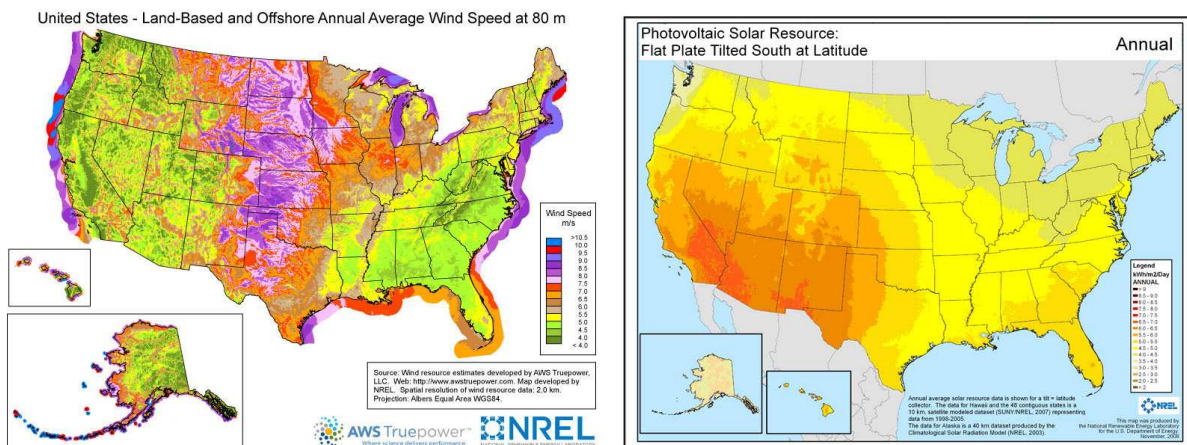
## LIST OF TABLES

|     |   |     |
|-----|---|-----|
| 3.1 | Case of study microgrid $H_{12}$ . . . . .  | 67  |
| 3.2 | State matrix of the gradient based droop . . . . .  | 67  |
| 3.3 | State matrix of the conventional droop . . . . .  | 68  |
| 3.4 | Lyapunov matrix derived for the gradient based droop . . . . .                            | 69  |
| 3.5 | Lyapunov matrix derived for the conventional droop . . . . .                              | 69  |
| 4.1 | Matrix game between the main grid and a microgrid . . . . .                               | 92  |
| 4.2 | Matrix game for example 1, where $\{\star, \star\}$ stands for $\{J_\mu, J_t\}$ . . . . . | 93  |
| 4.3 | Cost function optimizations . . . . .   | 99  |
| 4.4 | The values of power flow $P_\mu^{ref}$ and $\alpha_p^{ref}$ . . . . .                     | 100 |
| 4.5 | The energy prices: $\beta_i$ , $\beta_i^{avg}$ , and $\hat{\beta}_i^{avg}$ . . . . .      | 102 |
| C.1 | $J_\mu$ cost function game table . . . . .  | 112 |
| C.2 | $J_t$ cost function game table . . . . .  | 113 |

# CHAPTER 1: INTRODUCTION

The global increase of the electricity demand, combined with both, the economical and the environmental constraints of conventional energy sources such as fossil or nuclear energy, is putting more demand on finding alternative energy sources. Renewable energy sources are of special interest as alternative energy. This has led to the outburst of the distributed generators (DGs) and smart grid concepts.

United States is among the countries, which are rich on different kinds of the renewable energy sources. Figure 1.1 shows the US maps of the solar and wind energy; provided by the National Renewable Energy Laboratory (NREL). It is seen that some states, such as Colorado and Kansas, are rich in both wind and solar energy sources. Most of the others, either have a great wind speed or solar radiation. Especially, Florida receives a great deal of solar energy radiation. Therefore, it is clear that United States is an ideal country for investing and harvesting such unlimited and clean energy sources.



(a) US map of 80m altitude wind speed

(b) US map of solar energy

Figure 1.1: US maps of the solar energy and the wind speed, courtesy of NREL



Other factor that motivates concepts such as microgrids and smart grid is improving the power reliability. With the conventional power system structure, any event that causes a system failure results in the loss of the electricity to the consumers. For instance, the blackouts happened in USA in 2003 [1] and India in 2012 [2] caused thousands of homes loss electricity for several days. Another concern is natural phenomena and disasters. Such unpredictable events may cause the destruction of infrastructures and result in the loss of electricity. For instance, the Sandy hurricane which hit the USA northeast in Oct. 2012, caused millions of people loss electricity for several days, despite the extreme coldness [3].

In fact, a microgrid may be as small as a home and as big as a city. If houses were equipped with solar panels or small wind turbines, they could survive such massive blackouts. Or in case of hurricane, the homes that had survived the disaster could disconnect from the grid and provide their own needed electricity. The figure 1.2a shows a home with roof top solar panels. If a majority of homes in an area get equipped with solar panels, as in the figure 1.2b, not only the power reliability would improve, but also such a high PV penetration could help the main grid in several ways.



(a) An individual house with roof top solar panels



(b) An area with majority of the homes equipped with solar panels

Figure 1.2: Homes getting equipped with solar panels

According to the United States Department of Energy's Modern Grid Initiative report [4], a modern smart grid must motivate consumers to actively participate in operations of the grid and accommodate different generation sources. This motivates decentralization of power generation. Such distributed generation allows individual consumers to generate power on site, using whatever generation method they find appropriate and tailor their generation directly to their load, making them independent from grid power failures. A major source of the distributed generation is the renewable energy. To increase the harness of such alternative energy, DGs will be installed near the loads and be spread widely across the distribution network.

Figure 1.3 shows the typical block diagram of a smart grid. A smart grid consists of several generation sources, including large scale renewable sources such as wind farms or solar farms, and conventional power stations. Small sized distributed generators, such as rooftop solar panels and

home installed small wind turbines are also important elements of the smart grid which will be able to provide a high aggregated power dispatch.

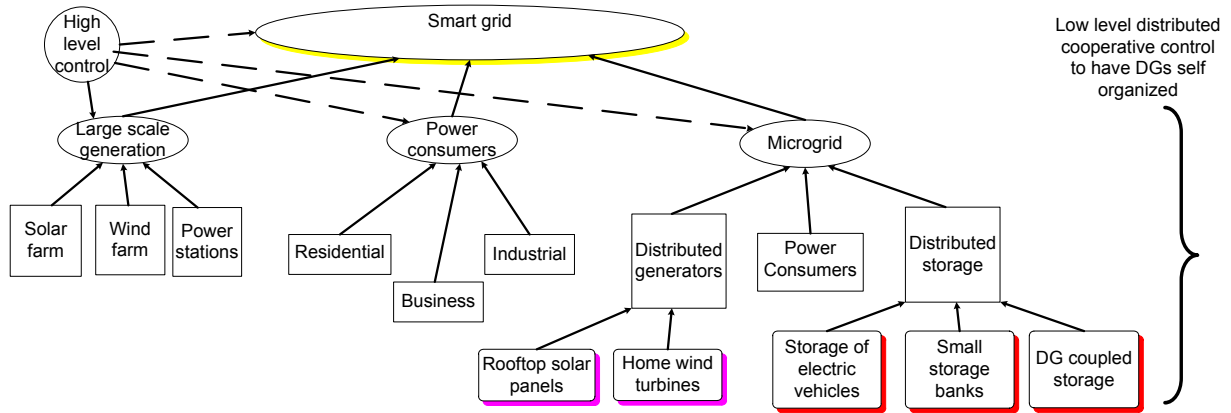


Figure 1.3: Typical smart grid block diagram

The best way to organize and control such highly dispersed and individually small sized generation is to group them in the form of microgrids [5], as shown in the figure 1.3. Then, a low-level control is applied to organize and properly dispatch the DGs.

A smart grid consists of several buses to which loads, conventional generators and microgrids may be connected. An example of a smart grid, based on the IEEE 5-bus system is shown in the figure 1.4, where a microgrid is connected to the bus 5.

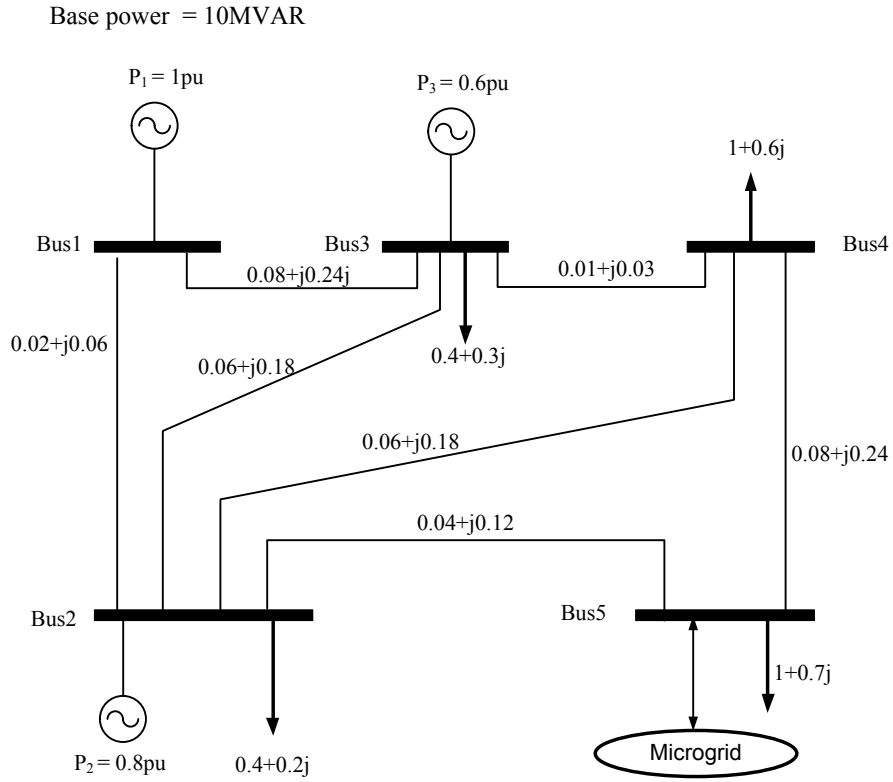


Figure 1.4: A smart grid diagram based on IEEE 5-bus system

The dynamics of the synchronous generators are described as follows:

$$\begin{cases} \dot{\theta}_i = \omega_i \\ M_i \dot{\omega}_i = P_{Di} - P_{Gi} \end{cases} \quad i = 1, 2, \dots, N_b^t$$

On the buses to which microgrids are connected, the aggregated generation on the bus is considered in the above equation. The power flows on the system buses are constrained by the following power

flow equations:

$$\left\{ \begin{array}{l} P_{Gi} - P_{Di} = \sum_{j \in N_b^t} V_i V_j [G_{ij} \cos \delta_{ij} + B_{ij} \sin \delta_{ij}] \\ Q_{Gi} - Q_{Di} = \sum_{j \in N_b^t} V_i V_j [G_{ij} \sin \delta_{ij} - B_{ij} \cos \delta_{ij}] \end{array} \right. \quad i, j = 1, 2, \dots, N_b^t \quad (1.1)$$

The small size of DGs and their potential high penetration in the future smart grids, make the application of the conventional optimal power flow (OPF) neither practical nor economical. When it comes to the control and management of such highly dispersed and small scale generators, organizing them in the form of microgrids is the viable solution. Microgrids are the innovation zone for a smart grid, as they provide flexibility and scalability to control DGs and realize smart grid objectives. A microgrid connects to the main grid through the point of common coupling (PCC). There maybe several buses through which, capacitor banks, motors, generators and DGs are connected to the microgrid.

Microgrids, these small power systems, are gaining popularity because they offer increased reliability and efficiency, use environmental friendly renewable energy and other forms of distributed generation [6] as shown in the figure 1.5.

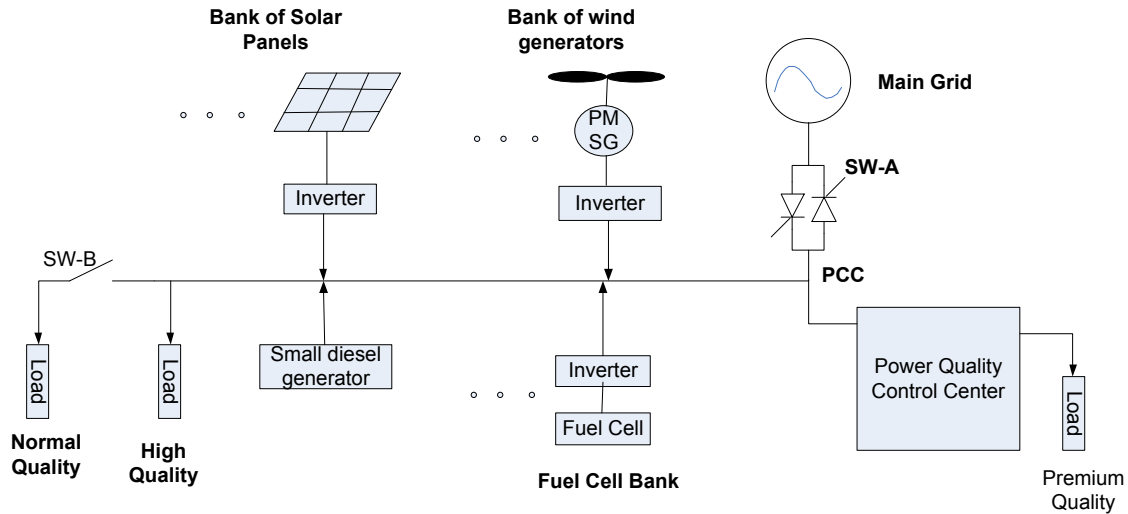


Figure 1.5: A typical microgrid, consisting of DGs and loads

A microgrid can be operated either in the grid connected mode or in the stand-alone (intentional islanding). In the grid connected mode, DGs feed their available energy to the grid and most of the system-level dynamics are dictated by the main grid, due to the relatively small size of micro sources. If the grid is tripped, microgrid disconnects and forms an intentional island and DGs provide the demanded energy of the loads. In the stand-alone mode, the system dynamics are dictated by micro sources, the network and the nature of the power regulation control.

It is believed that the microgrid concept and a high penetration of DGs will result in the reduction of power losses, voltage profile improvement, meeting future load demands, and optimizing the use of non-conventional energy sources [7]. However, more serious problems will arise if a decent control mechanism is not exploited. An improperly managed high DG penetration may cause voltage profile disturbance, make conflict with conventional network protection devices, interfere with transformer tap changers, and as a result, cause network instability.

Many forms of distributed generation (DG) systems such as fuel-cells, photo-voltaic and micro-turbines are interfaced to the network through power electronic converters [8, 9, 10]. These interfacing devices make them more flexible in their operation and control compared to the conventional power systems. Usually, the final stage of such power electronic converters is a DC/AC inverter [11, 12, 13]. Grid-tie inverters are at the heart of today's renewable energy conversion systems and future smart grids. These inverters convert the energy harnessed from the various renewable energy sources, such as wind, sun, etc., into a grid quality AC power that can be fed into the utility grid. As such, the appropriate control and management of inverters will have a significant effect on the performance of the microgrids.

### Review of the Existing Microgrid Inverter Controls

Currently, existing inverter control strategies include the current source inverter (CSI) [14, 15] , the voltage/frequency droop control [16, 17] and the generator emulation control (GEC) [18]. In the following sections, an introduction about these techniques is provided.

#### *Current Source Inverters (CSI)*

CSI mainly has the inverter feed all its available power to the grid and has been shown to cause stability problems on high penetrations [19]. Current source inverters without reactive power control, also may impose a high level of the voltage fluctuation across the system.

The highly intermittent nature of renewables is also a source of certain issues. Renewable energy sources, such as solar or wind, are very intermittent in nature. As such, the intermittency of the active power generation by the DGs would be intense. Such intermittency may result in an array of problems, if the DGs control and the reactive power compensation are not coordinated properly.

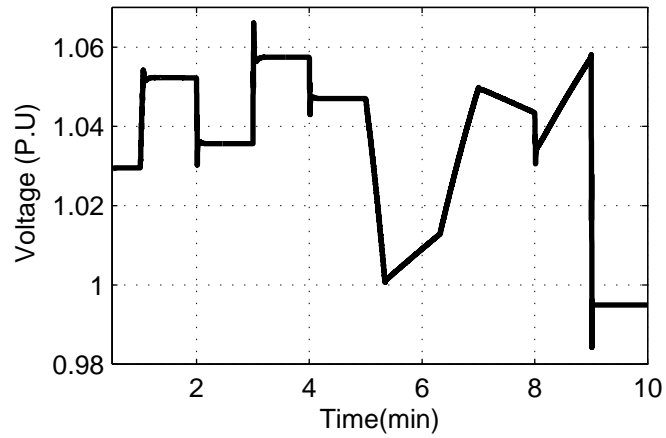
Potential issues are voltage variation [20, 21], transient stability issues, and even voltage collapse [22, 23]. For instance, Fig. 1.6a shows the end point voltage of a short feeder in a typical microgrid<sup>1</sup>, when the solar farm connected to it is exposed to a radiation intermittency as shown in the Fig. 1.6b. Such intermittencies are quite normal due to the varying weather conditions, passing clouds and etc. It is noticed how such sun radiation intermittencies directly cause voltage fluctuation.

Therefore, if the CSI control is followed without reactive power generation in high penetrations, such voltage fluctuations could trigger conventional voltage regulators on and off (such as on load tap changers (OLTC) or capacitor banks), and cause conflict. As such, a proper reactive power generation mechanism should be devised to not only prevent such voltage disturbances and conflicts, but also improve the overall system performance.

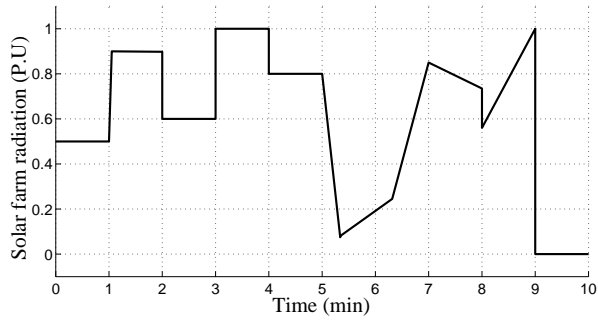
---

<sup>1</sup>This simulation is based on the feeder 5 of Fig. 3.4





(a) Feeder end point voltage



(b) A typical solar radiation intermittency

Figure 1.6: Voltage disturbance caused by a typical radiation intermittency

Different derivatives of the droop control and GEC use communicationless control to imitate the behavior of the synchronous generators. These controllers regulate their point of connection voltage and frequency. More details of the droop and GEC are provided as follows.

## Droop

Droop controllers [24, 25, 26, 27] try to mimic the behavior of the synchronous generators in an inverter. The electrical equivalent circuit of a typical synchronous generator is shown in the figure 1.7. Usually, the output stage of the generator can be simply assumed as a voltage source in series with an inductor and the series resistance is negligible. The power flow equations for such a system may be written as follows:

$$P = \frac{V_S V_o}{X_s} \sin \delta, \quad (1.2)$$

$$Q = \frac{V_S(V_S - V_o)}{X_s}. \quad (1.3)$$

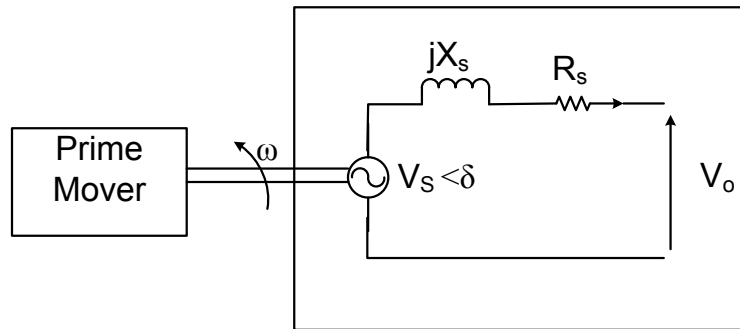


Figure 1.7: Electrical equivalent circuit of a typical synchronous generator

Equations (1.2) and (1.3), show that the power angle depends predominantly on  $P$ , whereas the voltage difference depends predominantly on  $Q$  [24]. In other words, the angle  $\delta$  can be controlled by regulating  $P$ , whereas the voltage is controllable through  $Q$ . Control of the frequency, dynamically controls the power angle and thus, the real power flow. Therefore, by adjusting  $P$  and  $Q$  independently, frequency and amplitude of the grid voltage are determined. These conclusions

form the basis for the well-known frequency and voltage droop regulation through respectively active and reactive power:

$$f - f_0 = -k_p(P - P_0), \quad (1.4)$$

$$V_S - V_o = -k_q(Q - Q_0). \quad (1.5)$$

$f_0$  and  $V_0$  are the grid rated frequency and voltage respectively, and  $P_0$  and  $Q_0$  are the (momentary) set points for the active and the reactive power of the inverter. The typical frequency and voltage droop control characteristics are shown graphically in the figure 1.8.

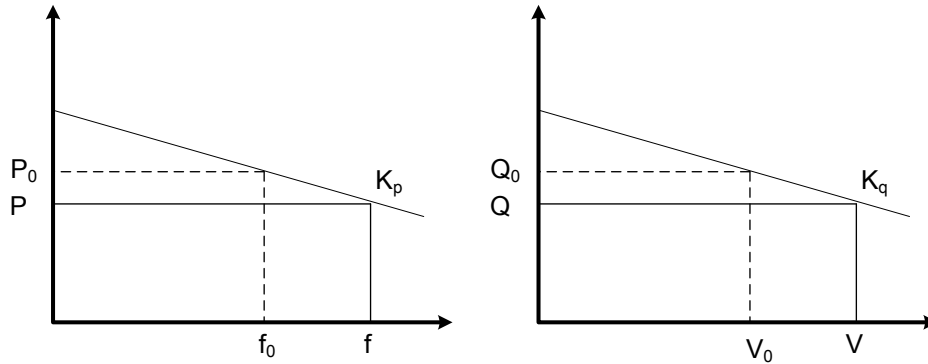


Figure 1.8: frequency and voltage droop control characteristics.

There are several issues associated with the droop control. To provide a fair power share among inverters, steeper droops should be used, which result in larger frequency and voltage deviations from the desired values. This implies the need for a mechanism to restore the system frequency and voltage to nominal values, following a change in the system load/generation [25, 28]. Following the term used in the electric power system control, this restoration mechanism is termed as the secondary control of the voltage and frequency, and takes place over a longer period of time.

To overcome this issue, the use of a low-bandwidth communication channel between DGs, for the secondary control functions of restoration, load sharing and management, has been proposed [26, 27, 29].

Conventional droop, following the conventional power system control practice, assumes the lines to which modules are connected, are mainly inductive. As such, this method has the limitations when the microgrid interconnecting impedances have a significant resistive component [24, 30, 31]. In this situation, the active power vs. the frequency droop ( $P - f$  droop) and the reactive power vs. the voltage droop ( $Q - E$  droop) are no longer valid. As such, the real and the reactive power are affected by both, the voltage magnitude and the phase angle difference[30]. In such situations, the droop technique should be modified to include the effect of the line resistances.

However, one of the most important drawbacks of the droop is that it fails to meet the actual system demands in a high DG penetration and larger scale microgrid. The main reason is that in droop, every module only regulates its own coupling point voltage and frequency, without considering the higher level system demands. For instance, as shown in the figure 1.6a, the DGs closer to the beginning of the feeder, produce less reactive power, due to the less voltage drop seen by them. On the other hand, those closer to the end of the feeder, produce more reactive power, due to higher voltage drop, sensed by them. That is while there may be a high demand of the reactive power on that area as a whole. As such, this power management fails to control DGs power generation optimally, to benefit a larger scale microgrid.

### *Impedance Emulation*

The output impedance of the inverter has a significant role on its control performance and dynamics. It affects the power sharing accuracy and determines the P/Q droop control strategy. Furthermore, the proper design of this output impedance can reduce the impact of the line-impedance

unbalance on the droop [30], which was discussed earlier.

However, large inductors are way bulky and expensive. Therefore, it is impractical to use the actual large inductors in the output of inverters. For instance, figure 1.9 shows a  $1H$  inductor next to a typical micro inverter. As such, it is desired to avoid the use of such actual impedances and instead, it is of interest to program the inverters in such a way to emulate the existence of the demanded impedances.



Figure 1.9: Comparing the size of a large inductor and an actual micro inverter, courtesy of Petra Solar Inc.

It was shown by [30] that to program a stable output impedance, the inverter output voltage reference,  $v_{ref}$ , can be dropped proportionally to the output current, using the following instantaneous droop scheme:

$$v_{ref} = v_o^* - Z_D(s)i_o$$

where  $Z_D(s)$  is the virtual output impedance, which may be chosen to be resistive, inductive or a desired network. The parameter  $v_o^*$  is the output voltage reference at no load, which is usually a sinusoidal waveform with unity magnitude. The variable  $i_o$  is the output current feedback.  $Z_D(s)$

The use of the resistive virtual impedance to decouple the voltage and the frequency droop controllers, was discussed in [32]. The use of an inductive virtual impedance at the converter output is reported in [33, 34]. The output current feedback is used to implement a controller, that presents a virtual inductor at the inverter output. The frequency and the voltage droops are decoupled with a virtual inductor at the output, and the conventional droop schemes can be used.

Reference [18] proposed emulating a large inductor at the output of the inverter. Therefore, the use of the conventional droops of (1.4) and (3.12) to emulate the behavior of the synchronous generators was facilitated. Also, a large inductor being emulated, reduces the circulating power among the inverters and improves the power share [18]. As the emphasize has been of emulating the behavior of the synchronous generators on that work, it has been dubbed generator emulation control (GEC).

The control core of the GEC is a single loop current controller. There is an outer loop controller, which generates the reference current. This reference current is generated based on the virtual impedance network and the related droop curve.

The simplified inverter model is shown in the figure 1.10 , where  $V_S$ ,  $V_o$  and  $X_s$  are the inverter emulated EMF (reference voltage), line voltage and the inductor impedance to be emulated, respectively.

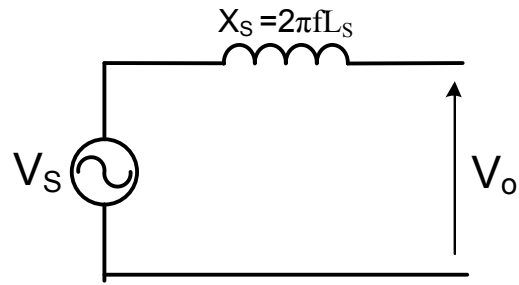


Figure 1.10: GEC simplified inverter model

The GEC active power droop curve is shown in the figure 1.11, where  $f_0$  and  $f_{Max}$  are the line nominal and the max frequency, respectively. As long as the the line frequency is below the nominal, the maximum available power, provided by the maximum power point tracking (MPPT) mechanism of the inverter, is fed to the grid. However, in case the line frequency is increased above the nominal, mainly due to the excessive active power generation, the produced active power is decreased linearly, down to zero at  $f_{Max}$ . The units active power generation is controlled by accordingly controlling the inverter phase with respect to the line, according to the figure 1.10 and (1.2).

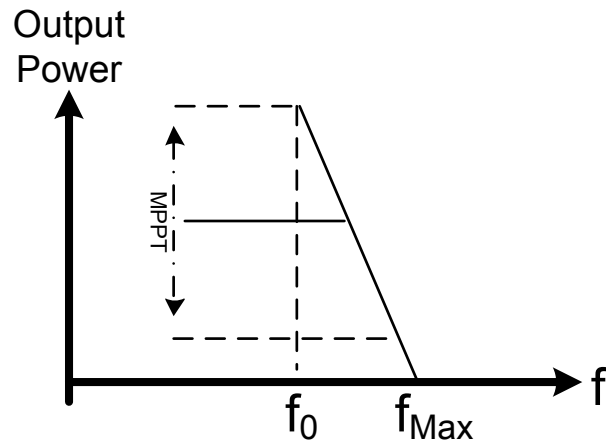


Figure 1.11: GEC active power droop curve

The inverter emulated EMF,  $V_S$ , is kept at a constant value, mainly one per unit. According to (3.12), this results in a linear volt/VAR droop characteristics, as shown in the figure 1.12. The inverter provides voltage regulation support by sinking reactive power, if the line voltage is higher than normal and sourcing reactive power, if the line voltage drops. This very simple droop profile results naturally with a constant emulated EMF amplitude.



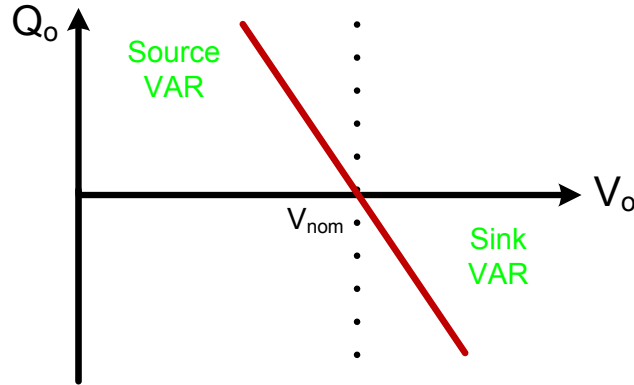


Figure 1.12: Volt-VAR droop characteristics of GEC

Respectively, the output current reference, to be sent to the internal current controller, is calculated as follows:

$$i_o^{ref} = \frac{V_S - V_o}{X_S}$$

As discussed earlier, the magnitude of  $V_S$  is kept constant at unity and its phase is controlled to produce the desired output active power, as shown by the figure 1.11 and (1.2)

#### Statement of the Contribution

A microgrid needs to organize its DGs to realize predetermined objectives. The ultimate goal is to have DGs operate fairly together to help provide stability, to keep voltage profile within the acceptable range and to provide a desired power flow.

In a wide system, with high DG penetration, every DG just regulating its coupling point voltage could result in an array of problems. For instance, the effects of DG operations on the other parts

of the system are neglected. As an illustrative example, in a typical feeder as shown in the figure 1.6a by the solid line, voltage is the highest at the top, and naturally drops, as going down the line. Droop based controllers produce a reactive power, proportional to their voltage difference from unity. As such, the units at the top of the feeder produce less reactive power, while the units at the end of the feeder produce more. That is while, there may be a high reactive power demand on the area as a whole. This non optimal dispatch of DG's reactive power results in a non-optimal voltage profile across the system and increases the system losses. Other side effect of the droop based controllers is the impose of a high reactive power flow to the main grid [35].

The highly intermittent nature of PVs is also a source of certain issues. Considering the wide spread of PVs on a high penetration and potential variation of PV profiles on different locations, the intermittency of the active power generation by the DGs would be intense. Such intermittency may result in an array of problems if the DGs control are not coordinated properly. Potential issues are voltage variation [20, 21], transient stability issues, and even voltage collapse [22, 23], making it desirable to develop a practical and robust scheme of controlling the total output of the PVs. As such, an appropriate control scheme extends far beyond just regulating inverters coupling point voltage and frequency.

Cooperative control provides the possibility for different agents in a networked area to operate together and realize some desired objectives [36] and already has been successfully applied to the autonomous vehicle control [37]. In this work, the application of the cooperative control for managing the DGs in a power system is introduced.

Chapter 2 introduces and formulates the design of the cooperative control of DGs. It is shown how DGs can utilize the intermittent, asynchronous, and low bandwidth communication links and get organized to work cooperatively together to fulfill the demanded power objectives. Cooperative control can be applied to helps DGs cooperatively satisfy multiple power objectives. Introduction

of the fair utilization ratio also makes DGs contribute proportional to their capacity. Individual DGs cooperative law is derived, based on the inverter dynamics. The closed loop system stability is also investigated.

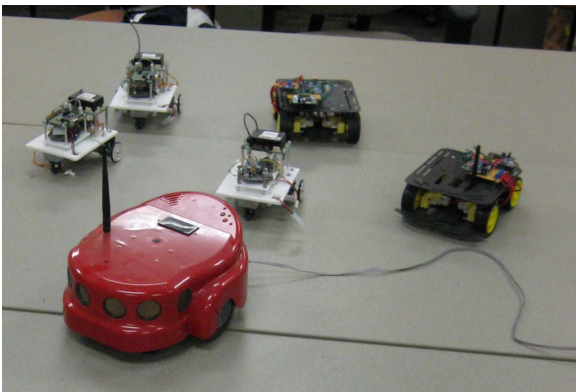
Chapter 3 elaborates the application of the cooperative distributed optimization in controlling the DGs reactive power. It is shown how DGs can cooperatively minimize an additive cost function. In this work, the minimization of the overall system voltage errors is of interest. It is shown how the application of the distributed optimization results in a unified microgrid voltage profile and active power loss minimization. The detailed design and stability analysis are provided. It is also shown that in case the communication is not available, the proposed technique results in an adaptive droop. The proposed adaptive droop, exhibits an improved transient response in terms of eliminating the overshoots and oscillations, compared with the conventional droop.

Chapter 4 formulates the interaction between the microgrid and the main grid. A game approach is proposed and fully investigated that not only optimizes the economical interests of both, the main grid and the microgrid, but also improves the power flow between the main grid and the microgrid.

## CHAPTER 2: COOPERATIVE CONTROL OF DISTRIBUTED GENERATORS

### GENERATORS

Cooperative control helps individual agents in a system use a shared communication network and make the overall system act as a group. System is pliable to network disconnection, topology changes, latency and intermittenencies. Cooperative control originally was introduced for the control of autonomous robots and vehicles [38]. For instance, the figure 2.1a shows a group of robots that are following a leader robot. The group of robots use the communication network and try to be oriented according to the leader. Another example is shown in the figure 2.1b; where a group of submarines communicate with each other to follow the leader and be organized accordingly.



(a) Application of cooperative control in autonomous robots



(b) Application of the cooperative control in autonomous submarines

Figure 2.1: Different applications of the cooperative control

In both cases of the figure 2.1 the communication network may undergo serious abrupciones, intermittenencies and not all the modules have access to the leader. Also the leader may change during the time. Cooperative control helps the agents in any group, in which the leader is subject to change, utilize the available non-consistent communication network and behave as a robust and

united group. This facilitates the overall group realize the desired objectives.

In a smart grid, DGs should be controlled properly to cooperatively satisfy multiple objectives. In this chapter, at first the desired power objectives are discussed. Then, the cooperative control law, based on the inverter modeling, is introduced. It is shown that the system is stable and the simulation results show the effectiveness of this technique, compared with the state of the art.

## Power Objectives

### *Active Power*

In a high DG penetration, every unit regulating its own point voltage/frequency, is not much to the benefit of the system. In such a system, the power demands on the other places of the microgrid should be considered and all the agents should work cooperatively together to achieve an appropriate performance. To this end, the proper definition of the power objectives of the microgrid plays an important role.

As it will be discussed in the Chapter 4, the economical constraints of both the main grid and the microgrid, make it of especial interest to secure a desired active power flow between the microgrid and the main grid. As such, the active power flow policy is to keep the active power flow between the main and the microgrid at a specified value.

The microgrid power management should be in such a way not only meet certain power policies, but also provide the possibility that all DGs contribute proportional to their capacity. Therefore, active power fair utilization ratio,  $\alpha_p$ , is introduced to determine how many percentage of the

available active power is to be generated by every DG:

$$\alpha_{p_i} = \frac{P_i}{\bar{P}_i}, \quad (2.1)$$

where the  $P_i$  and  $\bar{P}_i$  are the  $i$ th unit generation and the maximum available active power respectively. DGs are to operate together and converge to the same utilization ratio to secure the desired power objective.

### *Reactive Power*

Each inverter has a nominal power rating,  $S_i$ . If the active power generated by a DG is less than this nominal rating, the excessive power capacity may be exploited to generate reactive power:

$$\begin{cases} \bar{Q}_i = \sqrt{S_i^2 - P_i^2} \\ Q_i = \alpha_{q_i} \bar{Q}_i \end{cases}, \quad (2.2)$$

where  $Q_i$  and  $\bar{Q}_i$  are the generated and the maximum available reactive power of the  $i$ th unit respectively. Similar to the active power,  $\alpha_q$  is the reactive power fair utilization ratio and indicates what percentage of the available reactive power is to be fed to the grid.

The reactive power flow objective may be set as minimizing the aggregated reactive power flow to the main grid and regulating one or several critical points across the system. Therefore, in terms of the reactive power control, the DGs form different groups to cooperatively satisfy these power objectives, as shown in the figure 2.2.

As such, two sets of DG groups are required as follows to satisfy the above mentioned reactive power objectives:

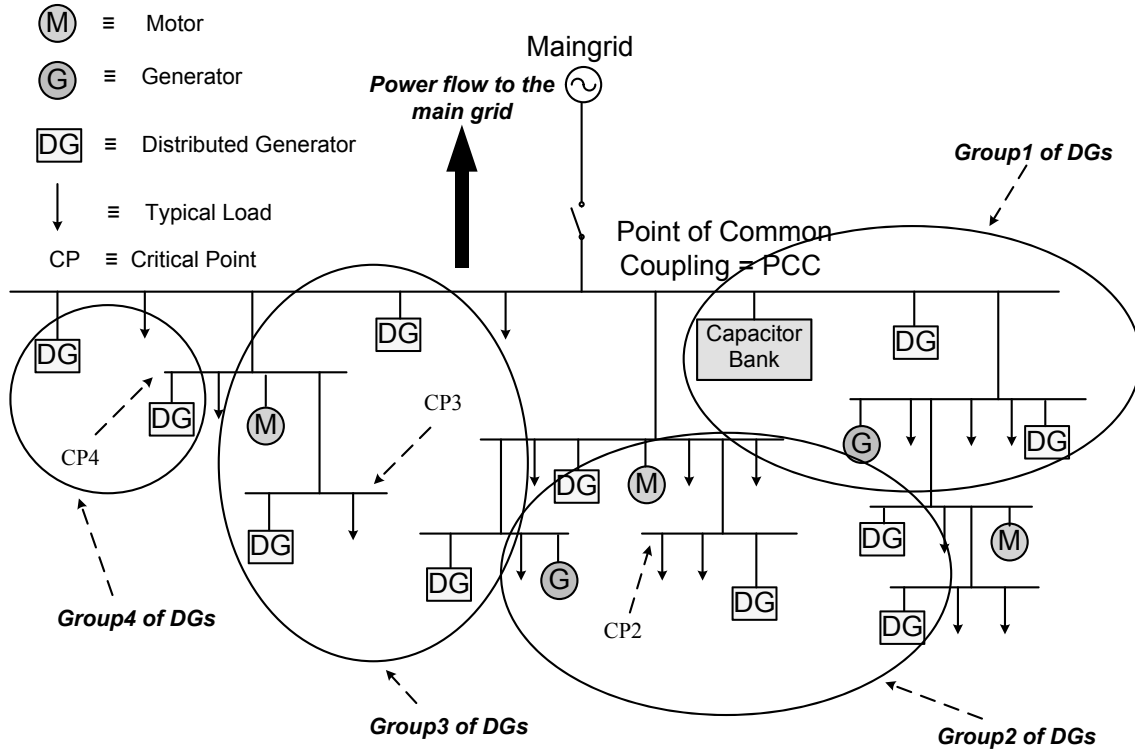


Figure 2.2: Typical structure of a microgrid with distributed generators, organized in groups

- Power objective1:

$$Q_{\mu-G} \rightarrow 0,$$

- Power objective2:

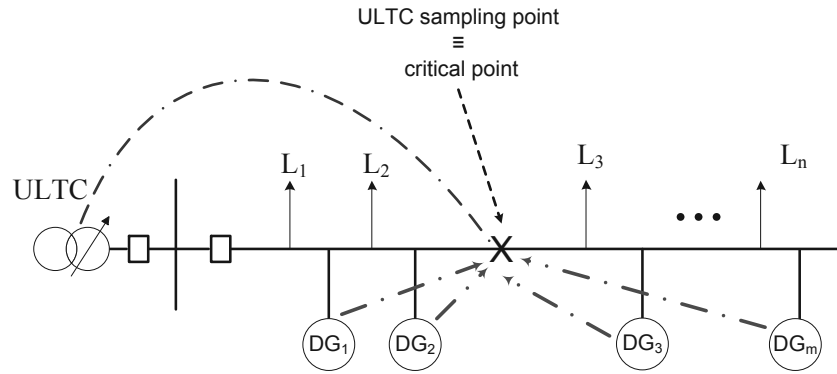
$$V_{cp_i} \rightarrow 1P.U \quad 1 \leq i \leq N_{CP}.$$

where  $Q_{\mu-G}$  is the reactive power flow from the microgrid to the main grid,  $V_{cp_i}$  is the  $i$ th critical point voltage and  $N_{CP}$  is the number of critical points on the microgrid.

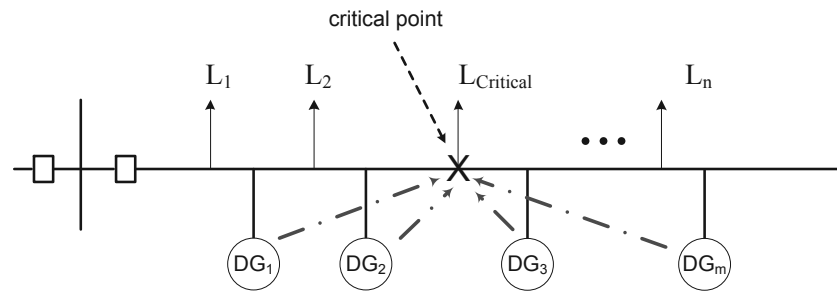
Figure 2.2 illustrates the clustering discussed above. DGs in group 1 are supposed to support power objective 1, minimizing the reactive power flow to the main grid. groups 2-4 try to regulate the marked critical point voltages.

The number of DG groups depends on the select critical points. DGs from one or several feeders may form a group to regulate a critical point voltage. The choice of the critical point depends on the system requirements and configurations. Figure 2.3 shows some possible choices. As shown, critical point may be the downstream point in a feeder, as it usually undergoes the highest voltage drop due to more distance from the source, or a specific location with critical loads, such as special business area. Other alternative for a critical node in a distribution network is the sampling point of the under load transformer tap changer (ULTC), as shown in the figure 2.3a. This way, the conflict between inverters operation and ULTCs is minimized, the DGs capacity is effectively utilized to maintain the desired voltage profile and also the transformer tap changer operation is minimized. In the next section, the inverter modeling is provided and then the cooperative control is formulated based on the inverter dynamics.

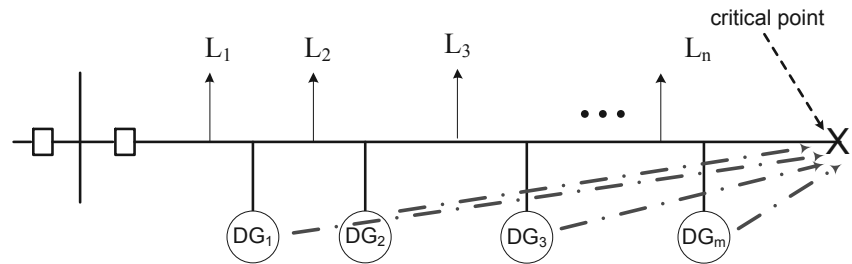




(a) ULTC sampling point as the critical point



(b) Critical loads as the critical point



(c) End of the feeder as a critical point

Figure 2.3: Different choices of the critical point on a typical feeder

## Inverter Modeling

DGs are usually connected to the grid through fast responding DC/AC converters (inverters) [17]. The typical structure of a DG, coupled to the grid by an inverter, is shown in the figure 2.4.

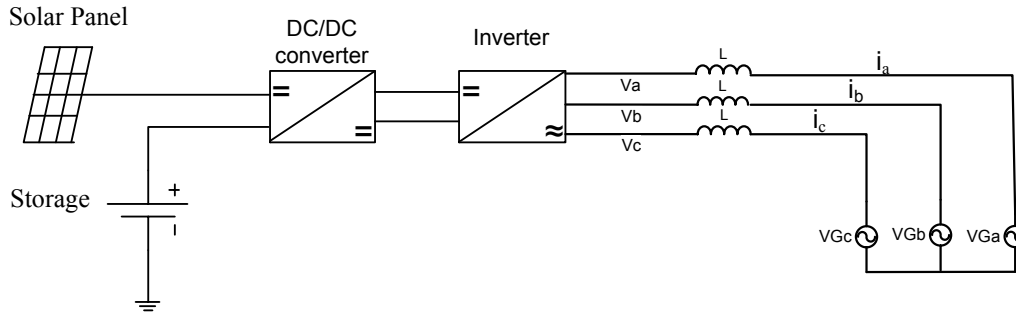


Figure 2.4: Typical structure of a PV based DG, coupled to the grid using a three phase inverter

The system equation of the figure 2.4 is as follow:

$$\begin{cases} V_{abc} = L \frac{di_{abc}}{dt} + V_{Gabc} \\ V_{abc} = KV_{c_{abc}} \end{cases}, \quad (2.3)$$

where  $K$  is the inverter gain and  $V_{c_{abc}}$  is the overall controller output which is applied to the inverter. In power systems, it is customary to take variables in the  $d - q$  reference frame and have calculation in terms of the  $d - q$  variables. That is because sinusoidal variables turn into constants at the  $d - q$  frame and this makes it easy to work, especially makes the application of simple PI controllers viable [14, 16, 15]. Applying the park transformation on the above equations provides the  $d - q$

equivalent equations [16, 39]:

$$\frac{di}{dt} = \begin{bmatrix} 0 & \omega \\ -\omega & 0 \end{bmatrix} i + \frac{1}{L}(KV_c - V_G), \quad (2.4)$$

where

$$i = [i_d \quad i_q]^T, V_c = [V_{cd} \quad V_{cq}]^T, V_G = [V_{Gd} \quad V_{Gq}]^T.$$

Here,  $i$  is the output current,  $V_c$  is the input voltage command to the inverter,  $K$  is the inverter PWM gain, and  $V_G$  is the grid voltage at the inverter terminals.

The model (2.4) indicates that current components  $i_{d,q}$  are coupled through  $\omega i_d$  and  $\omega i_q$  terms. This coupling can be eliminated by introducing the new variables  $V$ , as given by:

$$V = KV_c - V_G + \omega L[i_q \quad -i_d]^T, \quad (2.5)$$

where  $V = [V_d \quad V_q]^T$ . Substituting (2.5) in (2.4) yields:

$$\frac{di}{dt} = \frac{1}{L}V$$

This equation represents decoupled  $i_{d,q}$  currents. Once the decoupled variables have been defined as in (2.5), a PI controller may be applied to control the overall system. This system block diagram is shown in the figure 2.5

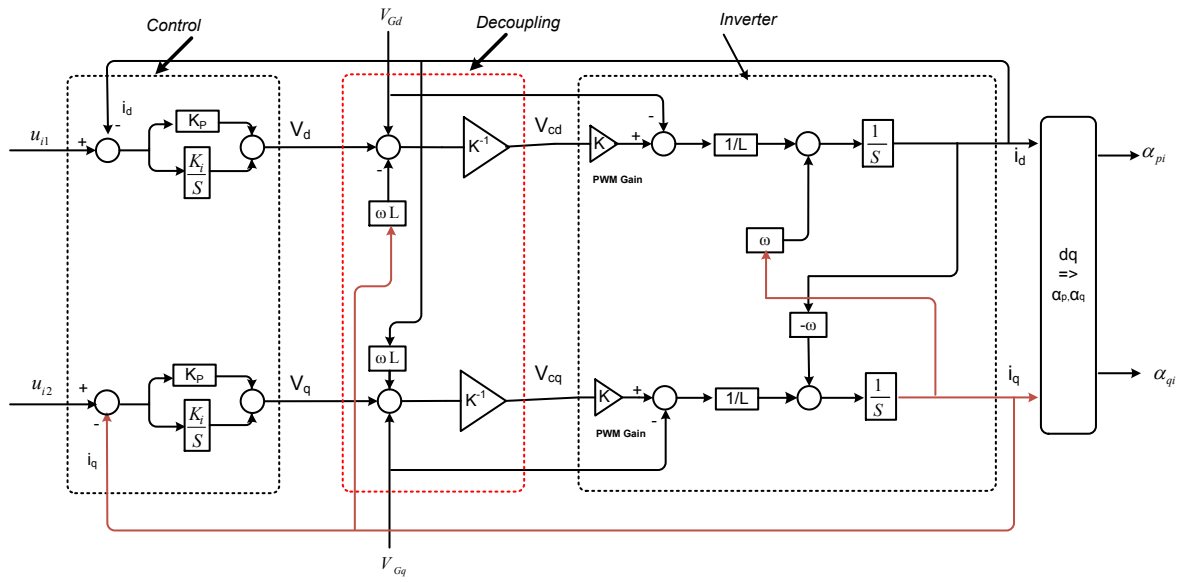


Figure 2.5: Inverter model block diagram with PI control

Combining the inverter plant, decoupling section and controller in the figure 2.5, the following inverter state space dynamic model is obtained:

$$\begin{cases} \dot{x}_i = A_i x_i + B_i u_i \\ y_i = C_i x_i \end{cases}, \quad (2.6)$$

where

$$x_i = \begin{bmatrix} \int (u_i - I_i) dt \\ I_i \end{bmatrix}, \quad I_i = \begin{bmatrix} i_{di} \\ i_{qi} \end{bmatrix}, \quad y_i = \begin{bmatrix} \alpha_{pi} \\ \alpha_{qi} \end{bmatrix}, \quad u_i = \begin{bmatrix} u_{i1} \\ u_{i2} \end{bmatrix},$$

$$A_i = \begin{bmatrix} 0 & 0 & -1 & 0 \\ 0 & 0 & 0 & -1 \\ \frac{K_i}{L} & 0 & -\frac{K_p}{L} & 0 \\ 0 & \frac{K_i}{L} & 0 & -\frac{K_p}{L} \end{bmatrix}, \quad B_i = \begin{bmatrix} 1 & 0 \\ 0 & 1 \\ \frac{K_p}{L} & 0 \\ 0 & \frac{K_p}{L} \end{bmatrix}, \quad C_i = \begin{bmatrix} 0 & 0 & \frac{V_{Gi}}{P_i} & 0 \\ 0 & 0 & 0 & -\frac{V_{Gi}}{Q_i} \end{bmatrix}.$$

Here,  $I_i$  is the output current. It is noteworthy that all the measurements on the inverter are with respect to the voltage measured at the output terminal. As such,  $V_{di} = V_{Gi}$  and  $V_{qi} = 0$ . Therefore, the output power of the  $i$ th inverter can be expressed as:

$$P_i = i_{di}V_{Gi}, \quad Q_i = -i_{qi}V_{Gi}.$$

## Cooperative Control Formulation

### *Communication Network*

The objective is utilizing the available communication network, control the DGs in the microgrid in such a way to both, meet the power objectives and have all the DGs converge to the same utilization ratios. However, the communication links may have limited bandwidth, be intermittent and asynchronous. Cooperative control has the advantage that utilizing such non consistent communication links, can have a group of agents/modules exhibit cooperative behaviors and make the system act as one group. Cooperative control has been already applied to the autonomous vehicle control [37] and its basic application for DG control on power systems was introduced in [40]. In this section, to facilitate all DGs to self-organize, the design of the cooperative control with respect to the dynamics of the inverters is provided.

The instantaneous communication topology is defined by the following matrix:

$$S(t) = \begin{bmatrix} s_{00}(t) & s_{01}(t) & s_{02}(t) & \cdots & s_{0n}(t) \\ s_{10}(t) & s_{11}(t) & s_{12}(t) & \cdots & s_{1n}(t) \\ s_{20}(t) & s_{21}(t) & s_{22}(t) & \cdots & s_{2n}(t) \\ \vdots & \vdots & \vdots & \ddots & \vdots \\ s_{n0}(t) & s_{n1}(t) & s_{n2}(t) & \cdots & s_{nn}(t) \end{bmatrix} \quad (2.7)$$

In (2.7),  $s_{ii} = 1$  for all  $i$ ;  $s_{ij} = 1$  if the output of the  $j$ th DG is known to the  $i$ th DG at time  $t$ , and  $s_{ij} = 0$  if otherwise. Heuristically, the more communication channels be available, the more information propagates within the group, and the faster the convergence is achieved. However, It follows from the cooperative control theory [38] that the minimum requirement on the communication topologies is the so-called sequential completeness condition. Mathematically, this requirement is that the sequence of communication matrices  $S_{\infty:0} = \{S(t_0), S(t_1), \dots\}$  be sequentially complete in the sense that, over an infinite sequence of finite consecutive intervals, the composite graph over each of the intervals (or the binary product of all the matrices of  $S$  over the interval) has at least one globally reachable node (in the sense that all other nodes can be reached from the globally reachable node by following the directed branches of the graph) [38]. Precisely, it is a necessary and sufficient condition for the cooperative system to converge that the Communication matrix  $S$  be piecewise constant, and the corresponding sequence  $S_{\infty:0} = \{S(t_0), S(t_1), \dots\}$  be sequentially complete [40].

A more restrictive (sufficient but not necessary) condition is that the composite graph is strongly connected (which implies that, by following the directed branches, every node can be reached from any other node). To illustrate its application, consider communication matrix  $S(t_k)$  and construct the corresponding graph by linking the nodes according to nonzero entries in  $S$ . One can easily determine whether the resulting graph has at least one globally reachable node or not. For instance,

consider the graphs in the figure 2.6. figure 2.6(a) has node 0 as the unique globally reachable node; and none of the nodes in the figure 2.6(b) is globally reachable, because there are two isolated groups of nodes.

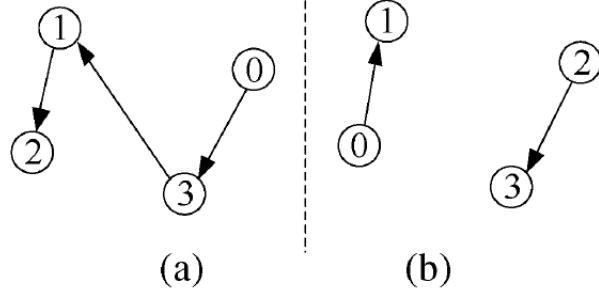


Figure 2.6: Sample graphs of the communication topology. (a) Existence of one globally reachable node. (b) Absence of a globally reachable node.

The above general method can be used to verify or establish the sequential completeness condition, and the details can be found in [38, 41]. In designing distributed control for PVs in a distribution network, the focus is to the following very special case of the local communication topology: If matrix  $S(t_k)$  has at least one globally reachable node for every  $k \geq 0$ , then sequence  $S_{\infty,0}$  is guaranteed to be sequentially complete. The following example further explains this special case for the sequential completeness condition. Consider a communication network which may have any of the following  $S_0, S_1$  or  $S_2$  communication matrices:

$$S_0 = \begin{bmatrix} 1 & 0 & 0 & 0 \\ 1 & 1 & 0 & 0 \\ 1 & 0 & 1 & 0 \\ 0 & 0 & 1 & 1 \end{bmatrix}, S_1 = \begin{bmatrix} 1 & 0 & 0 & 0 \\ 1 & 1 & 0 & 1 \\ 0 & 0 & 1 & 1 \\ 1 & 0 & 0 & 1 \end{bmatrix} \& S_2 = \begin{bmatrix} 1 & 0 & 0 & 0 \\ 1 & 1 & 0 & 1 \\ 1 & 0 & 1 & 1 \\ 0 & 1 & 0 & 1 \end{bmatrix}$$

Figure 2.7 plots the graphs corresponding to those communication topologies. It follows from the

figure 2.7 that the information can propagate from node 0 to the nodes 1, 2, and 3. Therefore, all of the communication matrices are complete by themselves, and so are their sequences.

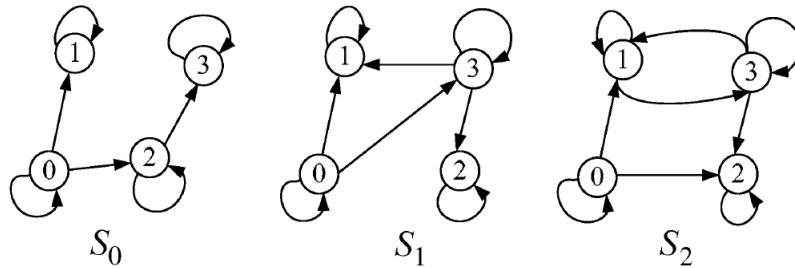


Figure 2.7: Graphs for time-varying communication topologies.

While not necessarily required, this special case can be used to design and implement a redundant local communication network, which satisfies the so-called rule of N-n. Namely, when  $n$  communication channels cannot work properly in some amount of time, the communication matrix corresponding to the remaining communication channels should be kept to be complete. It should be also noted that the convergence rate of the closed loop system depends upon connectivity of the communication network, so it is important to design a reasonably connected local communication network within certain physical and economic constraints.

### *Cooperative Law*

The control algorithms are implemented in the discrete form in the practical systems. The discrete time closed loop cooperative control law, for the  $i$ th DG is as follows [38]:

$$\alpha_i(k+1) = \sum_{j=1}^{N_{DG}} d_{ij} \alpha_j(k) + d_{i0} \alpha^{ref} \quad (2.8)$$



where

$$d_{ij} = \frac{\omega_{ij}s_{ij}}{\sum_{l=0}^{N_{DG}} \omega_{il}s_{il}}, \quad i, j = 0, 1, \dots, N \quad (2.9)$$

$s_{ij}$  is a generic entry of the  $S$  communication matrix, defined by (2.7) and  $\omega_{ij}$  are the weighting factors. For a symmetric control system,  $\omega_{ij} = 1, \forall i, j$ .

The closed loop system description of (2.8) in the matrix form is as follows:

$$\alpha(k+1) = D\alpha(k) + D_0\alpha^{ref} \quad (2.10)$$

where  $\alpha = [\alpha_1, \dots, \alpha_{N_{DG}}]^T$ ,  $D_0 = [d_{10}, \dots, d_{N_{DG}0}]^T$ ,  $D \in \mathbb{R}^{N_{DG} \times N_{DG}}$  and  $D = [d_{ij}]|_{i,j=1, \dots, N_{DG}}$ .

The continuous time equivalent form of (2.8) is as follows [38, 42]:

$$\dot{\alpha}_i = k_c \left[ -\alpha_i + d_{i0}\alpha_p^{ref} + \sum_{j=1}^{N_{DG}} d_{ij}\alpha_j \right], \quad (2.11)$$

Based on (2.11), the cooperative control law for the system of (2.6) for a group of  $N_{DG}$  inverters is as follows.

$$\begin{cases} u_{i1} = \frac{L}{K_p V_{Gi}} \{ \bar{P}(d_{i0}\alpha_p^{ref} - \alpha_{pi} + \sum_{j=1}^{N_{DG}} d_{ij}\alpha_{pj}) - [(\dot{V}_{Gi} - V_{Gi}\frac{K_p}{L})x_{3i} + V_{Gi}\frac{K_i}{L}x_{1i}] \} \\ u_{i2} = \frac{L}{K_p V_{Gi}} \{ -\bar{Q}(d'_{i0}\alpha_q^{ref} - \alpha_{qi} + \sum_{j=1}^{N_{DG}} d'_{ij}\alpha_{qj}) - [(\dot{V}_{Gi} - V_{Gi}\frac{K_p}{L})x_{4i} + V_{Gi}\frac{K_i}{L}x_{2i}] \} \end{cases}, \quad (2.12)$$

where

$$d_{ij} = \frac{s_{ij}}{\sum_{j=0}^{N_{DG}} s_{ij}}, \quad i = 0, 2, \dots, N_{DG} \quad (2.13)$$

$s_{ij}$  is a generic entry of the matrix  $S$  defined in (2.7). The variables  $\alpha_p^{ref}$  and  $\alpha_q^{ref}$  respectively are the active and reactive power fair utilization ratios, provided by the virtual leaders. In (2.7), unit 0 is assumed to be the virtual leader. Virtual leader needs to have access to either the top level

control agent, the power flow information or the voltage profile of the lines. As such, if any of the operating modules have access to such information, it may acquire the position of the virtual leader.

*The effect of the Communication Frequency on the Convergence Rate*

**Theorem 1.** *The convergence rate of the system of (2.10) is proportional to the system communication frequency.*

*Proof.* In order to calculate the convergence rate of (2.10), the largest in magnitude eigenvalue of  $D$  should be mapped into the  $S$ -domain [43].  $Z$ -domain and  $S$ -domain are related by the formula  $z = e^{Ts}$ , where  $T$  is the sampling (or discretizing) period of the system. As a reminder, the  $Z$ -domain and  $S$ -domain diagrams are shown in Fig. 2.8. As shown in Fig. 2.8, the system time

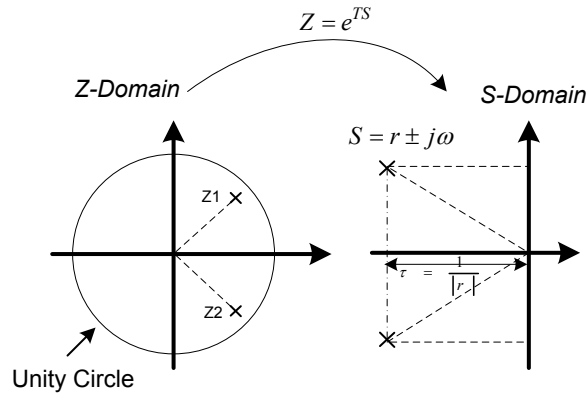


Figure 2.8: Z-domain to S-domain mapping

constant,  $\tau$ , is the inverse of the dominant eigenvalue real part magnitude. Therefore, assuming

$S = r + j\omega$ :

$$\begin{aligned} Z &= e^{ST} = e^{rT + j\omega T}, \\ \Rightarrow |Z| &= e^{rT} = e^{-\frac{T}{\tau}} \\ \Rightarrow \tau &= -\frac{T}{\ln|Z|} \end{aligned} \tag{2.14}$$

Equation (2.14) shows that the system time constant is directly proportional to the communication period. This implies that faster communication frequencies result in lower time constants and faster convergence rates are achieved.  $\square$

### *ZigBee Communication*

ZigBee is becoming a preferred communication protocol for home applications and other low range communication devices [44]. Recently, some of the inverter producers also have incorporated ZigBee communication modules within their devices, including Petra Solar Inc. ([petrasolar.com](http://petrasolar.com)).

ZigBee is a low cost, low power and low range communication protocol. It targets the devices which require a secure networking, low data rate and long battery life. It is based on the IEEE 802.15.4 physical radio standard. ZigBee operates in unlicensed bands worldwide at 2.4GHz (global), 915Mhz (Americas) and 868Mhz (Europe). It provides data rates of 250Kbs at 2.4GHz (16 channels), 40Kbs at 915Mhz (10 channels) and 20Kbs at 868Mhz (1 channel) and best suites the applications that need periodic or intermittent data. It also boosts the privilege of being lower cost compared with bluetooth or conventional Wi-Fi devices.

As shown in the figure 2.9, ZigBee devices may connect together in a mesh or star network. A typical ZigBee network consists of the following elements:

- ZigBee Co-ordinator (ZC): This forms the root of the network and performs similar to a virtual leader.
- ZigBee Router (ZR): Routers may pass data through different devices, mainly to increase the effective operating range.
- ZigBee End Device (ZED): This may be the actual device, communicating with the rest of the network.

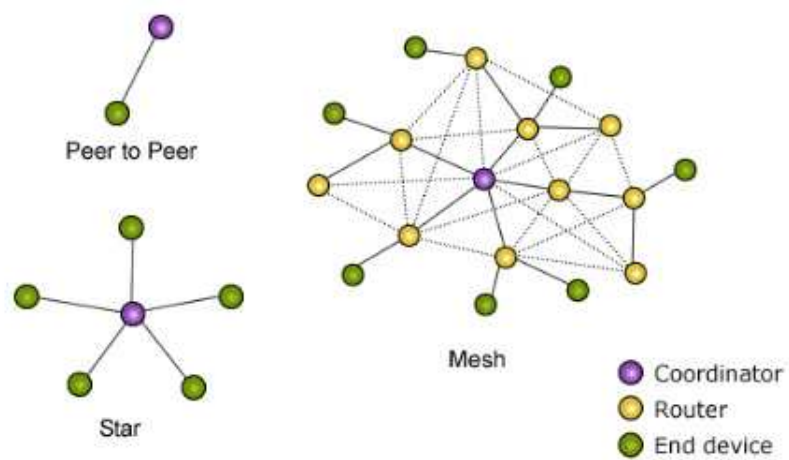


Figure 2.9: ZigBee communication network

Based on the ZigBee specifications, cooperative control may easily be operated on the networks, which utilize such communication modules.

## Virtual Leaders Control

### Active Power

Active power objective is to keep active power flow to the main grid at a desired level. As such, all DGs form a group and cooperatively try to realize this objective. Therefore, a virtual leader monitors the active power flow and adjusts the active power utilization ratio,  $\alpha_p^{ref}$ , accordingly. Then, all DGs will follow this utilization ratio, utilizing the cooperative control. The virtual leader uses an integrator controller to search for the proper utilization ratio as follows and shown in the figure2.10 :

$$\dot{\alpha}_p^{ref} = k_p(P_\mu^{ref} - P_\mu), \quad (2.15)$$

where  $k_p$  is the controller gain and  $P_\mu^{ref}$  and  $P_\mu$  are the reference and actual active power flow to the main grid, respectively.

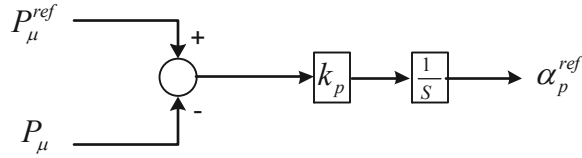


Figure 2.10: Search for the active power flow fair utilization ratio

### Reactive Power

Usually the active power that DGs produce is less than the power ratings of the inverters. As such, the excessive power capacity of the inverters may be used to produce reactive power to help microgrid voltage regulation.

One approach in managing the reactive power capacity of the inverters is to regulate a critical point voltage. However, in large scale microgrids, all DGs focusing on regulating one point may cause some other problems. For instance, voltage profile on other locations may be disturbed or excessive reactive power may flow to the main grid.

The proper reactive power management should both, keep a unified voltage profile across the microgrid and at the same time, minimize the reactive power flow to the main grid. As such, as shown in the figure2.2, DGs need to be organized in different groups.

The number of DG groups depends on the select critical points. DGs from one or several feeders may form a group to regulate a critical point voltage.  $N_{CP}$  DG group is required to regulate the  $N_{CP}$  critical points. One more group is needed to minimize the reactive power flow to the main grid. Considering one inverter in each group as a minimum requirement, the lower bound for the number of demanded inverters on the microgrid,  $N_{DG}$ , is:

$$N_{DG} \geq N_{CP} + 1.$$

The closest DGs to the critical points or PCC, which have access to the demanded power flow or voltage measurements, take virtual leader responsibility and set the power policies. DGs join the group of the closest virtual leader and clusters of DGs are formed accordingly:

$$DG_i \in G_j \quad , if D_{ij} < D_{il}, \begin{cases} l = 1, \dots, L, \\ l \neq j \end{cases} \quad (2.16)$$

where  $DG_i$  is the  $i$ th DG in the microgrid,  $G_j$  is the  $j$ th DG group in the microgrid,  $D_{ij}$  is the distance between the  $i$ th DG and the  $j$ th virtual leader, and  $L$  is the number of virtual leaders at the microgrid.

Virtual leader uses an integrator controller to search for its group reference fair utilization ratio,  $\alpha_{qi}^{ref}$ , as follows for the  $i$ th critical point:

$$\begin{cases} \dot{\alpha}_{q0}^{ref} = k_q(Q^{ref} - Q), & \text{To regulate reactive power flow,} \\ \dot{\alpha}_{qi}^{ref} = k_v(V_c^{ref} - V_{ci}), & \text{To regulate } i\text{th critical point,} \\ 1 \leq i \leq N_{CP}, \end{cases} \quad (2.17)$$

where  $V_c^{ref} = 1P.U$ ,  $Q^{ref} = 0$  and  $k_q$  and  $k_v$  are the controllers gains.

### *Closed Loop System Analysis*

The closed loop system for any microgrid of interest, can be expressed by substituting (2.12) in (2.6) as follows:

$$\dot{z}_i = k_c \left[ -z_i + d_{i0}z_0 + \sum_{j=1}^{N_{DG}} d_{ij}z_j \right],$$

where  $z_i = \alpha_{pi}$ , the fair utilization ratio of the  $i$ th inverter. As such, the overall dynamics of the microgrid system can be expressed as follows:

$$\dot{z}_0 = k_p \left[ P_{\mu}^{ref} - P_{\mu}(z_1, \dots, z_{N_{DG}}, X_p) \right], \quad (2.18)$$

$$\dot{z}_i = k_c \left[ -z_i + d_{i0}z_0 + \sum_{j=1}^{N_{DG}} d_{ij}z_j \right], \quad (2.19)$$

$$0 = g_p(P_1, \dots, P_{N_{DG}}, X_p), \quad (2.20)$$

where  $z_0 = \alpha_p^{ref}$  and (2.18) is a restatement of (2.15) for a desired microgrid. (2.20) is the power flow equation of the system. The stability of the closed loop system is proved based on the following lemma.

**Lemma 1.** *If  $A \in \mathbb{R}^{N_{DG} \times N_{DG}}$  is a row-stochastic, connected matrix and can be expressed as*

$$A = D + D_0,$$

*where  $D \in \mathbb{R}^{N_{DG} \times N_{DG}}$  and  $D_0 = \text{diag}\{d_{01}, d_{02}, \dots, d_{0N_{DG}}\}$  are non-negative, then*

*(i) matrix  $(D - I)$  is Hurwitz,*

*(ii) matrix  $(I - D)^{-1}$  exists and is non-negative.*

*proof:* For (i), a square matrix is called a Hurwitz matrix if all its eigenvalues have strictly negative real parts [45]. Toward that, since  $A$  is row-stochastic and connected, the spectral radius  $\rho(A)$  is equal to 1. Suppose that the eigenvalues of  $A$  are  $\lambda_1, \dots, \lambda_{N_{DG}}$ . Then, the eigenvalues of  $(I - A)$  are

$$1 - \lambda_1, \dots, 1 - \lambda_{N_{DG}}.$$

Hence, the eigenvalues of  $(I - A)$  are either zero or have positive real parts, and matrix  $(I - A)$  is called a singular M-matrix [38]. According to Corollary 4.33 in [38], matrix

$$I - A + D_0$$

is a non-singular M-matrix. Since

$$I - A + D_0 = I - D - D_0 + D_0 = I - D,$$

matrix  $(I - D)$  is a M-matrix. Therefore,  $(D - I)$  is Hurwitz.



For (ii), since  $(I - A)$  is a singular M-matrix, according to Theorem 4.27(c) in [38],

$$(I - A + D_0)^{-1} = (I - D)^{-1}$$

exists and is non-negative for positive diagonal matrix  $D_0$ . ■

**Theorem 2.** *For a microgrid system whose dynamics is given by (2.18)-(2.20), if the following conditions are satisfied*

- (1)  $k_p/k_c$  is sufficiently small,
- (2) Communication among the DGs are cumulatively connected (sequentially complete),
- (3)  $|\sin(\delta_i - \delta_j)| \ll |\cos(\delta_i - \delta_j)|$ ,

the system is asymptotically stable in the sense that  $z_i \rightarrow z_0$ .

*proof:* The equilibrium of the system (2.18) and (2.19) is obtained by setting the right hand side of them to zero, that is, in vector form,

$$0 = P_\mu^{ref} - P_\mu(z_1, \dots, z_{N_{DG}}, X_p), \quad (2.21)$$

$$0 = - \begin{bmatrix} z_1 \\ z_2 \\ \vdots \\ z_{N_{DG}} \end{bmatrix} + \begin{bmatrix} d_{10} \\ d_{20} \\ \vdots \\ d_{N_{DG}0} \end{bmatrix} z_0 + \begin{bmatrix} d_{11} & \cdots & d_{1N_{DG}} \\ \vdots & \ddots & \vdots \\ d_{N_{DG}1} & \cdots & d_{N_{DG}N_{DG}} \end{bmatrix} \begin{bmatrix} z_1 \\ z_2 \\ \vdots \\ z_{N_{DG}} \end{bmatrix}. \quad (2.22)$$

From (2.21), it is straight forward to obtain

$$P_\mu(z_1, \dots, z_{N_{DG}}) = P_\mu^{ref},$$

which gives the equilibrium of  $z_0$  denoted by  $z_0^*$ . From (2.22), if  $d_0 = \begin{bmatrix} d_{10} & d_{20} & \cdots & d_{N_{DG}0} \end{bmatrix}^T$  and  $D = [d_{ij}] \in \mathbb{R}^{N_{DG} \times N_{DG}}$  for  $i, j = 1, 2, \dots, N_{DG}$ , then (2.22) can be expressed as

$$(-I + D) \begin{bmatrix} z_1 \\ z_2 \\ \vdots \\ z_{N_{DG}} \end{bmatrix} + d_0 z_0 = 0. \quad (2.23)$$

Then, based on (2.13), one can verify the following relationship:

$$d_0 = (I - D)\mathbf{1}_{N_{DG}}, \quad (2.24)$$

where  $\mathbf{1}_{N_{DG}}$  is a  $N_{DG}$ -by-1 vector with all the elements being equal to 1. Substituting (2.24) into (2.23) yields

$$(-I + D) \left( \begin{bmatrix} z_1 \\ z_2 \\ \vdots \\ z_{N_{DG}} \end{bmatrix} - \begin{bmatrix} z_0 \\ z_0 \\ \vdots \\ z_0 \end{bmatrix} \right) = 0 \implies \begin{cases} z_1 = z_0 \\ z_2 = z_0 \\ \vdots \\ z_{N_{DG}} = z_0 \end{cases}.$$

Therefore, the equilibrium of the system is given by

$$\begin{cases} z_0 = z_0^* \\ z_1 = z_0^* \\ \vdots \\ z_{N_{DG}} = z_0^* \end{cases}.$$

Near the equilibrium, linearizing the system (2.21) and (2.22) yields

$$\begin{cases} \dot{z}_0 = -k_p \sum_{j=1}^{N_{DG}} e_j (z_j - z_0^*) \\ \dot{z}_i = k_c \left[ -z_i + d_{i0} z_0 + \sum_{j=1}^{N_{DG}} d_{ij} z_j \right] \end{cases}, \quad (2.25)$$

where

$$e_j = \left. \frac{\partial P_\mu}{\partial z_j} \right|_{z_j=z_0^*} > 0, \quad \forall j = 1, 2, \dots, N_{DG}.$$

The derivatives at the equilibrium is positive because in the microgrid,  $P_\mu$  increases as  $z_j$  increases.

Applying the following coordinate transformations

$$\begin{cases} x_0 = z_0 - z_0^* \\ x_1 = \begin{bmatrix} z_1 - z_0^* \\ z_2 - z_0^* \\ \vdots \\ z_{N_{DG}} - z_0^* \end{bmatrix} \end{cases}$$

and denoting  $\tau = k_c t$ , the linearized system (2.25) can be expressed as

$$\begin{bmatrix} \frac{dx_0}{d\tau} \\ \frac{dx_1}{d\tau} \end{bmatrix} = \begin{bmatrix} 0 & -\frac{k_p}{k_c} e^T \\ d_0 & D - I \end{bmatrix} \begin{bmatrix} x_0 \\ x_1 \end{bmatrix}, \quad (2.26)$$

where  $e = [e_1 \ \dots \ e_{N_{DG}}]^T$ . Since  $k_p/k_c$  is sufficiently small, the dynamics of  $x_1$  is much faster than that of  $x_0$ . According to the singular perturbation theory [46], if  $x_0$  would be constant, then  $x_1$  will

be asymptotically stable and converge to

$$x_1 = -(D - I)^{-1}d_0x_0, \quad (2.27)$$

since  $(D - I)$  is Hurwitz from (i) in Lemma 1. Substituting (2.27) to the dynamics of  $x_0$  in (2.26) yields

$$\frac{dx_0}{d\tau} = \frac{k_p}{k_c}e^T(D - I)^{-1}d_0x_0. \quad (2.28)$$

According to (ii) in lemma 1,  $(D - I)^{-1}$  is a non-positive matrix. Since  $\frac{k_p}{k_c}$ ,  $e^T$ , and  $d_0$  are all positive,  $\frac{k_p}{k_c}e^T(D - I)^{-1}d_0$  is negative. Hence,  $x_0$  is asymptotically stable and converge to 0. Therefore,  $z_i \rightarrow z_0$  for  $i = 1, 2, \dots, N_{DG}$ . ■

### Cooperative Control Nash Equilibrium

For the system

$$\dot{z}_i = k_c \left( w_i + d_{i0}z_0 + \sum_{j=1}^{N_{DG}} d_{ij}z_j \right) \quad i = 1, 2, \dots, N_{DG}; \quad (2.29)$$

the following theorem shows that

$$w_i = w_i^* = -z_i \quad i = 1, 2, \dots, N_{DG}; \quad (2.30)$$

form a Nash equilibrium with respect to certain performance indices.

**Theorem 3.** *If the system dynamics is given by (2.29), then  $w_i = w_i^*$  in (2.30) for  $i = 1, 2, \dots, N_{DG}$  form a Nash equilibrium with respect to the following performance indices*

$$J_i = \frac{1}{2} \sum_{j=1}^{N_{DG}} z_j^2(t_f) + \int_{t_0}^{t_f} \left[ q_i(z_0, z_1, \dots, z_{N_{DG}}) + \frac{k_c}{2} w_i^2 \right] dt \quad (2.31)$$

for  $i = 1, 2, \dots, n$ , where

$$q_i = \frac{k_c}{2} z_i^2 - \sum_{j=1}^{N_{DG}} k_c z_j^2 + \sum_{j=1}^{N_{DG}} k_c d_{j0} z_j z_0 + \sum_{j=1}^{N_{DG}} [k_c z_j (\sum_{k=1}^{N_{DG}} d_{jk} z_k)] \quad (2.32)$$

for  $i = 1, 2, \dots, n$ .

*Proof.* Consider the following Lyapunov functions

$$V = \frac{1}{2} \sum_{j=1}^{N_{DG}} z_j^2,$$

Differentiating  $V$  yields

$$\begin{aligned} \dot{V} &= \sum_{j=1}^{N_{DG}} z_j \dot{z}_j \\ &= \sum_{j=1}^{N_{DG}} \left[ k_c z_j \left( w_j - w_j^* - z_j + d_{j0} z_0 + \sum_{k=1}^{N_{DG}} d_{jk} z_k \right) \right] \\ &= \sum_{j=1, j \neq i}^{N_{DG}} [k_c z_j (w_j - w_j^*)] + k_c z_i (w_i - w_i^*) - \sum_{j=1}^{N_{DG}} k_c z_j^2 + \sum_{j=1}^{N_{DG}} k_c d_{j0} z_j z_0 + \sum_{j=1}^{N_{DG}} [k_c z_j (\sum_{k=1}^{N_{DG}} d_{jk} z_k)] \\ &= \sum_{j=1, j \neq i}^{N_{DG}} [k_c z_j (w_j - w_j^*)] + k_c z_i (w_i - w_i^*) - \sum_{j=1}^{N_{DG}} k_c z_j^2 + \sum_{j=1}^{N_{DG}} k_c d_{j0} z_j z_0 + \sum_{j=1}^{N_{DG}} [k_c z_j (\sum_{k=1}^{N_{DG}} d_{jk} z_k)] \\ &\quad + \frac{k_c}{2} (w_i - w_i^*)^2 - \frac{k_c}{2} (w_i - w_i^*)^2. \end{aligned} \quad (2.33)$$

Since

$$\begin{aligned} \frac{k_c}{2} (w_i - w_i^*)^2 &= \frac{k_c}{2} w_i^2 + \frac{k_c}{2} (w_i^*)^2 - k_c w_i w_i^* \\ &= \frac{k_c}{2} w_i^2 + \frac{k_c}{2} z_i^2 + k_c w_i z_i, \end{aligned} \quad (2.34)$$

substitute (2.34) into (2.33) yields

$$\begin{aligned}
\dot{V}_i &= \sum_{j=1, j \neq i}^{N_{DG}} [k_c z_j (w_j - w_j^*)] + k_c z_i (w_i - w_i^*) - \sum_{j=1}^{N_{DG}} k_c z_j^2 + \sum_{j=1}^{N_{DG}} k_c d_{j0} z_j z_0 + \sum_{j=1}^{N_{DG}} [k_c z_j (\sum_{k=1}^{N_{DG}} d_{jk} z_k)] \\
&\quad + \frac{k_c}{2} (w_i - w_i^*)^2 - \frac{k_c}{2} w_i^2 - \frac{k_c}{2} z_i^2 - k_c w_i z_i \\
&= \sum_{j=1, j \neq i}^{N_{DG}} [k_c z_j (w_j - w_j^*)] + \frac{k_c}{2} (w_i - w_i^*)^2 - \frac{k_c}{2} w_i^2 - q_i(z_0, z_1, \dots, z_{N_{DG}}),
\end{aligned}$$

where  $q_i$  is defined in (2.32). By integrating the above equation over  $[t_0, t_f]$  and using (2.31), we have

$$J_i = V_i(t_0) + \int_{t_0}^{t_f} \left[ \frac{k_c}{2} (w_i - w_i^*)^2 + \sum_{j=1, j \neq i}^{N_{DG}} k_c z_j (w_j - w_j^*) \right] dt. \quad (2.35)$$

Since equation (2.35) is applicable for all  $i = 1, 2, \dots, N_{DG}$ , we can conclude that

$$J_i(w_1^*, w_2^*, \dots, w_i^*, \dots, w_{N_{DG}}^*) \leq J_i(w_1^*, w_2^*, \dots, w_i, \dots, w_{N_{DG}}^*)$$

for all  $i = 1, 2, \dots, N_{DG}$ . Therefore,  $(w_1^*, w_2^*, \dots, w_{N_{DG}}^*)$  form a Nash equilibrium.  $\square$

**Remark 1.** According to the nature of Nash equilibrium, by suitably choosing  $k_c$ , performance index (2.31) can be assigned to each DG so that they have no choice but to stick to the Nash equilibrium.

## Simulation Results

A modified version of the bus system proposed by the IEEE 399-1997 standard is used to represent the microgrid case of study for simulations as shown in the figure 2.11. Simulations are performed using the Simpower System Toolbox of Simulink to demonstrate the performance of the single and multiple critical points voltage regulation controls. There are 5 feeders and 8 DGs are distributed

across the microgrid with a total of 12.5MVA generation capacity. The total load is 9.85KW + 4.17KVAR. Inverters connect to the microgrid at  $t = 0.4$ . Two asynchronous motors, each 300KVA,

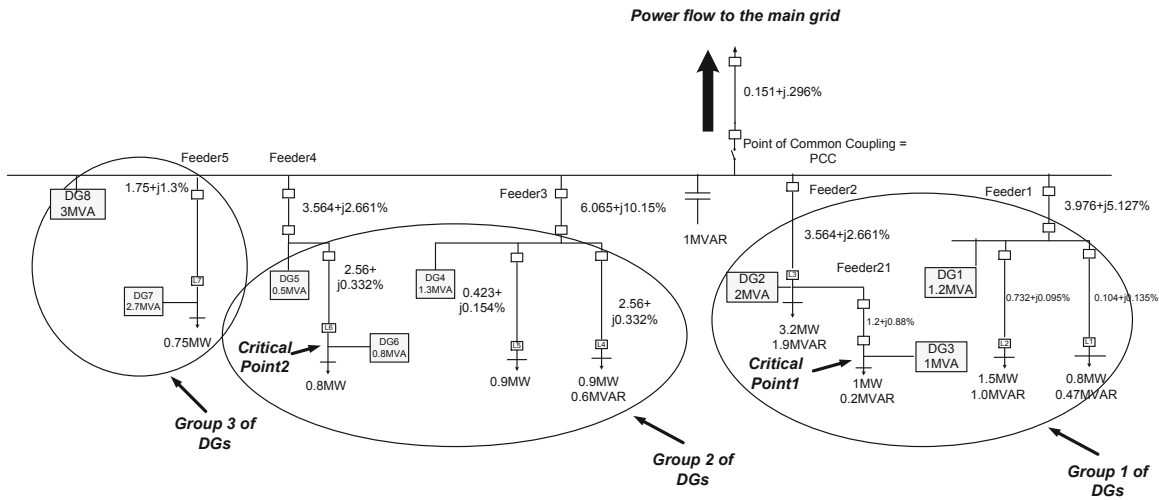


Figure 2.11: The system diagram of the case of study microgrid

connect to the first feeder at  $t = 4s$ . The startup of these motors causes voltage dip on the microgrid and this transient takes couple of seconds to be damped.

The objective is to keep the active power flow to the main grid constant at 5.85MW, minimize the reactive power flow to the grid, and secure a unified voltage profile across the microgrid.

For single critical point regulation, the end point of feeder2 is selected as the critical point. For multiple critical points regulation technique, end points of feeders2 and 4 are selected as the critical points and DG clusters are organized accordingly. DG3 and DG6 are connected to these points and as such, are the virtual leaders. DGs are clustered into three groups. DG1, DG2 and DG3 form group one, with DG3 as the virtual leader, to regulate critical point1. DG4, DG5 and DG6 form the second group with DG6 as the virtual leader to regulate the second critical point. DG7 and DG8 form the third group to minimize the reactive power flow to the main grid with DG8 as the virtual leader. DG8 is also the active power fair utilization ratio virtual leader to lead all the DGs

as a group, realize the active power objective. DGs in each group are managed by the cooperative control.

Simulation results are shown in figures 2.12-2.14b. Waveforms of DGs operation without reactive power generation are also included as a reference. Figures 2.12, 2.13a and 2.13b show voltages of PCC, critical point1 and critical point2 respectively. Figure 2.14a and figure 2.14b also show the active and reactive power flow to the main grid. It is seen that the single critical point regulation has resulted in the unity voltage at its critical point, but at the expense of increasing the voltage at other nodes and imposing a great deal of the reactive power flow to the main grid. Contradictorily, DG clustering (multiple critical point regulation), results in a fair voltage regulation of its critical points and PCC and at the same time, minimizes the reactive power flow to the main grid. The DG clustering also shows better dynamic response in damping the voltage transient, caused by the motors start up.

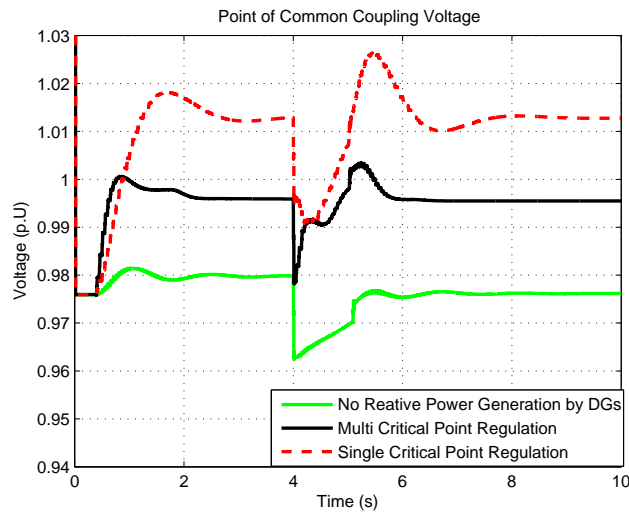
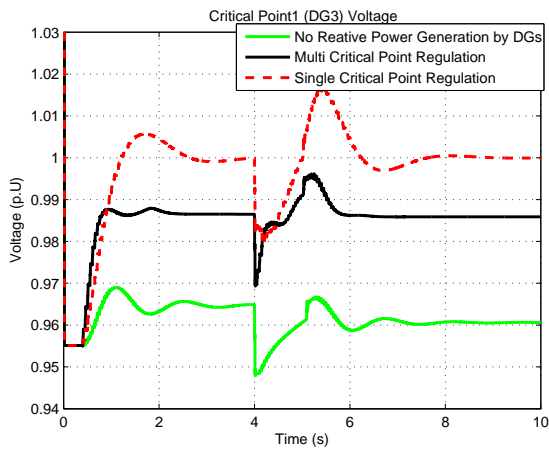
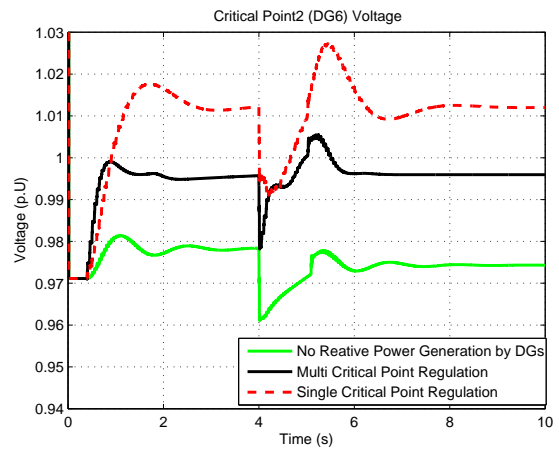


Figure 2.12: Point of common coupling (PCC) voltage



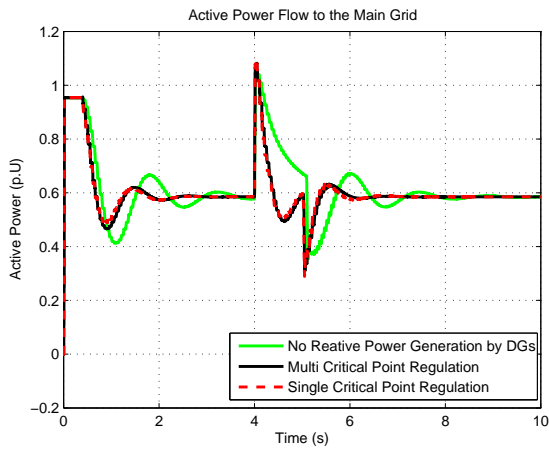


(a) Critical point1 voltage

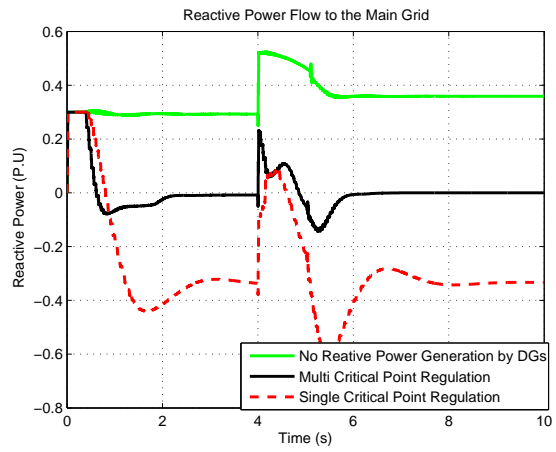


(b) Critical point2 voltage

Figure 2.13: Critical points voltages



(a) Main grid-microgrid active power flow



(b) Main grid-microgrid reactive power flow

Figure 2.14: Main grid-microgrid power flow

## Conclusion

In this chapter the application of the cooperative control to control DGs in a microgrid is investigated. Initially, the power objectives in a typical microgrid are discussed. The major power objectives of interest are proposed to be:

- Securing a desired active power flow from the main grid to the microgrid
- Minimizing the reactive power flow to the main grid
- Regulating some critical points voltages across the microgrid.

A brief introduction to the inverter dynamic model is presented. Then, the cooperative control law is provided based on the dynamics of the conventional three phase inverters. The closed loop system stability is investigated and proved. The simulated results show the efficiency of the proposed control in achieving the power objectives. It is also noticed that in terms of the reactive power control, clustering the DGs into several groups is more efficient than just having all the units regulate one critical point. One group of DGs may minimize the aggregated reactive power flow to the main grid and others regulate their respective critical points. Such a DG clustering shows improvement in realizing multiple power objectives in a typical microgrid.

## CHAPTER 3: COOPERATIVE DISTRIBUTED OPTIMIZATION

In any power system, it is always of especial interest to improve the voltage profile and minimize the losses. In the conventional power systems, this may be achieved by using under load tap change transformers (ULTC) or capacitor banks. Capacitor banks improve the voltage level by generating the reactive power. A typical ULTC and capacitor bank, installed in local power stations, are shown in the figure 3.1.



(a) A typical ULTC

(b) A typical capacitor bank

Figure 3.1: A typical ULTC and capacitor bank, installed in local power stations

Generally, voltage control of large magnitude is done by the means of OLTC and/or switches of capacitor banks. Such devices roughly regulate the node voltages to be within the ANSI standard limits,  $\pm 5\%$ . However, it is advantageous to take use of the DGs in improving the voltage quality. Once the voltages are adjusted to be close to unity by the OLTCs or capacitor banks, DGs can exert their finer controls to further regulate these voltages.

In this chapter, it is shown how the DGs reactive power generation capacity can be utilized to

further regulate voltages and achieve a more unified voltage profile. It is also shown that a unified voltage profile yields loss minimization. Furthermore, a unified voltage profile around the unity provides a larger safe zone for the voltage swing, which may be caused by any potential system disturbance.

From the perspective of the distribution generators, improving the system level voltage profile or loss minimization are global objectives. Therefore, an optimization technique should be distributed among the DGs and they all together, by their contribution, should realize such objectives. To this end, the application of the cooperative distributed optimization [47] to optimally dispatch the reactive power of DGs is introduced in this chapter. A global cost function is defined and DGs cooperatively try to minimize this cost function.

In a microgrid, there may be some critical nodes without a DG, but with the required measurement and communication modules installed. A method is introduced that enables such critical nodes also contribute in the optimization. A subgradient method is distributed among the modules. The subgradient method facilitates the application of the distributed optimization even when detailed system information are not known. The system active power loss is also formulated. It is shown that the unified voltage profile leads to the overall system active power loss minimization as well.

Two scenarios for the global cost function are considered. The first case is when the objective is to minimize the overall system voltage errors to realize a unified microgrid voltage profile. Stability analysis and criteria are also provided. As a further study, the case in which the overall active power loss is formulated as the global cost function is also provided. It is noticed that the latter not only is more complicated and difficult to implement, but neither yields any improvement upon the first case, as revealed by the simulations. Therefore, minimizing the overall system voltage error is recommended as the preferred cost function; which not only results in a unified voltage profile, but also results in the loss minimization.

The distributed optimization is further studied for the case the communication is down, or there is no communication available among the units. It is shown that the application of the gradient based optimization, takes the units to an adaptive droop, which improves the system dynamics. Even though this adaptive droop is reduced to a form of the conventional droop at steady state, but it improves the transient response significantly. Adaptive droop, which is a gradient based approach compared to the linear droop, eliminates the well known droop overshoots. This is well shown by the case of study system simulations, accompanied by the related analysis.

### Active Power Loss Analysis

The current flowing between two nodes,  $i$  and  $j$ , in a power system, is expressed as:

$$I_{ij} = (V_i \angle \theta_i - V_j \angle \theta_j)(G_{ij} + jB_{ij}).$$

The complex power over the line is:

$$\begin{aligned} S_{Loss_{ij}} &= (V_i \angle \theta_i - V_j \angle \theta_j) I_{ij}^*, \\ &= (V_i \angle \theta_i - V_j \angle \theta_j)(V_i \angle -\theta_i - V_j \angle -\theta_j)(G_{ij} - jB_{ij}), \\ &= (V_i^2 + V_j^2 - 2V_i V_j \cos(\theta_i - \theta_j))(G_{ij} - jB_{ij}), \end{aligned} \quad (3.1)$$

In the power systems, usually the phase difference between two adjacent nodes is close enough to approximate its cosine to be unity, i.e  $\cos(\theta_i - \theta_j) \simeq 1$ . Therefore, active power loss in the  $ij$  branch can be evaluated based on (3.1) as follows:

$$P_{Loss_{ij}} \simeq G_{ij}(V_i - V_j)^2. \quad (3.2)$$

Therefore, the system total losses follows to be:

$$P_{Loss} = \sum_{i=1}^{N-1} \sum_{j=i+1}^N G_{ij} (V_i - V_j)^2 \quad (3.3)$$

Equation (3.3) shows that the power losses of the system are proportional to the voltage differences among the adjacent nodes. As such, realizing a unified voltage profile across the microgrid will result in the loss minimizations as well.

### Cooperative Control based on the Distributed Optimization

The scenario in which the DGs cooperatively minimize a common additive cost function is considered here. Each agent has information only about one cost component, and minimizes that component, while exchanging information with the other units. In particular, the agents want to cooperatively solve the following optimization problem:

$$F^* = \min_{\alpha_q} \sum_{i=1}^N f_i, \quad (3.4)$$

where  $f_i$  are the DGs local cost function. The control variables are DGs reactive power fair utilization ratios. The optimal value of this problem,  $F^*$ , is achieved by an optimal solution set of  $\alpha_q^*$ ; i.e.:

$$\alpha_q^* = \{ \alpha_q \in [-1, 1]; \sum_{i=1}^N f_i = F^* \}. \quad (3.5)$$

In this setting, the information state of the  $i$ th DG, is an estimate of an optimal solution of the problem 3.4. The variable  $\alpha_{q_i}(k)$  is the estimate, maintained by the agent  $i$ , at the time  $t_k$ . When generating a new estimate, unit  $i$  combines its current estimate,  $\alpha_{q_i}$ , with the estimates received from some of the other units. In particular, unit  $i$  updates its estimates according to the following

relation:

$$\alpha_{q_i}(k+1) = \sum_{j=1}^N d_{ij} \alpha_{q_j}(k) - \beta_i g_i, \quad (3.6)$$

where  $d_{ij}$  is defined by (2.13),  $\beta_i > 0$  is a step size gain, used by the agent  $i$  and  $g_i = \frac{\partial f_{v_i}}{\partial \alpha_{q_i}}$  is a gradient of the  $i$ th DG objective function. If the detailed value of  $g_i$  cannot be calculated due to lack of the system information, a subgradient of it,  $g'_i$ , may be used instead.

A quantity  $g'_i$  is said to be a subgradient of  $f_i$  at  $\alpha_{q_i}^*$ , if for all  $-1 < \alpha_{q_i} < 1$

$$f_i(\alpha_{q_i}) \geq f_i(\alpha_{q_i}^*) + g'_i(\alpha_{q_i} - \alpha_{q_i}^*) \quad (3.7)$$

As such, if the detailed value of  $g_i$  is not available to the units, any approximation of  $g'_i$  to satisfy (3.7) may be used alternatively.

The choice of the cost functions,  $F^*$  and  $f_i$ , depend on the system objectives and requirements. On the rest of this section, two scenarios will be considered. One case is when realizing a unified voltage profile is the objective and the other one when minimizing the system active power loss is the objective.

### Realizing a Unified Voltage Profile as the Global Objective

In the chapter 2, it was shown how cooperative control can be used to organize DGs in a microgrid to satisfy multiple power objectives. Power objectives included regulating some critical points voltages. It was shown that multiple critical points regulation provides improvements compared with the single critical point regulation in terms of realizing a more unified voltage profile and less voltage fluctuation across the system.

The case in which each DG node is considered as a critical point is of interest. Trying to regulate all

DG nodes together will result in a more unified microgrid voltage profile. Cooperative distributed optimization is proposed to optimally dispatch the reactive power of the distributed generators (DGs). The objective is to minimize the global cost function, that is the sum of the quadratic voltage errors of all the DG nodes on the system. It is assumed that each DG, only knows its own local cost function, which is defined as the quadratic voltage error of its respective node. The method involves every DG, minimizing its own objective function, while exchanging information locally, with the other units on the network. Therefore, the cost function of (3.4) will be as follows:

$$F_v^* = \min_{\alpha_q} \sum_{i=1}^N f_{v_i}, \quad (3.8)$$

$$f_{v_i} = \frac{1}{2}(1 - V_i)^2.$$

To apply the cooperative control law of (3.6), the sub-gradients of  $f_{v_i}$  should be calculated. This is covered on the next sections.

#### *Calculation of the Units Sub-Gradient: Agents with DG installed*

In (3.6),  $g_i$  is the gradient (or a subgradient) of the  $i$ th unit, in respect to its state,  $\alpha_{q_i}$ . Considering equations (2.2) and (3.8), yields:

$$\begin{aligned} g_i &= \frac{\partial f_{v_i}}{\partial \alpha_{q_i}} \\ &= \frac{\partial f_{v_i}}{\partial V_i} \frac{\partial V_i}{\partial Q_i} \frac{\partial Q_i}{\partial \alpha_{q_i}} \\ &= -\overline{Q_i}(1 - V_i) \frac{\partial V_i}{\partial Q_i} \end{aligned} \quad (3.9)$$



The system power flow equations are expressed as follows:

$$\begin{cases} P_{G_i} - P_{D_i} = \sum_{j=1}^N V_i V_j [G_{ij} \cos \delta_{ij} + B_{ij} \sin \delta_{ij}] \\ Q_{G_i} - Q_{D_i} = \sum_{j=1}^N V_i V_j [G_{ij} \sin \delta_{ij} - B_{ij} \cos \delta_{ij}] \end{cases} \quad (3.10)$$

where  $\delta_{ij}$  is the phase difference between nodes  $i$  and  $j$ . Quantities  $B_{ij}$  and  $G_{ij}$  are the real and imaginary parts of the system  $Y$  bus matrix. Symbols  $P_{G_i}$ ,  $P_{D_i}$ ,  $Q_{G_i}$  and  $Q_{D_i}$  are the  $i$ th node active power generation, active power load, reactive power generation and reactive power load respectively.

The reactive power flow in (3.10) may be rewritten as follows:

$$\begin{aligned} Q_i &= Q_{G_i} - Q_{D_i} = \sum_j V_i V_j [G_{ij} \sin \delta_{ij} - B_{ij} \cos \delta_{ij}] \\ &= -V_i^2 B_{ii} + V_i \sum_{j \neq i} V_j [G_{ij} \sin \delta_{ij} - B_{ij} \cos \delta_{ij}], \end{aligned} \quad (3.11)$$

From (3.11), the required gradients can be derived, as follows:

$$\frac{\partial Q_i}{\partial V_i} = -2V_i B_{ii} + \sum_{j \neq i} V_j [G_{ij} \sin \delta_{ij} - B_{ij} \cos \delta_{ij}] \quad (3.12)$$

$$= -V_i B_{ii} + \frac{Q_i}{V_i}. \quad (3.13)$$

Hence, we have

$$\begin{aligned} g_i = \frac{\partial f_{V_i}}{\partial \alpha_{q_i}} &= -\bar{Q}_i (1 - V_i) \frac{\partial V_i}{\partial Q_i} \\ &= -\bar{Q}_i (1 - V_i) \frac{V_i}{Q_i - V_i^2 B_{ii}}. \end{aligned} \quad (3.14)$$

The (3.14) implies that the only system information needed is  $B_{ii}$ , that is the sum of the imaginary

parts of the line conductances, connecting node  $i$  to the neighboring nodes. However, if this information is not available to the DGs, a subgradient of (3.14),  $g'_i$ , may be used instead [47]. Usually, the range of the  $B_{ii}$  is known in a particular power system,  $B_{ii} \in [\underline{B}_{ii}, \overline{B}_{ii}]$ . Therefore, by definition, the subgradient of (3.14) is given by:

$$g'_i = \begin{cases} -\overline{Q}_i(1 - V_i) \frac{V_i}{Q_i - V_i^2 \overline{B}_{ii}}, & V_i \leq 1; \\ -\overline{Q}_i(1 - V_i) \frac{V_i}{Q_i - V_i^2 \underline{B}_{ii}}, & V_i > 1. \end{cases}$$

#### *Calculation of the Units Sub-Gradient: Agents without a DG Installed*

If there is no DG installed on a node, then the  $\overline{Q}_i$  of that node is zero. This makes the gradient/subgradient defined by (3.14) zero, and hence, such modules will not contribute into the optimization. For these nodes, the definition of the virtual leader as discussed in the section 2 is applied. Typically, a virtual leader tries to regulate the voltage of its respective node by utilizing all other units reactive power capacity.

For the cooperative distributed optimization discussed here, the same concept of a virtual leader may be applied to the nodes without a DG installed. That means they should utilize the other units reactive power generation to regulate their respective node. As such, the  $\overline{Q}_i$  in (3.14) will be replaced by the average of all the units available reactive power capacity.

As the optimization is being performed, units may utilize the same communication links to find the average of all units available reactive power capacity as well. Every unit tries to keep the track of the average by a state,  $x_i$ . The initial value of  $x_i$  is the units available reactive power. Units update their states, according to the following cooperative law:

$$x_i(k+1) = \sum_{j=1}^N d'_{ij} x_j \quad (3.15)$$

$d'_{ij} = 0$ , provided that  $s_{ij} = 0$ . Similar to  $D = [d_{ij}]$  matrix, defined by (2.13),  $D' = [d'_{ij}]$ . However,  $D'$  should be designed to be double stochastic [38]. That is:

$$\begin{cases} D'\mathbf{1} = \mathbf{1}, \\ \mathbf{1}^T D' = \mathbf{1}^T. \end{cases}$$

where  $\mathbf{1}$  is a  $N \times 1$  vector, with all elements equal to one. For instance, the  $D'$  matrix associated with the communication topology shown in figure the 3.2 may be designed as follows:

$$D' = \begin{bmatrix} \frac{2}{3} & \frac{1}{3} & 0 \\ \frac{1}{3} & \frac{1}{3} & \frac{1}{3} \\ 0 & \frac{1}{3} & \frac{2}{3} \end{bmatrix}$$

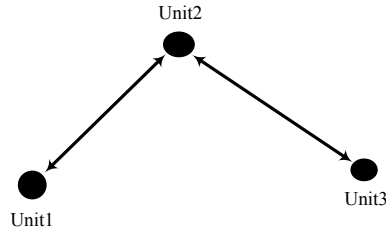


Figure 3.2: A simple, three node communication topology

Following the law in (3.15), results in all the states,  $x_i$ , converge to the desired value:

$$x_i \rightarrow \frac{1}{N} \sum_{j=1}^N \bar{Q}_i.$$

Hence, the gradient term of (3.14) for such units is formulated as follows:

$$g_i = -x_i(1 - V_i) \frac{V_i}{Q_i - V_i^2 B_{ii}},$$

where  $x_i$  was formulated in (3.15).

The detailed system stability and analysis is provided in the appendix D.

### *Choosing the Gradient Gains, $\beta$*

The  $\beta$  gains in (3.6) should be chosen in such a way to give the best performance. Heuristically, small gains will slow down the pace of the distributed optimization; and on the other hand, large gains tend to introduce overshoots that induce oscillations, and even may cause system instability on extremes.

Theorem 4 of the appendix D shows that for a particular power system, there exists a range of the  $\beta$ , which secures the system stability. This theorem may be used to numerically calculate the desired  $\beta$  gains, or equivalently, a best choice of  $\beta$  may be found out by running the simulations.

### Minimizing the Active Power Losses as the Global Objective

To minimize the system active power losses, the cost function to minimize will be the  $P_{Loss}$  in (3.3) which is repeated here:

$$P_{Loss} = \sum_{i=1}^{N-1} \sum_{j=i+1}^N G_{ij} (V_i - V_j)^2$$

The local cost function of a unit  $k$ , may be defined as the sum of the power losses in the lines, connected to module  $k$ :

$$P_{Loss_k} = \sum_{i=1, i \neq k}^N G_{ki} (V_k - V_i)^2.$$

The gradient of  $P_{Loss_k}$  may be calculated as follows:

$$\begin{aligned} g_k &= \frac{\partial P_{Loss_k}}{\partial \alpha_{qk}} = \frac{\partial P_{Loss_k}}{\partial V_k} \frac{\partial V_k}{\partial Q_k} \frac{\partial Q_k}{\partial \alpha_{qk}}, \\ &= \left[ \sum_{i=1, i \neq k}^N 2G_{ki} (V_k - V_i) \right] \frac{\partial V_k}{\partial Q_k} \overline{Q_k}. \end{aligned} \quad (3.16)$$

$\frac{\partial V_k}{\partial Q_k}$  is denoted by (3.12). Then, the same cooperative law of (3.6) may be used to cooperatively minimize the losses. Comparing (3.16) and (3.14) shows that the loss minimization demands much more system information compared with the realizing the unified voltage profile. The performance of these two techniques will be compared by the simulations.

### Single Units Applying Optimization: Gradient based Droop

It is of interest to study the proposed optimization technique, in case the communication is not available. In this case, units will utilize just their own local measurement and apply the control law. In such a case, the control law of (3.6) will reduce to the following form for a particular DG:

$$\alpha_{q_i}(k+1) - \alpha_{q_i}(k) = \beta_i \left[ \overline{Q}_i \frac{V_i}{Q_i - V_i^2 B_{ii}} \right] (1 - V_i), \quad (3.17)$$

where  $g_i$  is replaced with its relation from (3.14).

Using the assumptions of  $V_i \simeq 1$  and  $|Q_i| \ll |B_{ii}|$ , (3.17) may be simplified as:

$$\alpha_{q_i}(k+1) - \alpha_{q_i}(k) = \beta_i \frac{\bar{Q}_i}{-B_{ii}} (1 - V_i), \quad (3.18)$$

Equation (3.18) has an integrator form and will cause the  $\alpha_{q_i}$  to saturate. This is also noticed by applying the control law of (3.18) on the system in the figure 3.4. The figure 3.3 shows the voltages and utilization ratios of  $DG_3$  and  $DG_6$  in this case. The  $\alpha_q$  saturation is clear and the voltage profiles are somehow distorted.

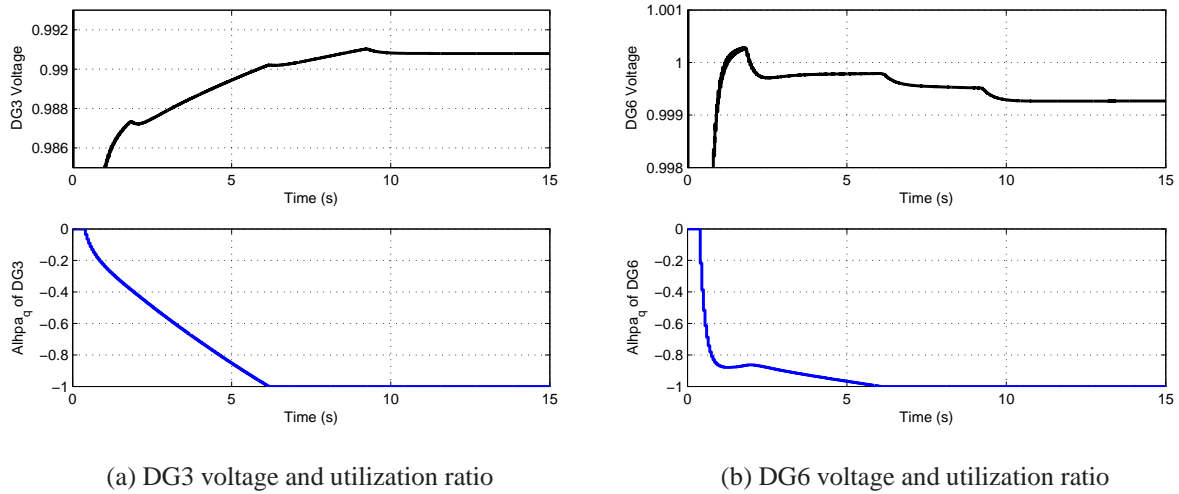


Figure 3.3: Saturation effect of the single unit optimization application

In a control system, when the parameters are time varying, the old data are not representative of the process as much as the recent data. Therefore, it is desirable to base the identification on the most recent data. As such, and as a well known rule in the adaptive control [48], a forgetting factor should scale down the old data. This prevents the aforementioned saturation. To this end,

the control law of (3.18) may be rewritten as follows:

$$\alpha_{q_i}(k+1) - \gamma\alpha_{q_i}(k) = \beta_i \frac{\bar{Q}_i}{-B_{ii}} (1 - V_i), \quad (3.19)$$

where  $\gamma$  is chosen as the forgetting factor. Typically, forgetting factor is a value between zero and one. It should not be too close to one, to neutralize its effect and not too small, to negatively affect the control law. A typical value of  $\gamma = 0.95$  is chosen for this case.

As  $B_{ii}$  is a negative quantity, the final rule may be written as:

$$\alpha_{q_i}(k+1) = \gamma\alpha_{q_i}(k) + k_{a_i}(1 - V_i). \quad (3.20)$$

where:

$$K_{a_i} = \beta_i \frac{\bar{Q}_i}{|B_{ii}|} > 0$$

The conventional droop equivalent control law is as follows:

$$\alpha_{q_i}(k) - \alpha_{q_i}^{ref} = k_v(1 - V_i), \quad (3.21)$$

where  $\alpha_{q_i}^{ref}$  may be chosen to be zero in this case.

The similarities between (3.20) and (3.21) are eminent. However, the main difference is that (3.20) is a gradient based approach, while (3.21) is a linear relation.

The control rule of (3.20) is reduced to a form of the conventional droop at steady state. At steady state,  $\alpha_{q_i}(k+1) = \alpha_{q_i}(k)$  and therefore:

$$\begin{aligned}
(1 - \gamma)\alpha_{q_i} &= k_{a_i}(1 - V_i), \\
\alpha_{q_i} &= \frac{k_{a_i}}{(1 - \gamma)}(1 - V_i).
\end{aligned} \tag{3.22}$$

The main advantage of this gradient based droop is the improvement of the transient response. In the next section, it is shown that it eliminates the overshoots that the conventional droop usually exhibits. This is further justified by the simulation results.

### *Analysis*

The control rule of (3.20) may be written in the matrix form as follows:

$$\alpha_q(k+1) = \gamma\alpha_q(k) + K_a(\mathbf{1} - V) \tag{3.23}$$

where  $\alpha_q = [\alpha_1, \dots, \alpha_N]^T$ ,  $K_a = \text{diag}[K_{a_1}, \dots, K_{a_N}]$ ,  $\mathbf{1}$  is a  $N \times 1$  vector with all elements equal to 1 and  $N$  is the number of the available modules.

Substituting  $V$  from the linearized power flow equation, (D.5), provides the following:

$$\alpha_q(k+1) = [\gamma I - K_a H_{12}] \alpha_q(k) - K_a [\mathbf{1} + H_{12} \alpha_q^* - V^* - H_{11}(P - P^*)]. \tag{3.24}$$

The continuous time equivalent of (3.24) may be derived as follows:



$$\frac{\alpha_q(k+1) - \alpha_q(k)}{T} = \frac{1}{T} [-I + \gamma I - K_a H_{12}] \alpha_q(k) - \frac{1}{T} K_a [\mathbf{1} + H_{12} \alpha_q^* - V^* - H_{11}(P - P^*)],$$

$$\dot{\alpha}_q = k_c [-I + \gamma I - K_a H_{12}] \alpha_q - k_c K_a [\mathbf{1} + H_{12} \alpha_q^* - V^* - H_{11}(P - P^*)],$$

where  $k_c = \frac{1}{T}$  and  $T$  is the time interval between two consecutive iterations. Therefore, the system dynamics depend on the state matrix:

$$A = k_c [(\gamma - 1)I - K_a H_{12}] \quad (3.25)$$

In this regard, the difference between the gradient based droop and the conventional droop is:

- For droop,  $\gamma = 0$ , for the gradient based droop  $\gamma = 0.95$
- for the gradient based droop,  $K_a = \text{diag}[K_{a_1}, \dots, K_{a_n}]$ . However, for the droop,  $K_a$  should be replaced by the scalar gain of  $K_v$ .

Detailed analysis of a nonlinear system for studying the transient response and the overshoot, if not impossible, is very difficult. As such, the transient response analysis here is performed for the case of study microgrid shown in the figure 3.4 and the simulations of the section 3.

For the case of study microgrid of figure 3.4,  $H_{12}$  is derived as follows:

Table 3.1: Case of study microgrid  $H_{12}$

|        |        |        |        |        |        |
|--------|--------|--------|--------|--------|--------|
| 0.0522 | 0.0044 | 0.0022 | 0.0031 | 0.0012 | 0.0019 |
| 0.0026 | 0.0435 | 0.0218 | 0.0028 | 0.0011 | 0.0017 |
| 0.0025 | 0.0424 | 0.0282 | 0.0028 | 0.0011 | 0.0017 |
| 0.0028 | 0.0043 | 0.0022 | 0.1085 | 0.0012 | 0.0019 |
| 0.0028 | 0.0044 | 0.0022 | 0.0031 | 0.0118 | 0.0189 |
| 0.0028 | 0.0044 | 0.0022 | 0.0031 | 0.0118 | 0.0210 |

For a choice of  $k_c = 1$  and based on the  $H_{12}$  provided by the Table (3.1), the state matrix of (3.25) can be calculated. The state matrix for the gradient based droop is as follows:

Table 3.2: State matrix of the gradient based droop

|         |         |         |         |         |         |
|---------|---------|---------|---------|---------|---------|
| -0.0545 | -0.0004 | -0.0002 | -0.0003 | -0.0001 | -0.0002 |
| -0.0000 | -0.0505 | -0.0003 | -0.0000 | -0.0000 | -0.0000 |
| -0.0001 | -0.0013 | -0.0509 | -0.0001 | -0.0000 | -0.0001 |
| -0.0004 | -0.0006 | -0.0003 | -0.0642 | -0.0002 | -0.0002 |
| -0.0004 | -0.0006 | -0.0003 | -0.0004 | -0.0517 | -0.0027 |
| -0.0011 | -0.0017 | -0.0008 | -0.0012 | -0.0046 | -0.0581 |

The conventional droop is designed to release the maximum available reactive power on the maximum voltage deviation,  $\pm 5\%$ . Therefore,  $K_v = 20$  is chosen and the state matrix is derived as follows:

Table 3.3: State matrix of the conventional droop

|         |         |         |         |         |         |
|---------|---------|---------|---------|---------|---------|
| -3.0860 | -0.1743 | -0.0871 | -0.1222 | -0.0470 | -0.0753 |
| -0.1046 | -2.7408 | -0.8703 | -0.1131 | -0.0435 | -0.0696 |
| -0.1018 | -1.6948 | -2.1293 | -0.1101 | -0.0424 | -0.0678 |
| -0.1128 | -0.1740 | -0.0870 | -5.3381 | -0.0469 | -0.0751 |
| -0.1129 | -0.1741 | -0.0870 | -0.1220 | -1.4726 | -0.7562 |
| -0.1129 | -0.1741 | -0.0870 | -0.1220 | -0.4726 | -1.8412 |

Even though, most of the properties of the linear systems may be derived by studying the eigenvalues of their state matrixes, for the non-linear systems, the study of the Lyapunov matrix,  $P$ , is preferred. The ratio of the maximum to the minimum eigenvalue of  $P$  is an indication of the potential system overshoots [38]. The Lyapunov matrix is the solution to the following Lyapunov equation:

$$PA + AP = -I,$$

where  $A$  is the system state matrix and  $I$  is the unity matrix. Based on the previously derived state matrixes, the Lyapunov matrixes may be derived as follows:

Table 3.4: Lyapunov matrix derived for the gradient based droop

|         |         |         |         |         |         |
|---------|---------|---------|---------|---------|---------|
| 9.1792  | -0.0317 | -0.0219 | -0.0425 | -0.0359 | -0.0931 |
| -0.0317 | 9.9071  | -0.1525 | -0.0379 | -0.0450 | -0.1288 |
| -0.0219 | -0.1525 | 9.8264  | -0.0249 | -0.0249 | -0.0681 |
| -0.0425 | -0.0379 | -0.0249 | 7.7848  | -0.0375 | -0.0954 |
| -0.0359 | -0.0450 | -0.0249 | -0.0375 | 9.7210  | -0.6012 |
| -0.0931 | -0.1288 | -0.0681 | -0.0954 | -0.6012 | 8.6331  |

The eigenvalues of this matrix are:

$$[7.7621, 8.3583, 9.1911, 9.7247, 9.9873, 10.0281] \quad (3.26)$$

Table 3.5: Lyapunov matrix derived for the conventional droop

|         |         |         |         |         |         |
|---------|---------|---------|---------|---------|---------|
| 0.1629  | -0.0052 | -0.0041 | -0.0032 | -0.0068 | -0.0054 |
| -0.0052 | 0.2781  | -0.1523 | -0.0028 | -0.0085 | -0.0059 |
| -0.0041 | -0.1523 | 0.2977  | -0.0025 | -0.0047 | -0.0041 |
| -0.0032 | -0.0028 | -0.0025 | 0.0940  | -0.0045 | -0.0035 |
| -0.0068 | -0.0085 | -0.0047 | -0.0045 | 0.3831  | -0.1333 |
| -0.0054 | -0.0059 | -0.0041 | -0.0035 | -0.1333 | 0.3270  |

The eigenvalues of this matrix are:

$$[0.0931, 0.1324, 0.1639, 0.2215, 0.4406, 0.4913] \quad (3.27)$$

The eigenvalues of (3.26) and (3.27) provide a maximum to minimum eigenvalue ratio of 1.2919 and 5.2786 for the gradient based droop and the conventional droop, respectively. This proves a great transient response improvement and less overshoots gained by the gradient based droop, compared to the conventional droop.

### Simulation Results

To run the simulations, a modified version of the bus system proposed by the IEEE 399-1997 standard is used to represent the microgrid case of study, as shown in figure 3.4. Simulations are performed using the Simpower System Toolbox of Simulink. Main grid is 69KV and the microgrid

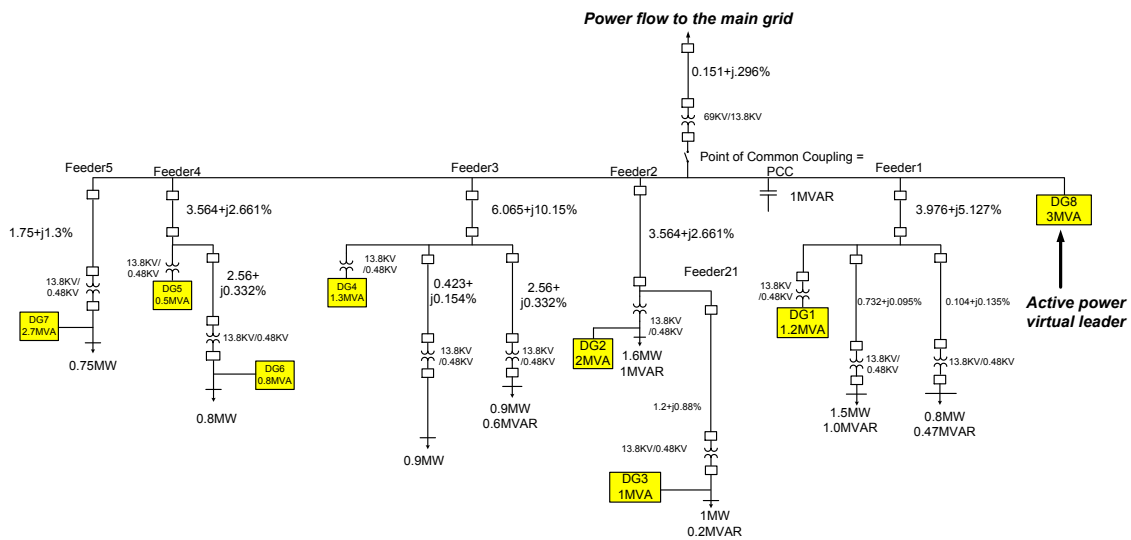


Figure 3.4: The system diagram of the case of study microgrid

consists of five 13.8KV distribution feeders. Eight DGs are distributed across the microgrid with a total of 15.5MVA generation capacity. The total load is 8.25MW + 2.27MVAR. Loads and DGs operate on a lower voltage of 430V.

### *Simulations of the cooperative distributed optimization*

Simulations are performed for the time period of 9:00 A.M up to 6:00 P.M. DG profiles are provided in figure 3.5. *DG2,3,4* are wind farms and *DG1,5,6,7,8* are solar farms. The weather effect and sun radiation intermittencies are considered in these profiles.

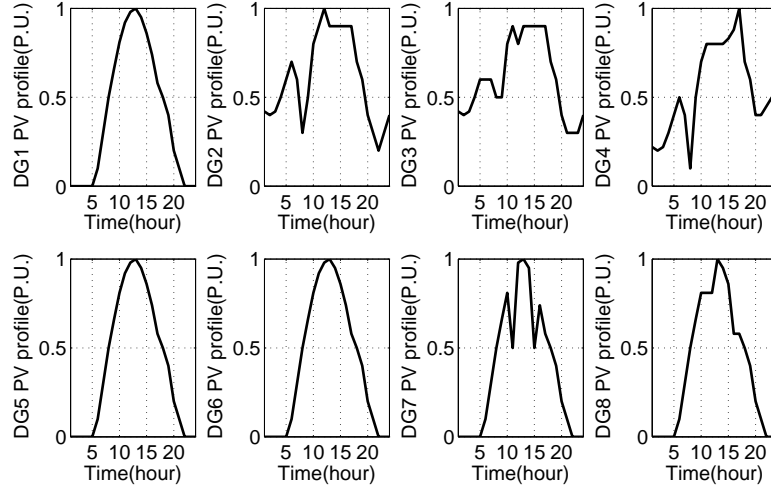


Figure 3.5: PV profile of DGs

Three different microgrid inverter control schemes, droop, multiple critical points voltage regulation, and the cooperative distributed optimization, proposed in this chapter, are evaluated. The performance of these controllers in realizing the microgrid power objectives are compared.

In droop, every DG just regulates its grid coupling point voltage and frequency. Other two techniques, utilize communication links and the cooperative control. Their active power flow objective is to regulate the power flow from the main grid at 2.5MW. DG8, is their active power virtual leader. For the reactive power control, DGs are controlled as follows: In multiple critical points regulation, DGs are clustered into three groups. First group, consisting of DGs 7,8, minimizes the reactive power flow to the main grid. Second group, DGs 1,2,3, regulate the DG3 voltage, as a

critical point. The third group, DGs 4,5,6, regulate the other critical point, DG6. In the cooperative distributed optimization, similar to the multiple critical points regulation, DGs 7,8 minimize the aggregated reactive power flow to the main grid. All other DGs participate in the distributed optimization to cooperatively minimize the sum of their nodes voltage error, which is expressed by the following cost function:

$$F_v = \sum_{i=1}^6 \frac{1}{2} (1 - V_i)^2$$

Simulation results are provided in Figs. 3.6-3.10. Figure 3.6 shows the system cost function,  $F_v$ . It is seen that the droop achieves the highest value of the cost function, while the cooperative distributed optimization has well minimized it, and as such, has realized the most unified voltage profile.

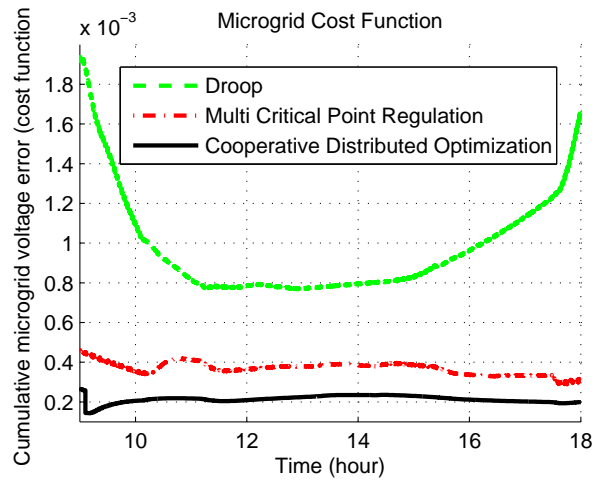


Figure 3.6: Global cost function of the microgrid,  $F_v$

Figure 3.7 shows the active power flow from the main grid to the microgrid. Despite the intermitencies, the cooperative controls have succeeded in regulating the active power flow at the desired level of  $2.5MW$ . Droop has no control over the aggregated active power flow.

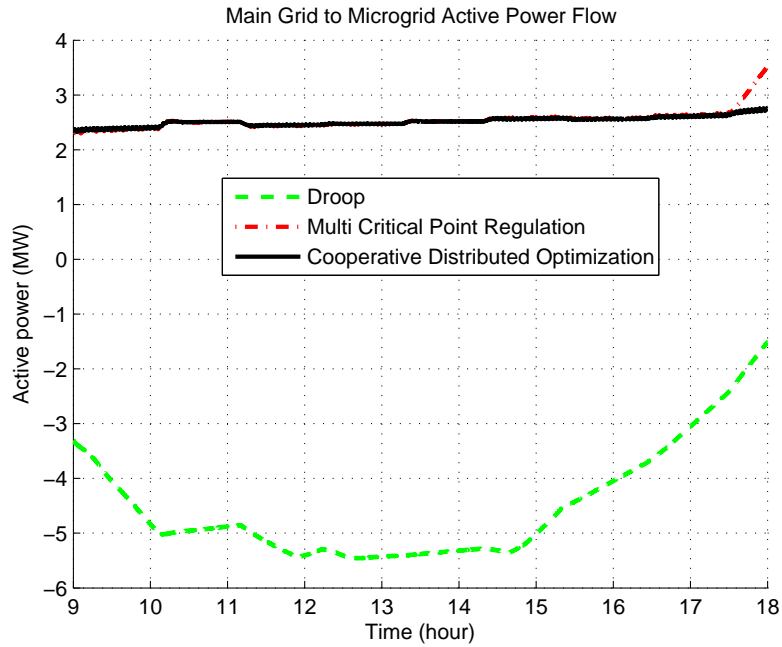


Figure 3.7: Main grid to the microgrid active power flow

Figure 3.8 shows the main grid reactive power flow to the microgrid. It is clear that droop has induced a high reactive power to the main grid, while cooperative control techniques successfully have minimized it, despite the intermittencies.



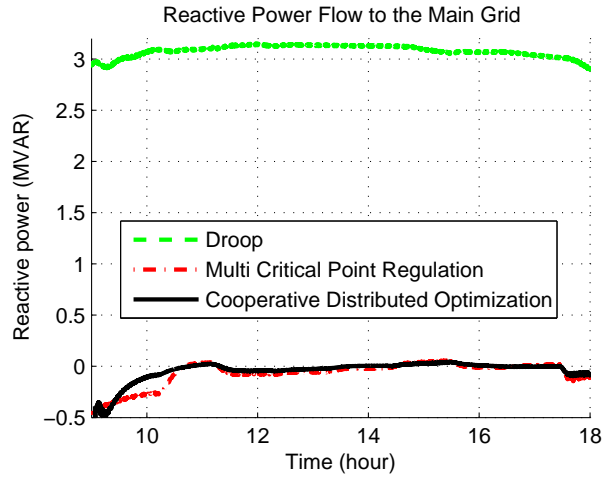


Figure 3.8: Main grid reactive power flow to the microgrid

Figure 3.9 shows the system active power losses. The cooperative distributed optimization has realized the minimum losses and the droop has led to the highest loss. This certifies the previous discussion that a more unified voltage profile results in a lower active power loss.

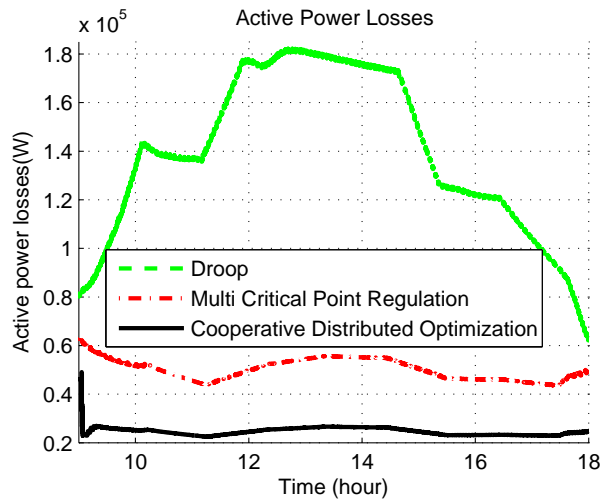
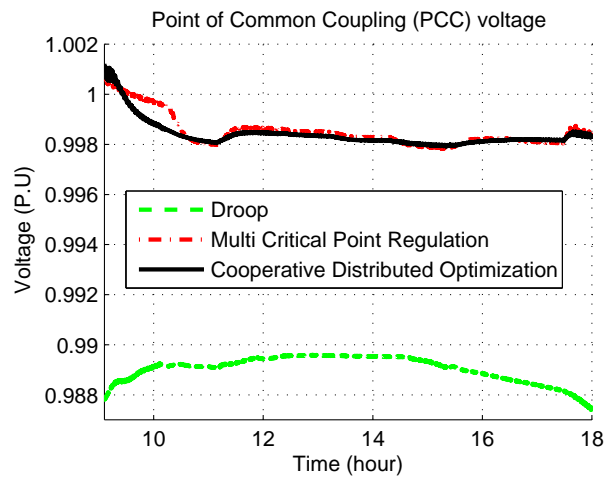


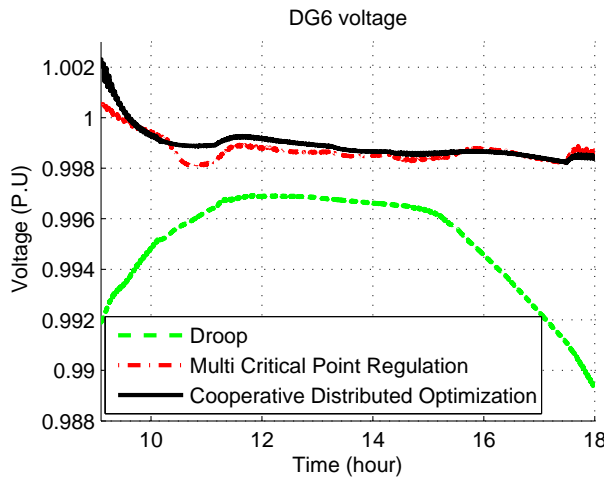
Figure 3.9: Microgrid active power loss

Figure 3.10 shows the voltages at two different system nodes, point of common coupling (PCC)

and DG6 terminals. This figure illustrates how cooperative distributed optimization has maintained a unified voltage profile, close to unity, across the microgrid. Also it is notable that this technique well regulates the voltages despite the daily intermittencies. Other point learned from this figure is that droop fails to keep the voltage at different nodes as close. That means a non-unified voltage profile, as already was shown by figure 3.6. Also the sun radiation intermittencies have caused major voltage fluctuations, when DGs are controlled by the droop.



(a) Voltage of point of common coupling



(b) voltage of DG6

Figure 3.10: Voltages of DG6 and point of common coupling

The simulations regarding the microgrid active power loss minimization are shown in figures 3.11 and 3.12. It is noticed that the performances of the two techniques are comparable and close. However, figure 3.11 shows that the loss minimization technique has not resulted in less active power losses compared with the unified voltage approach. Figure 3.12 also shows that the performance of the two techniques are comparable in minimizing the overall voltage deviations from unity. however, unified voltage profile technique has shown being more consistent despite the PV intermittencies.

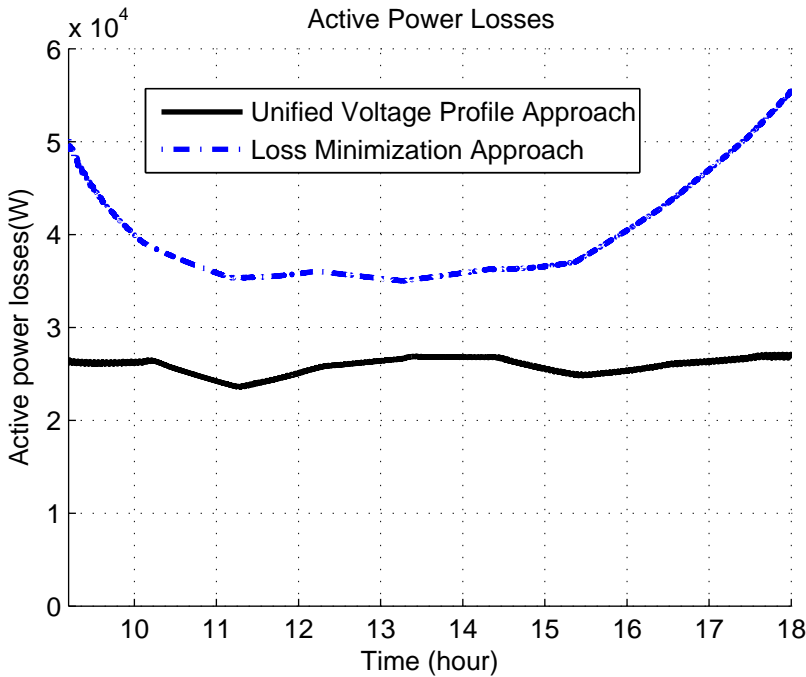


Figure 3.11: Comparing the microgrid active power loss for loss minimization and unified voltage profile techniques

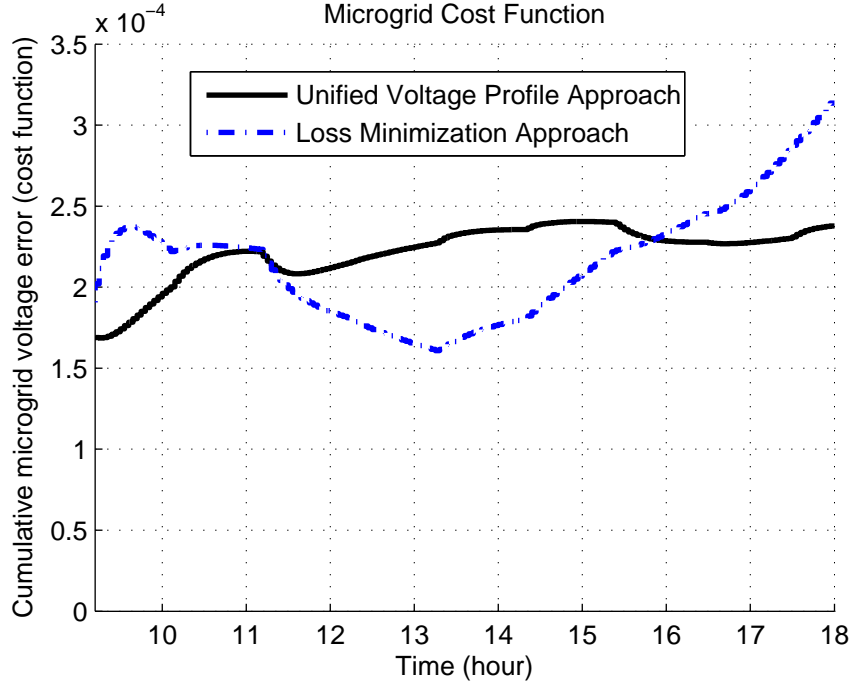


Figure 3.12: Comparing the microgrid global cost function ,  $F_v$ , for loss minimization and unified voltage profile techniques

### *Simulations of the Gradient based Droop*

For comparing the performance of the gradient based droop, discussed on the section 3, and the conventional droop, the same microgrid structure of figure 3.4 is used. It is assumed that the full active power is available to units and the active power fair utilization ratio reference,  $\alpha_p^{ref}$ , is set to be 0.6.

Figure 3.13 shows the  $\alpha_q$  and voltage waveforms of the  $DG_1$ . The huge oscillations and the overshoots are noticed for the conventional droop, while the gradient based droop fairly has suppressed such overshoots and oscillations.

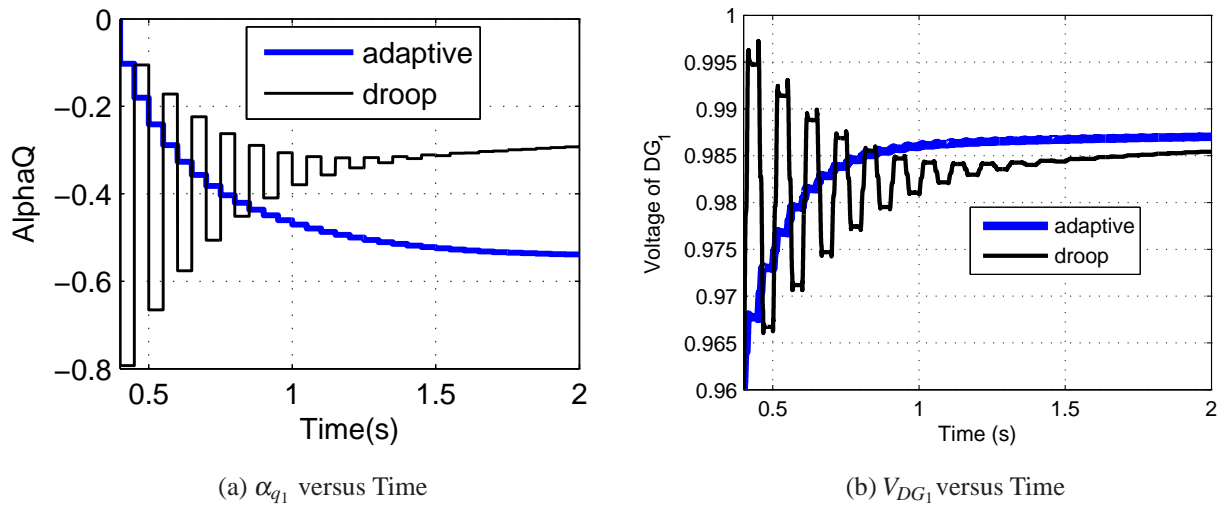


Figure 3.13: Voltage and  $\alpha_q$  waveforms of  $DG_1$

Figure 3.14 shows the  $\alpha_q$  and voltage trajectory for the  $DG_1$ . It is seen that the gradient based droop directly converges to the final value, while for the conventional droop, the trajectory is a spinal waveform that finally converges to the final value. This depicts the extreme oscillation and overshoot, associated with the conventional droop.

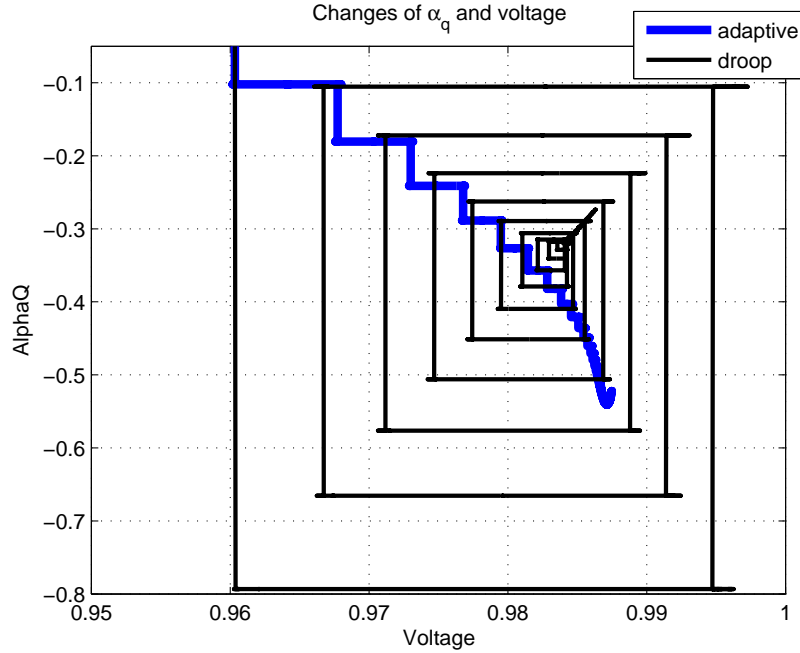


Figure 3.14: Trajectory of  $\alpha_{q1}$  and  $V_1$

### Conclusion

In this chapter, the application of the cooperative distributed optimization to optimally dispatch the reactive power generation of DGs in a microgrid is investigated. In a large scale microgrid, there may be some critical nodes without a DG installed, but with the required measurements and communication modules available. A method also is provided to facilitate the contribution of such nodes in the optimization process. The system active power losses are formulated and it is shown that how a unified voltage profile results in a lower loss minimization as well.

Two different global system objectives have been evaluated as the minimization cost function. One approach is minimizing the overall system quadratic voltage errors from unity, to realize a unified voltage profile. It is expected that a unified voltage profile also results in the loss minimization, as

well. The stability and the convergence analysis are provided.

The only system information required to implement this technique is an approximation of the line conductances, connecting DG nodes together. However, it is shown that the application of the subgradient technique makes it possible to use this method, even when such detailed information is not available. The simulation results applied over a typical microgrid are provided. It is shown that even despite the daily PV intermittencies, this technique realizes a unified microgrid voltage profile and lower losses and is superior compared with the state of the art microgrid inverter controls.

The other evaluated objective is minimizing the system active power losses as the primary objective. It is shown that not only this requires a great deal of the system information, but does not result in a better performance in terms of the loss minimization and an improved voltage profile either. Therefore, using the voltage error minimization is advised as a practical choice.

The performance of this optimization, in case the communication is not available among the DGs, is also scrutinized. In this case, every module only has access to its own information and local measurements. Applying the optimization in this case, results in a gradient based droop, which improves the transient response of the conventional droop in a great deal. The simulation results and the related analysis show how the proposed gradient based droop suppresses the overshoots, associated with the conventional droop control.

## CHAPTER 4: MAIN GRID-MICROGRIDS INTERACTION MANAGEMENT

A proper interaction between the microgrid and the main grid is an important aspect of the smart grid. A microgrid should look as a dispatchable load to the main grid. A proper smart grid control is expected to utilize the DGs and their related storage devices in such a way to both, optimize the overall system profit and also improve the power flow. In [40] it was shown how cooperative control may be applied to organize DGs in a microgrid and secure a desired upstream power flow to the main grid. However, this technique may be applied once the desired power flow is known. As such, another high level controller should be devised to properly search and come up with the most suitable power flow from the microgrid to the main grid. The desired power flow may be calculated based on the following constraints:

- (i) Both the microgrid and the main grid should be able to optimize their profit or minimize their cost.
- (ii) Improvement in the main grid daily generated power is an objective. It is desired to have less power fluctuations, which incur high stress and cost to the generators. To this end, the main grid generated power profile should be as smooth as possible. This means that the microgrids should assist the main grid to shave its power peak. To this end, microgrid may charge its storages when there is less power demand and release energy during peak hours.

The above requirements can be met by modeling the main grid-microgrid interaction as a game [49]. Game theory is briefly introduced in Appendix A. In terms of the conventional electric market, some of the previous works utilize different game theoretic approaches to deal with the optimal bidding strategy for the generating company, optimal load pricing, and reserve management prob-



lem. Towards this end, [50, 51, 52, 53, 54] focus on the Nash game, and [55, 56, 57, 58] focus on the Stackelberg game. In terms of future smart grid, [59] provided a demand-side management based on consumption scheduling game to optimize the energy cost and balance the load, and [60] analyzed the smart grid management with multiple intelligent players. However, the interaction between the main grid and the microgrid is an important aspect of the smart grid, which has not been fully considered using a game theoretic approach.

In this work, the main grid-microgrid interaction is modeled as a Stackelberg game. Specifically, by offering proper energy price to the microgrid, the main grid as the leader, can minimize its cost function and secure the power supply that microgrids, as the follower, are willing to dispatch. Once receiving the offered price from the main grid, microgrids decide what percentage of the available power to dispatch and how much to store. It is shown that this technique not only is helpful in terms of optimizing the cost functions, but also helps a proper power flow from the microgrid to the main grid to reduce load stresses and shave the power peak.

Introduction of the storage devices, makes some modifications to the microgrid variables defined on the Chapter 2 necessary. Next section provides the needed modifications.

### Redefining Some Microgrid Variables

In order to improve the performance of microgrids, such as flexibility and reliability, energy storages (batteries, super capacitors, etc.) will be available and bundled with DGs. As such, the available active power on the microgrid consists of both, stored and renewable energy.

To include the effect of storage devices, some of the variables defined on the Chapter 2 need to be modified. For instance, the maximum available active power of the  $i$ th inverter includes both, the

available renewable and the storage power, as follows:

$$\bar{P}_i = P_{DG_i} + P_{s_i}, \quad (4.1)$$

where  $P_{DG_i}(k)$  is the available renewable power and  $P_{s_i}$  is the power from storage. Assuming  $E_{s_i}$  to be the existing stored energy of the  $i$ th unit, the maximum power provided by discharging this energy in time interval  $T$  is

$$P_{s_i} = E_{s_i}/T.$$

The active power fair utilization ratio is also redefined as follows to include the effect of the stored energy:

$$\alpha_{p_i} = \frac{P_i}{P_{DG_i} + P_{s_i}}. \quad (4.2)$$

Accordingly, the energy stored in the unit  $i$  at the end of the time interval  $T$  is:

$$E_{s_i}(k+1) = [1 - \alpha_{p_i}][P_{DG_i}(k)T + E_{s_i}(k)] \quad (4.3)$$

### Microgrid Optimization

In any microgrid of interest, following (4.1) for a  $G$  group of DGs, the maximum available active power to be dispatched at hour  $k$  is:

$$\sum_{j \in G} [P_{DG_j}(k) + E_{s_j}(k-1)/T].$$

The relation between the aggregated active power generated,  $P_{DG}^a$ , at hour  $k$  and the available

renewable power,  $P_{DG_j}$ , and the storage energy,  $E_{sj}$ , of the  $j$ th unit are described as follows:

$$P_{DG}^a(k) = \begin{cases} \alpha_p(k) \sum_{j \in G} [P_{DG_j}(k) + E_{sj}(k-1)/T] & \text{if active power is available,} \\ \in (-\infty, 0] & \text{otherwise.} \end{cases} \quad (4.4)$$

Accordingly, the aggregated energy stored in the microgrid, at the end of the  $k$ th hour is:

$$E(k) = \begin{cases} [1 - \alpha_p(k)] \sum_{j \in G} [P_{DG_j}(k)T + E_{sj}(k-1)] & \text{if active power is available} \\ \sum_{j \in G} [E_{sj}(k-1)] - TP_{DG}^a & \text{otherwise} \end{cases} \quad (4.5)$$

Equations (4.4, 4.5) indicate that when there is active power available, some part of it may be sent to the grid and the rest be stored. Otherwise, some power may be absorbed from the grid to charge the storages.

The active power flow of the microgrid at bus  $i$  to the main grid is expressed as follows:

$$P_{\mu_i}(k) = P_{DG_i}^a(k) - P_{L_i}^\mu(k) - P_{losses_i}^\mu(k). \quad (4.6)$$

For simplicity, microgrid losses,  $P_{losses_i}^\mu$ , and load,  $P_{L_i}^\mu$ , may be lumped together.

To secure a desired power dispatch from the microgrid,  $P_{\mu_i}^{ref}$ , main grid proposes an energy price,  $\beta_i$ . This price is subject to the generation and load demand and is expected to increase during peak hours and be less at night and when there is less demand in general. As such, the microgrid cost function for the hours  $k$  up to  $N$  is calculated as follows:

$$J_{\mu_i}(\beta_i(k), P_{\mu_i}(k)) = \sum_{l=k}^N \beta_i(l) P_{\mu_i}^{ref}(l), \quad (4.7)$$

where  $J_{\mu_i}$  is the cost function which shows the microgrid profit by generating power. At every hour,  $k$ , based on the available power, load and the predicted generation and load for the upcoming hours, the microgrid tries to search for the best  $P_{\mu_i}^{ref}$  to maximize its profit. Then, the required DG active power generation,  $P_{DG_i}^a$ , is calculated using (4.6). Substituting this  $P_{DG_i}^a$  into (4.4), provides the  $\alpha_{p_i}^{ref}$ . However, in case the PV generation or load fluctuate, or real values deviated from the predicted ones, the  $\alpha_{p_i}^{ref}$  needs to be updated to keep the same power flow,  $P_{\mu_i}^{ref}$ . In such cases, the same mechanism explained in Section 2 may be utilized to search for the appropriate  $\alpha_{p_i}^{ref}$  to secure the desired  $P_{\mu_i}^{ref}$ .

### Main Grid Optimization

In general, at the main grid level with  $N_b^t$  buses, the real-time OPF problem of dispatching  $P_{\mu_i}$  is to minimize the following cost-to-go function for total power system at hour  $k$ :

$$J_t(k) = \sum_{i=1}^{N_b^t} \sum_{l=k}^N \left[ a_i P_{G_i}(l) + \beta_i(l) P_{\mu_i}^{ref}(l) \right], \quad (4.8)$$

where  $N$  indicates the final stage (in this case time = 24 P.M) and  $a$  is the per unit power price of the conventional generations,  $P_{G_i}$ , on the main grid.

The above optimization is subject to the power flow constraints of (3.10), which are non-linear and solved numerically [61]. As in the energy market only the active power flow is of interest, DC power flow which is a simplification of (3.10) can be used. The DC power flow neglects active power losses, assumes voltage angle differences are small and that the magnitude of nodal voltages are equal. As a result, the only variables are voltage angles and active power injections. Therefore, the problem becomes linear and there is no need for iterations. These assumptions cause errors as compared to the original power flow equations (3.10). Subject to keeping the error below 5%, the

following constraints should be met [62]:

1. Voltage angle differences,  $\delta_{ij}$ , be less than  $5^\circ$ ,
2. Lines impedances  $X/R$  ratio be greater than 2,
3. For a  $X/R$  ratio of 2, the voltage standard deviation be less than 0.012.

In case the above constraints are satisfied, the DC power flow may be used instead of (3.10) as follows:

$$P_{G_i}^a(k) - P_{D_i}^a(k) = \sum_{j=1}^{N_b^t} B_{ij} \delta_{ij}(k) \quad i = 1, \dots, N_b^t \quad (4.9)$$

The optimization of (4.8), is also subject to the steady state constraints:

$$\begin{aligned} \underline{P}_{G_i}(k) &\leq P_{G_i}(k) \leq \bar{P}_{G_i}(k), \\ \underline{P}_{\mu_i}(k) &\leq P_{\mu_i}(k) \leq \bar{P}_{\mu_i}(k) \end{aligned} \quad (4.10)$$

and thermal constraints:

$$-\underline{T}_i \leq T_i(k) \leq \bar{T}_i. \quad (4.11)$$

Note that  $P_{G_i}^a$  in (4.9) may be equal to 0 if there is no generation, equal to  $P_{G_i}$  if there is only conventional generation, equal to  $P_{\mu_i}$  if there is only microgrid connected to the bus, or equal to  $P_{G_i} + P_{\mu_i}$  if there are both conventional and microgrid generation.

### Interaction between the Main Grid and the Microgrid

Within a smart grid, there is an interaction between the main grid and the microgrids. The main grid tries to motivate microgrids to generate power by offering appropriate energy price,  $\beta_i$ , to them, and at the same time, tries to minimize its cost function (4.8). On the other hand, microgrids try to

maximize their profits of (4.7) by dispatching appropriate active power  $P_{\mu_i}$ . Since the optimization objectives of the main grid and the microgrids are different, such a problem can be formulated as a noncooperative game [63]. The concept of the noncooperative game is addressed in more detail in Appendix A. For our problem, because the main grid announces hourly energy price first and the microgrids dispatch active power after that, the game is indeed a Stackelberg game with the main grid as the leader and the microgrids as the followers. Hence, a Stackelberg solution can be obtained to secure demanded power from the main grid and improve the performance indices (4.7) and (4.8).

By predicting possible power price  $\beta_i$  and power dispatch  $P_{\mu_i}$  from hour 1 up to  $N$ , it is possible to play this game for  $N$  hours at once. However, there will be a large number of possible solutions to evaluate. For example, if  $N = 24$ , and there are five possible  $P_{\mu_i}$  at every hour  $k$ , then there will be  $5^{24}$  combinations of  $P_{\mu_i}$  (and the corresponding  $\beta_i$ ) to perform the whole game. This approach is thus impractical.

Also, at every hour  $k$ , the calculation of performance indices (4.7) and (4.8) requires information for all the hours  $k$  up to  $N$ . However, only data of the current hour,  $k$ , are known and for the remaining hours of  $(k + 1)$  up to  $N$ , the predicted PV generation and load are available. Yet, the prospective values of  $\beta_i(k + 1 \rightarrow N)$  and  $P_{\mu_i}(k + 1 \rightarrow N)$  neither are known nor have predicted profiles. These issues will then be difficult to handle if the game problem is to be solved effectively. Hence, a simplified game from hour  $k$  to  $N$  is proposed to carry out the original optimization with respect to the performance indices (4.7) and (4.8).

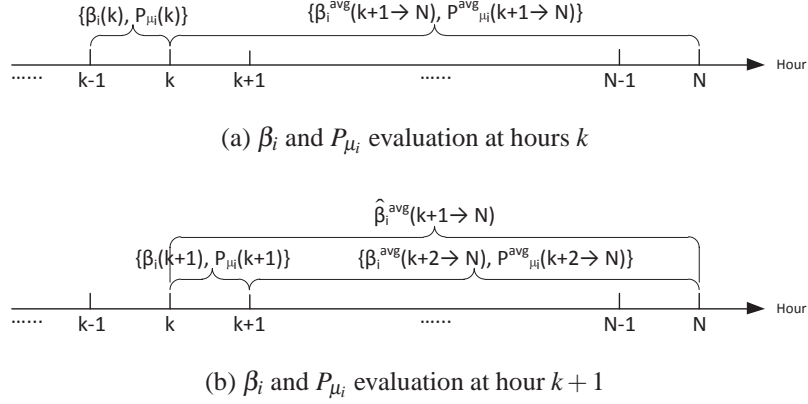


Figure 4.1: A simplified game model

A modification on (4.7) and (4.8) is then necessary in order to suit the simplified game approach, which is illustrated in the figure 4.1. In this case, the predicted PV generation, load profiles and the current hour choices of  $\beta_i(k)$  and  $P_{\mu_i}(k)$  are utilized; and the average values of the parameters for the upcoming hours are calculated and used to estimate the performance indices from hour  $(k + 1)$  to  $N$ . Thus, the performance indices (4.7) and (4.8) are modified as

$$J_{\mu}(\beta_i(k), P_{\mu_i}(k)) = \beta_i(k)P_{\mu_i}(k) + (N - k)\hat{\beta}_i^{avg}(k + 1 \rightarrow N)P_{\mu_i}^{avg}(k + 1 \rightarrow N), \quad (4.12)$$

and

$$\begin{aligned} J_t(\beta_i(k), P_{\mu_i}(k)) = & a_i P_{G_i}(k) + \beta_i(k)P_{\mu_i}(k) \\ & + (N - k) \left[ a_i^{avg}(k + 1 \rightarrow N)P_{G_i}^{avg}(k + 1 \rightarrow N) \right. \\ & \left. + \hat{\beta}_i^{avg}(k + 1 \rightarrow N)P_{\mu_i}^{avg}(k + 1 \rightarrow N) \right]. \end{aligned} \quad (4.13)$$

The optimizations of (4.12) and (4.13) are subject to the condition that the storage level of the microgrid, should return to its initial value after  $N$  hours. This requirement leads to a constraint on

the average increment or decrement stored energy,  $\Delta E_i^{avg}$ , as follows:

$$\Delta E_i^{avg}(k \rightarrow N) = \frac{\Delta E_i(k) + [N - (k)]\Delta E_i^{avg}(k + 1 \rightarrow N)}{N - (k + 1)}, \forall k \in [1, N - 2], \quad (4.14)$$

where

$$\Delta E_i(k + 1) = E_i(k + 1) - E_i(k). \quad (4.15)$$

Equation (4.14) is a recursive expression.  $\Delta E_i^{avg}(k \rightarrow N)$  is calculated on the previous hour,  $k - 1$ . It represents the hourly change of average stored energy from hour  $k$  to  $N$ . The consistency of this average for hour  $k$  and  $k + 1$  is imposed by (4.14). Then, for any proposed choice of  $\Delta E_i(k)$  by the microgrids, a  $\Delta E_i^{avg}(k + 1 \rightarrow N)$  is derived for the next hour.

When the game is not played, there is no storage involved and hence, the aggregated output power  $P_{DG_i}^a(k)$  is equal to the sum of the available power:

$$P_{DG_i}^a(k) = \sum_{j=1}^{N_{DG_i}} P_{DG_{ij}}(k). \quad (4.16)$$

where  $P_{DG_{ij}}$  is the available renewable power of the  $j$ th DG in a microgrid connected to the  $i$ th bus. However, when the game is played between the main grid and the microgrids, the aggregated output power  $P_{DG_i}^a(k)$  is represented as follows:

$$P_{DG_i}^a(k) = \sum_{j=1}^{N_{DG_i}} P_{DG_{ij}}(k) - \frac{\Delta E_i(k)}{T}, \quad (4.17)$$

where the second term on the right hand side of (4.17) is accounted for the energy storage change within time period  $T$ . Thus, by substituting (4.17) into (4.6), the constraint (4.14) can then be rewritten in terms of  $P_{\mu_i}$  and  $P_{\mu_i}^{avg}$  as follows:

$$P_{\mu_i}^{avg}(k + 1 \rightarrow N) = \frac{P_{\mu_i}(k + 1) + [N - (k + 1)]P_{\mu_i}^{avg}(k + 2 \rightarrow N)}{N - k}, \forall k \in [1, N - 1]. \quad (4.18)$$



Although the consistency of  $\beta_i^{avg}(k \rightarrow N)$  and  $\beta_i^{avg}(k+1 \rightarrow N)$  is not imposed, but it can be verified according to

$$\begin{cases} \hat{\beta}_i^{avg}(k+1 \rightarrow N) = \frac{\beta_i(k+1) + [N - (k+1)]\beta_i^{avg}(k+2 \rightarrow N)}{N - k}, \forall k \in [1, N-1] \\ \beta_i^{avg}(k+1 \rightarrow N) = \hat{\beta}_i^{avg}(k+1 \rightarrow N). \end{cases} \quad (4.19)$$

The term  $\hat{\beta}_i^{avg}(k+1 \rightarrow N)$  in (4.19) refers to the re-evaluation of  $\beta_i^{avg}(k+1 \rightarrow N)$  at hour  $(k+1)$ , using  $\beta_i(k+1)$  and  $\beta_i^{avg}(k+2 \rightarrow N)$ , which are obtained from the game at hour  $(k+1)$  as shown in the figure 4.1b. Evaluating (4.19) analytically is not straightforward and it can be checked numerically for any case of interest.

### Game Solution

To solve the game problem presented in Section 4, the following steps are carried out to calculate performance indices  $J_\mu$  in (4.12) and  $J_t$  in (4.13).

1. The active power  $P_{\mu_i}(k)$ , flowing from the microgrid (on the  $i$ th bus) to the main grid at hour  $k$  is given by (4.6).
2. Assume that the storage level of a microgrid should return to its initial value after  $N$  hours, then the average active power from hour  $(k+1)$  to  $N$ ,  $P_{\mu_i}^{avg}(k+1 \rightarrow N)$ , is given by:

$$P_{\mu_i}^{avg}(k+1 \rightarrow N) = \text{avg}[P_{\mu_i}(k+1 \rightarrow N)] + \frac{\sum_{l=1}^k \Delta E_i(l)}{N - k}, \quad (4.20)$$

where  $\text{avg}[P_{\mu_i}(k+1 \rightarrow N)]$  is the predicted average power flow from historical data without considering the storage.

3. Conventional generation  $P_{G_i}(k)$  (on the  $i$ th bus) at hour  $k$  is given by

$$P_{G_i}(k) = P_{D_i}(k) - P_{\mu_i}(k). \quad (4.21)$$

And the predicted average generation from hour  $(k+1)$  to  $N$  is given by

$$P_{G_i}^{avg}(k+1 \rightarrow N) = P_{D_i}^{avg}(k+1 \rightarrow N) - P_{\mu_i}^{avg}(k+1 \rightarrow N), \quad (4.22)$$

where  $P_{D_i}^{avg}(k+1 \rightarrow N)$  is the predicted average demand from hour  $(k+1)$  to  $N$ .

4. Using  $P_{G_i}(k)$  given by (4.21),  $\beta_i(k)$  is computed by the following equation:

$$\beta_i(k) = \beta_0 \left[ 1 + \eta_i(k) \frac{P_{G_i}(k) - P_{G_i}^*(k)}{P_{G_i}^*(k)} \right], \quad (4.23)$$

where  $P_{G_i}^*$  is the optimal operation power of the conventional generator (on the  $i$ th bus),  $\beta_0$  is a known base price (when  $P_{G_i} = P_{G_i}^*$ ,  $\beta_i = \beta_0$ ), and  $\eta_i(k)$  is a variable, which the main grid perturbs to find different energy price offers to play the game. Basically, equation (4.23) means that if  $P_{G_i}$  is larger than  $P_{G_i}^*$ , the main grid should increase the price  $\beta_i$  to motivate the DGs to produce more energy, and if the  $P_{G_i}$  is less than  $P_{G_i}^*$ , the price  $\beta_i$  should be decreased to encourage DGs to store more energy. This helps the generators operate near the optimal operation power,  $P_{G_i}^*$ .

5. Similarly,  $P_{G_i}^{avg}(k+1 \rightarrow N)$  in (4.22) will be used to calculate  $\beta_i^{avg}(k+1 \rightarrow N)$  as follows:

$$\beta_i^{avg}(k+1 \rightarrow N) = \beta_0 \left[ 1 + \eta_i(k) \frac{P_{G_i}^{avg}(k+1 \rightarrow N) - P_{G_i}^*(k)}{P_{G_i}^*(k)} \right].$$

Through the above steps, for every possible choice of  $\Delta E_i(k)$  and  $\eta_i(k)$ , the corresponding values of  $P_{\mu_i}(k)$ ,  $P_{\mu_i}^{avg}(k+1 \rightarrow N)$ ,  $\beta_i(k)$ , and  $\beta_i^{avg}(k+1 \rightarrow N)$  are obtained, and hence cost functions

(4.12) and (4.13) can be calculated.

In order to find the game solution, a matrix game can be constructed. Specifically, suppose that there exist  $M_1$  choices of  $\eta_i(k)$ ,

$$\{\eta_i(k, 1), \eta_i(k, 2), \dots, \eta_i(k, M_1)\},$$

and  $M_2$  choices of  $\Delta E_i(k)$ , which result in  $M_2$  choices of  $P_{\mu_i}(k)$ ,

$$\{P_{\mu_i}(k, 1), P_{\mu_i}(k, 2), \dots, P_{\mu_i}(k, M_2)\}.$$

Hence, a matrix game can be constructed as Table 4.1, where values of  $\eta_i(k)$  are located at the far left column and values of  $P_{\mu_i}(k)$  are located at the far top row. The other entries are pairs of  $\{J_t, J_{\mu_i}\}$  based on corresponding  $\eta_i(k)$  and  $P_{\mu_i}(k)$ .

Table 4.1: Matrix game between the main grid and a microgrid

| $\eta_i(k) \backslash P_{\mu_i}(k)$ | $P_{\mu_i}(k, 1)$   | $\dots$  | $P_{\mu_i}(k, M_2)$   |
|-------------------------------------|---|----------|---|
| $\eta_i(k, 1)$                      | $\left\{ \begin{array}{l} J_t[\eta_i(k, 1), P_{\mu_i}(k, 1)], \\ J_{\mu_i}[\eta_i(k, 1), P_{\mu_i}(k, 1)] \end{array} \right\}$     | $\dots$  | $\left\{ \begin{array}{l} J_t[\eta_i(k, 1), P_{\mu_i}(k, M_2)], \\ J_{\mu_i}[\eta_i(k, 1), P_{\mu_i}(k, M_2)] \end{array} \right\}$     |
| $\vdots$                            | $\vdots$  | $\ddots$ | $\vdots$  |
| $\eta_i(k, M_1)$                    | $\left\{ \begin{array}{l} J_t[\eta_i(k, M_1), P_{\mu_i}(k, 1)], \\ J_{\mu_i}[\eta_i(k, M_1), P_{\mu_i}(k, 1)] \end{array} \right\}$ | $\dots$  | $\left\{ \begin{array}{l} J_t[\eta_i(k, M_1), P_{\mu_i}(k, M_2)], \\ J_{\mu_i}[\eta_i(k, M_1), P_{\mu_i}(k, M_2)] \end{array} \right\}$ |

Using such a table, either the Nash equilibrium or the Stackelberg solution can be found. Since the main grid acts as a leader and the microgrids act as the followers, the search algorithm for

Stackelberg solution is presented here (please refer to Appendix B for the counterpart of Nash equilibrium).

1. For each  $\eta_i(k, j)$  for  $j = 1, 2, \dots, M_1$ , a corresponding  $P_{\mu_i}(k)$  can be found such that

$$J_{\mu_i}[\eta_i(k, j), P_{\mu_i}(k)] \text{ is maximized and that } P_{\mu_i}(k) \text{ is denoted as } P_{\mu_i}^S[\eta_i(k, j)].$$

2. The Stackelberg solution of the main grid is  $\eta_i(k, l)$  for some  $l$  such that

$$J_t[\eta_i(k, l), P_{\mu_i}^S(\eta_i(k, l))] \leq J_t[\eta_i(k, j), P_{\mu_i}^S(\eta_i(k, j))]$$

for all  $j = 1, 2, \dots, M_1$ .

To illustrate this algorithm, a simple example is provided as follows:

*Example 1:* Suppose that the matrix game is shown in Table 4.2.

Table 4.2: Matrix game for example 1, where  $\{\star, \star\}$  stands for  $\{J_{\mu}, J_t\}$ .

|             |                |             |             |
|-------------|----------------|-------------|-------------|
|             | $P_{\mu_i}(k)$ | 0.8         | 1           |
| $\eta_i(k)$ |                |             |             |
| 1           |                | $\{8, 10\}$ | $\{10, 9\}$ |
| 1.2         |                | $\{7, 5\}$  | $\{6, 7\}$  |

The Stackelberg solution with the main grid as the leader is obtained as follows:

1. For  $\eta_i(k) = 1$ ,  $P_{\mu_i}(k) = 1$  maximizes  $J_{\mu_i}$  because

$$J_{\mu_i}(1, 1) = 10 \text{ is greater than } J_{\mu_i}(1, 0.8) = 8.$$

For  $\eta_i(k) = 1.2, P_{\mu_i}(k) = 0.8$  maximizes  $J_{\mu_i}$  because

$$J_{\mu_i}(1.2, 0.8) = 7 \text{ is greater than } J_{\mu_i}(1.2, 1) = 6.$$

2. Since

$$J_t(1.2, 0.8) = 5 \text{ is less than } J_t(1, 1) = 9,$$

the Stackelberg solution of the main grid is  $\eta_i(k) = 1.2$ .

The Nash equilibrium counterpart of this particular example is also shown in the Appendix B. Note that for a game problem, a Nash equilibrium may happen to be the same as the Stackelberg solution, which is the case in Section 4.

## Simulations

To illustrate the smart grid control algorithm discussed earlier, the design and application of the game approach for the case of a microgrid versus one bus main grid is discussed in this section as shown in the figure4.2. A modified version of the bus system proposed by IEEE 399-1997 standard is used to represent the microgrid. There are 5 feeders and 8 DGs are distributed across the microgrid with a total of 8MVA generation capacity. The microgrid connects to the main grid through point of common coupling (PCC). Main grid is represented by a single bus into which an aggregated load and conventional generator is connected.

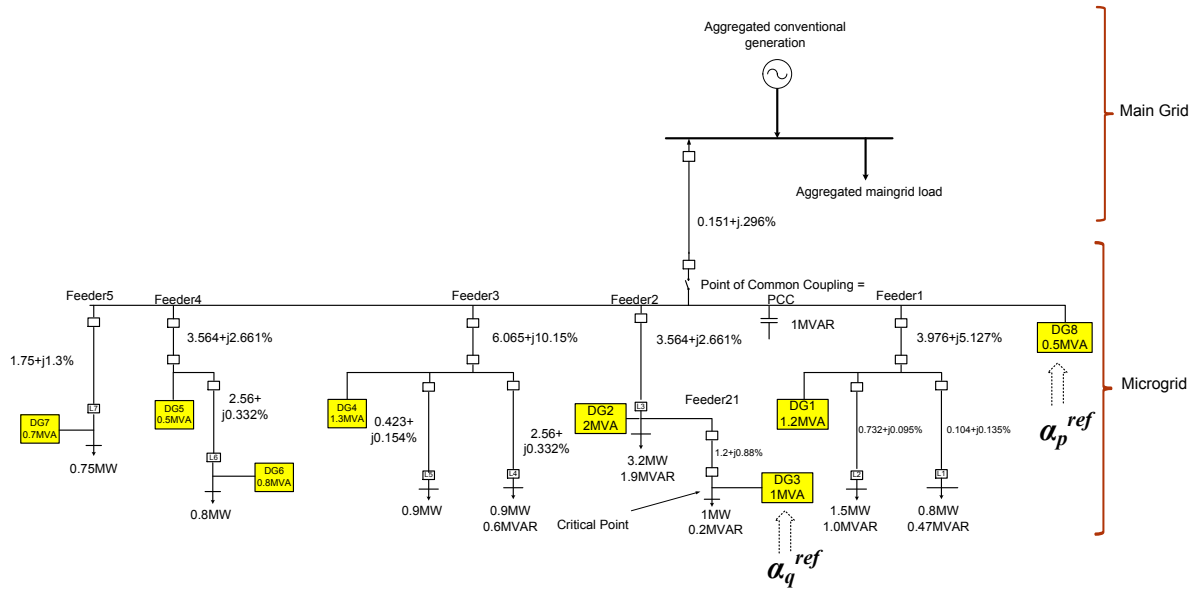


Figure 4.2: Case of study smart grid

Usually, solar power of DGs differ from each other due to variable environmental conditions, such as a passing cloud or storm. Especially, if the microgrid is geographically expanded, the sunshine intense for different DGs will also be different. As such, PV profiles should account for such non consistencies. Figure 4.3 provides proposed PV profiles used in the numerical example. These profiles, reflect the environmental and geographical differences, which may exist among DGs.

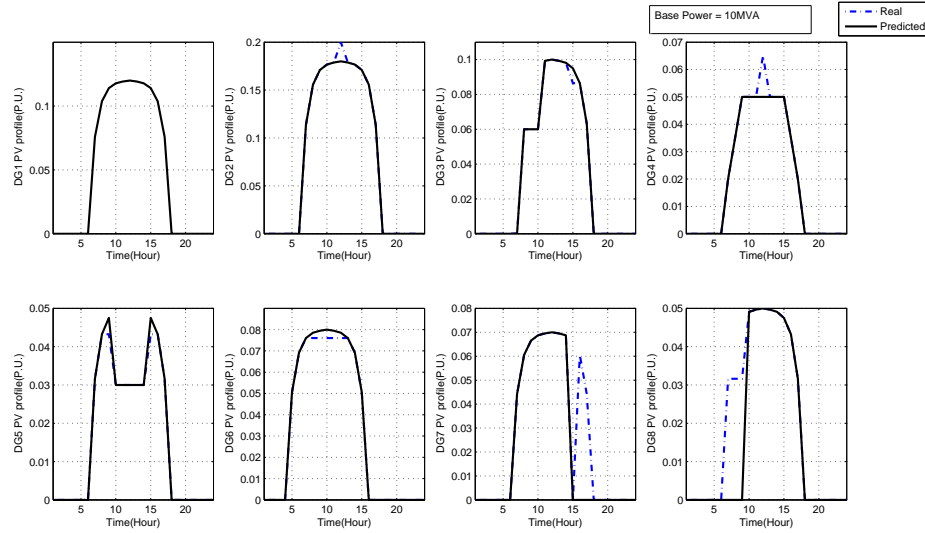


Figure 4.3: PV profiles of DGs of the microgrid

The microgrid case of study of figure 4.2, has five feeders. To account for the different kinds of possible consumers, different loads have been assumed to be connected to each feeder as follows and shown in the figure4.4. Each plot in the figure means:

- (1) Loads on feeder 1 represent industrial two shift workday.
- (2) Loads on feeder 2 are assumed to be of a commercial area.
- (3) Loads on feeder 3 represent an active night life area.
- (4) Loads on feeders 4 and 5 are assumed to be of small residential areas.

Load profile of the main grid is also shown in the figure4.5.

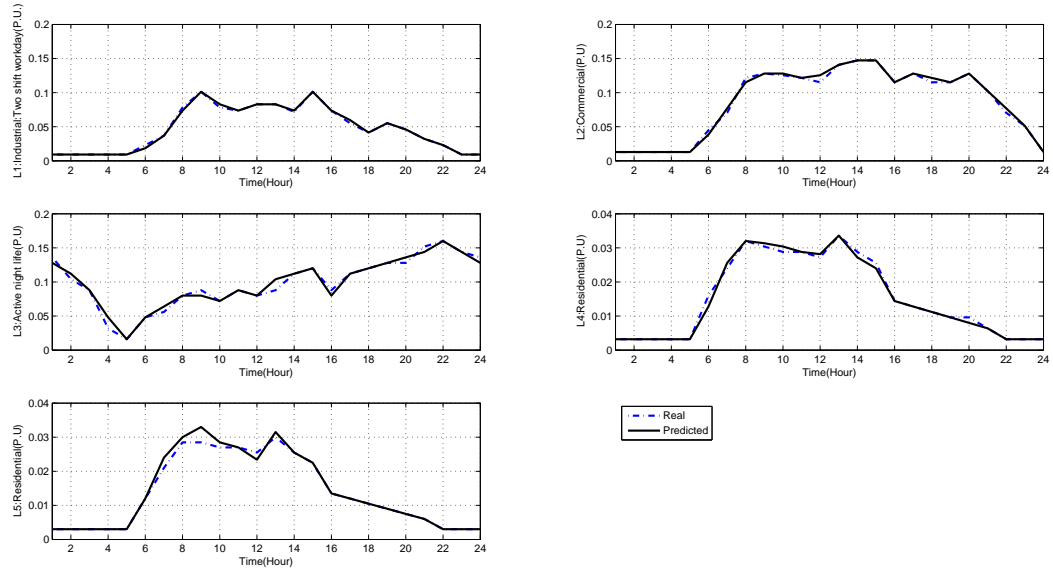


Figure 4.4: Load profiles of different feeders

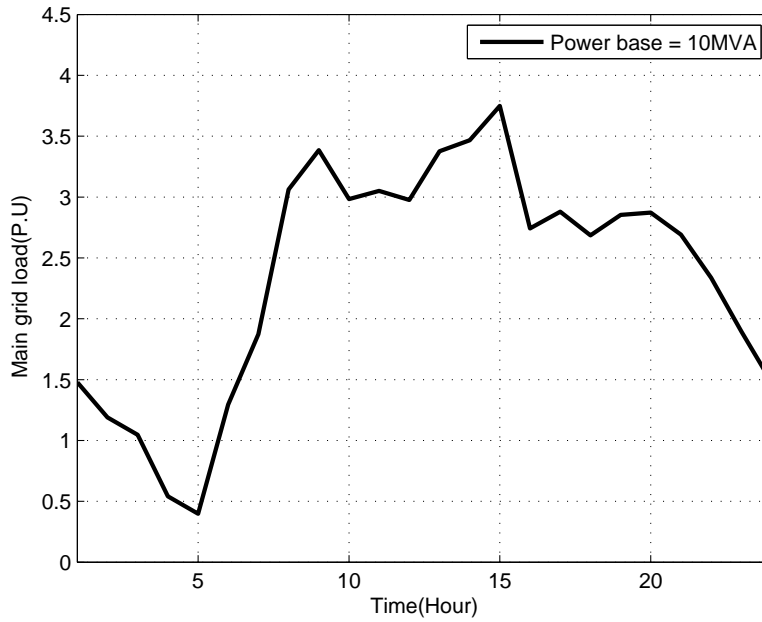


Figure 4.5: Main grid load profile



The per unit cost of the conventional generators of the main grid is shown in the figure 4.6. In this figure,  $P_G^*$  is the optimal operation point of the generators; that is the load on which they have the lowest cost. Due to the extra required fuel, the price increases quadratically beyond this point. Below this point also the cost per unit increases, however with a lower rate, due to the constant and permanent expenditures of generator stations such as human resources, maintenance fees and etc.

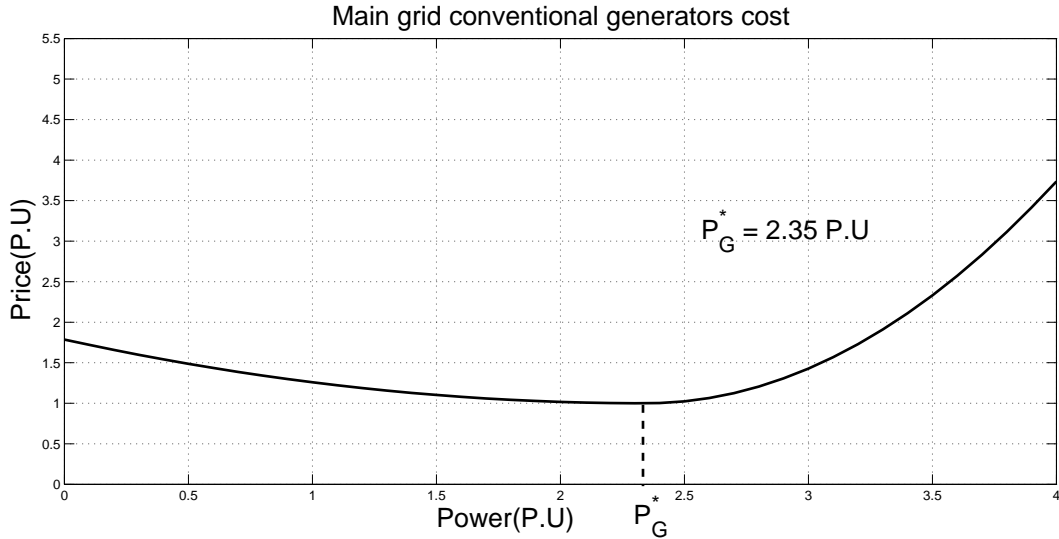


Figure 4.6: Conventional generation cost per unit

At each hour, based on the real time and predicted generation/load, the cost functions (4.7) & (4.8) are calculated for the different prices and power flows offered by the main grid and microgrid, respectively. Then, the Stackelberg solution with the main grid as the leader is found.

It is assumed that the microgrid has 1 P.U storage capacity. Hence, it can supply its local loads for about one hour in case of main grid disconnection. The initial storage is 0.5 P.U. Charge and discharge rates are limited to 0.25 P.U. Storage level at the end of the day (hour 24) should return to its initial value. The storage here makes the difference when the game is played or not. If there is no game in the smart grid control, all the available active power is fed to the grid.

When the game is played, to optimize the cost functions, sometimes some power is used to charge the storages (this power will come either from renewable sources (DGs) or the main grid) and sometimes storages are discharged. It is expected that during the night time when there is less power demand, microgrid buys power from the main grid to charge and during the day time when there is power peak demand, storages are released. As such, power peak shaving and improved power flow is expected.

As explained earlier in Section 4, the game is played between  $\eta$  in (4.23) and microgrid power flow  $P_\mu$ . Table 4.3 shows the improvements in the cost functions by running the game for 24 hours.

Table 4.3: Cost function optimizations

|              | $J_\mu(1 - 24)$ | $J_t(1 - 24)$ |
|--------------|-----------------|---------------|
| Without game | 6.4682          | 84.0155       |
| With game    | 10.5716         | 81.6979       |

It is seen that the game has reduced the main grid cost  $J_t$  and increased the microgrid profit  $J_\mu$ . The power flow of the main grid is shown in the figure 4.7a. The dashed line is the power flow without game and the solid one is the one with game. It is seen that the game has increased the load when originally was less load and has decreased the load when originally power demand is high. It is clear that this game strategy not only has helped cost optimization, but also resulted in peak power shave and improved power flow. For this particular case, the Nash solution was also considered which showed the same results of the Stackelberg solution.

Table 4.4: The values of power flow  $P_{\mu}^{ref}$  and  $\alpha_p^{ref}$ .

| Hour | $P_{\mu}^{ref}$ | $\alpha_p^{ref}$ | Hour | $P_{\mu}^{ref}$ | $\alpha_p^{ref}$ |
|------|-----------------|------------------|------|-----------------|------------------|
| 1    | -0.4142         | -0.5000          | 13   | 0.3123          | 0.4074           |
| 2    | -0.3822         | -0.3333          | 14   | 0.3519          | 0.4402           |
| 3    | -0.1162         | 0                | 15   | 0.4113          | 0.5463           |
| 4    | -0.0602         | 0                | 16   | -0.0163         | 0.2352           |
| 5    | 0.0064          | 0.0481           | 17   | 0.0038          | 0.2446           |
| 6    | -0.0746         | 0.0647           | 18   | -0.0483         | 0.2500           |
| 7    | 0.1910          | 0.2853           | 19   | -0.0670         | 0.3333           |
| 8    | 0.2360          | 0.3656           | 20   | -0.0691         | 0.5000           |
| 9    | 0.3138          | 0.4239           | 21   | -0.0490         | 1.0000           |
| 10   | 0.2494          | 0.3674           | 22   | -0.2596         | -                |
| 11   | 0.3485          | 0.4074           | 23   | -0.4606         | -                |
| 12   | 0.3998          | 0.4221           | 24   | -0.4142         | -1.0000          |

Playing a 24-hours game, results in  $P_{\mu}^{ref}$  and  $\alpha_p^{ref}$  as presented in Table 4.4. Note that at hour-22 and hour-23, the values of  $\alpha_p^{ref}$  (computed using (4.4) and (4.5)) do not exist because the active power is not available during those hours. Based on the data in Table 4.4, the figure 4.7b is then presented to graphically show a 24-hour profile of the power flow  $P_{\mu}^{ref}$ . Positive value of  $P_{\mu}^{ref}$  means that power flows from the microgrid to the main grid. It is shown that at night hours and when there is less power demand, power flow to the main grid has decreased as compared with the time that there is no game. That is because, at these time periods, when less power prices are offered by the main grid, the game results in charging the storages so that they may be released at the peak hours when power prices increase. As an illustration, the game procedure for hour-1 is

shown in the Appendix C and the process is similar for the next hours.

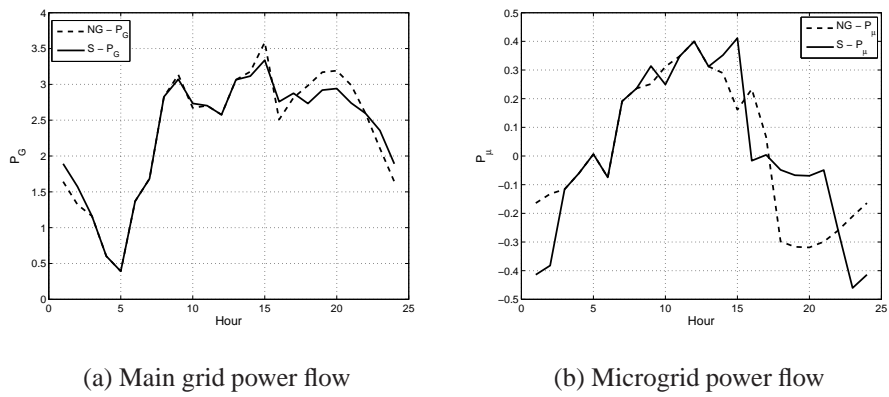


Figure 4.7: The effect of the proposed game approach on power flow and peak power shaving

Equation (4.19) is used to verify the accuracy of the estimations provided in the Section 4. The values of  $\beta$ ,  $\beta^{avg}$  and  $\hat{\beta}^{avg}$  are presented in Table 4.5; where  $\beta^{avg}$  and  $\hat{\beta}^{avg}$  match well except at hour-11,20 and 22 where there are discrepancies. The mismatch is less than 15% and as such, the estimation of (4.12, 4.13) has an acceptable accuracy.

Table 4.5: The energy prices:  $\beta_i$ ,  $\beta_i^{avg}$ , and  $\hat{\beta}_i^{avg}$ .

| Hour | $\beta_i$ | $\beta_i^{avg}$ | $\hat{\beta}_i^{avg}$ | Hour | $\beta_i$ | $\beta_i^{avg}$ | $\hat{\beta}_i^{avg}$ |
|------|-----------|-----------------|-----------------------|------|-----------|-----------------|-----------------------|
| 1    | 7.2204    | 7.9977          | 7.9977                | 13   | 11.6484   | 10.0497         | 10.0497               |
| 2    | 6.6757    | 8.0578          | 8.0578                | 14   | 11.9087   | 9.8638          | 9.8638                |
| 3    | 5.9779    | 8.1569          | 8.1569                | 15   | 13.0408   | 9.5108          | 9.5108                |
| 4    | 5.0247    | 8.3135          | 8.3135                | 16   | 10.0867   | 9.4388          | 9.4388                |
| 5    | 4.6663    | 8.5054          | 8.5054                | 17   | 10.6869   | 9.2605          | 9.2605                |
| 6    | 6.3299    | 8.6263          | 8.6263                | 18   | 9.9557    | 9.1447          | 9.1447                |
| 7    | 6.8643    | 8.7299          | 8.7299                | 19   | 10.9106   | 8.7915          | 8.7915                |
| 8    | 8.8114    | 8.7248          | 8.7248                | 20   | 11.0179   | 8.2349          | 8.0783                |
| 9    | 9.2273    | 8.6913          | 8.6913                | 21   | 8.6638    | 7.8831          | 7.8831                |
| 10   | 8.6529    | 8.6941          | 8.6941                | 22   | 8.4187    | 7.6153          | 6.8357                |
| 11   | 8.6000    | 8.7013          | 10.1040               | 23   | 8.0102    | 5.6613          | 5.6613                |
| 12   | 9.1565    | 10.1829         | 10.1829               | 24   | 5.6613    | -               | -                     |

### Conclusion

Main grid needs to pay for the renewable energy that the microgrids generate. The price is chosen dynamically and depends on the daily energy demand. At the same time that the main grid is trying to motivate microgrids produce more energy, it also needs to minimize its costs. Microgrids also try to optimize their profit by properly managing the energy they generate or store, based on the prices offered by the main grid.

In this chapter it is shown that such a relation between the main grid and the microgrids can be

formulated as a stackelberg game approach. in which the main grid as the leader, announces its hourly energy prices and the microgrids as the followers, have to decide the amount of power to dispatch. It is shown that this game strategy not only optimizes the performance indices of both sides, but also improves power flow on the main grid and the microgrid in term of peak power shaving.

## **APPENDIX A: INTRODUCTION TO THE GAME THEORY**

The game models strategic situations, in which an individual's success in making choices depends on the choices of others [64]. The modern game theory was first proposed by von Neuman and Morganstern in 1944. Basically, there are two major types of game. One is the cooperative game, where players collaborate with each other to achieve a common goal. The other is the non-cooperative game, which was developed by Nash in 1950s [65, 66], where each individual pursues its own interest or objective. For non-cooperative game, most of the results are summarized in [63]. In the non-cooperative game, if the players make their decisions simultaneously, then the game is called Nash game, and if the players make their decisions sequentially, then the game is called Stackelberg. The Stackelberg game was first established by the German economist, Heinrich von Stackelberg [67], and was extended to dynamic case by Simaan and Cruz [68, 69].

In a  $n$ -player Nash game, the strategy set  $\{\gamma_1^N, \gamma_2^N, \dots, \gamma_n^N\}$  for the  $n$  players is called a *Nash equilibrium* if and only if the following inequalities hold.

$$\begin{aligned} J_1(\gamma_1^N, \gamma_2^N, \dots, \gamma_n^N) &\leq J_1(\gamma_1, \gamma_2^N, \dots, \gamma_n^N), \\ J_2(\gamma_1^N, \gamma_2^N, \dots, \gamma_n^N) &\leq J_2(\gamma_1^N, \gamma_2, \dots, \gamma_n^N), \\ &\vdots \\ J_n(\gamma_1^N, \gamma_2^N, \dots, \gamma_n^N) &\leq J_n(\gamma_1^N, \gamma_2^N, \dots, \gamma_n) \end{aligned}$$

where  $\gamma_1, \gamma_2, \dots, \gamma_n$  are the decision variables for the  $n$  players belonging to the strategy space  $\Gamma_1 \times \Gamma_2 \times \dots \times \Gamma_n$  of all the admissible strategies, and  $J_i(\gamma_1, \gamma_2, \dots, \gamma_j, \dots, \gamma_n)$  is the objective function or performance index for the  $i$ th player. The philosophy of the Nash equilibrium is that if the players' strategies form a Nash equilibrium, then no player intends to unilaterally change its strategy. If it does so, its objective function or performance index will worsen.

In a 2-player Stackelberg game, the strategy set  $\{\gamma_1^S, \gamma_2^S\}$  is a *Stackelberg solution* with player 1 as



the leader if and only if

$$\gamma_1^S = \arg \min_{\gamma_1 \in \Gamma_1} J_1(\gamma_1, \gamma_2(\gamma_1)) \quad \text{and} \quad \gamma_2^S = \gamma_2(\gamma_1^S),$$

where

$$\gamma_2(\gamma_1) = \arg \min_{\gamma_2 \in \Gamma_2} J_2(\gamma_1, \gamma_2).$$

The philosophy of the Stackelberg solution is that if the leader knows the optimal response of the follower, then it can play the Stackelberg strategy to optimize its objective function or performance index.

## **APPENDIX B: SEARCH ALGORITHM FOR NASH EQUILIBRIUM**

Search algorithm for Nash Equilibrium is as follows:

1. For each  $\eta_i(k, j)$  for  $j = 1, 2, \dots, M_1$ ,  $P_{\mu_i}(k, l)$  can be found for some  $l$  such that  $J_{\mu_i}[\eta_i(k, j), P_{\mu_i}(k)]$  is maximized under  $P_{\mu_i}(k) = P_{\mu_i}(k, l)$ .
2. For  $P_{\mu_i}(k, l)$ , a corresponding  $\eta_i(k, m)$  can be found for some  $m$  such that  $J_t(\eta_i(k), P_{\mu_i}(k, l))$  is minimized under  $\eta_i(k) = \eta_i(k, m)$ .
3. If  $\eta_i(k, j) = \eta_i(k, m)$ , then the pair  $\{\eta_i(k, m), P_{\mu_i}(k, l)\}$  is a Nash equilibrium.

Applying the above algorithm to example 1 yields:

1. For  $\eta_i(k) = 1$ ,  $P_{\mu_i}(k) = 1$  maximizes  $J_{\mu_i}$  because

$$J_{\mu_i}(1, 1) = 10 \text{ is greater than } J_{\mu_i}(1, 0.8) = 8.$$

Then, for  $P_{\mu_i}(k) = 1$ ,  $\eta_i(k) = 1.2$  minimizes  $J_t$  because

$$J_t(1.2, 1) = 6 \text{ is less than } J_t(1, 1) = 9.$$

However,  $\eta_i(k) = 1.2 \neq \eta_i(k) = 1$ .

2. For  $\eta_i(k) = 1.2$ ,  $P_{\mu_i}(k) = 0.8$  maximizes  $J_{\mu_i}$  because

$$J_{\mu_i}(1.2, 0.8) = 7 \text{ is greater than } J_{\mu_i}(1.2, 1) = 6.$$

Then, for  $P_{\mu_i}(k) = 0.8$ ,  $\eta_i(k) = 1.2$  minimizes because

$$J_t(1.2, 0.8) = 5 \text{ is less than } J_t(1, 0.8) = 10.$$

Since  $\eta_i(k) = 1.2 = \eta_i(k) = 1.2$ ,  $\{\eta_i(k), P_{\mu_i}(k)\} = \{1.2, 1\}$  is the Nash equilibrium.

**APPENDIX C: DETAILS OF FINDING GAME SOLUTIONS FOR THE  
FIRST HOUR**

Here, the game approach for the first hour is provided to illustrate the game solution process. For the value of  $\Delta E$ , microgrid chooses five values between higher and lower bounds to play the game. Higher and lower bounds are determined by the facts that storage cannot be charged beyond 1 P.U or be discharged below 0. Also,  $|\Delta E| \leq 0.25$  P.U, which is the charge and discharge rate limitation. As such, and regarding the initial storage of 0.5 P.U, the chosen values for the first hour are as follows:

$$\Delta E(1) = [-0.25 \quad -0.125 \quad 0 \quad 0.125 \quad 0.25].$$

For every  $\Delta E$ , the microgrid power flow,  $P_\mu$ , can be calculated using (4.6) and (4.17). As such and according to the PV/Load profiles:

$$P_\mu(1) = [0.0938 \quad -0.0312 \quad -0.1562 \quad -0.2812 \quad -0.4062]. \quad (C.1)$$

To calculate the cost function for the remaining hours, the  $P_\mu^{avg}$  should be evaluated using (4.18) and PV profiles in the figure 4.3:

$$P_\mu^{avg}(2 \rightarrow 24) = [0.0021 \quad 0.0076 \quad 0.013 \quad 0.0184 \quad 0.0239].$$

Then, according to the load profile of the figure 4.5, the microgrid offers of  $P_\mu(1)$  in (C.1) and using (4.21, 4.22),  $P_G(1)$  and  $P_G^{avg}(2 \rightarrow 24)$  are calculated as:

$$P_G(1) = [1.384 \quad 1.509 \quad 1.634 \quad 1.759 \quad 1.884],$$

$$P_G^{avg}(2 \rightarrow 24) = [2.3816 \quad 2.3762 \quad 2.3708 \quad 2.3653 \quad 2.3599].$$

The price,  $\beta(1)$ , that the main grid offers to the microgrid is calculated using (4.23). The default value of  $\eta = 1$ . To get the best possible price to offer,  $\eta$  is perturbed around the default value. The

following five values of  $\eta$  are played against the microgrid proposed  $P_\mu$ :

$$\eta(1) = [0.5 \quad 0.75 \quad 1 \quad 1.25 \quad 1.5].$$

To calculate  $\beta^{avg}(2-23)$ ,  $P_G^{avg}(2-23)$  is substituted into (4.23).

Moreover,  $a(1)$  and  $a^{avg}(2-23)$  are calculated from the figure 4.6 for the  $P_G(1)$  and  $P_G^{avg}(2-24)$ , respectively. As such, (4.12, 4.13) are written as follows for the first hour:

$$J_\mu(1) = \beta(1)P_\mu(1) + 23\beta^{avg}(2-23)P_\mu^{avg}(2-23),$$

$$J_t(1) = a(1)P_G(1) + \beta(1)P_\mu(1) + 23\{a^{avg}(2-23)P_G^{avg}(2-23) + \beta^{avg}(2-23)P_\mu^{avg}(2-23)\}.$$

Therefore, the game matrix will be found as in Tables C.1 , C.2 for the first hour. The Stackelberg solution for these matrixes with the main grid as the leader yields  $\eta = 0.5$  and  $P_\mu = -0.4142$  as the solution. The same process is used for the remaining hours.

Table C.1:  $J_\mu$  cost function game table

| $J_\mu(1)$ |      | $P_\mu(1)$ |         |         |         |               |
|------------|------|------------|---------|---------|---------|---------------|
|            |      | 0.0858     | -0.0392 | -0.1642 | -0.2892 | -0.4142       |
| $\eta(1)$  | 0.5  | 3.0126     | 3.2084  | 3.3487  | 3.4336  | <b>3.4629</b> |
|            | 0.75 | 2.9479     | 3.2417  | 3.4522  | 3.5794  | 3.6234        |
|            | 1    | 2.8833     | 3.2750  | 3.5556  | 3.7253  | 3.7839        |
|            | 1.25 | 2.8187     | 3.3083  | 3.6591  | 3.8712  | 3.9445        |
|            | 1.5  | 2.7541     | 3.3416  | 3.7626  | 4.0170  | 4.1050        |

Table C.2:  $J_t$  cost function game table

| $J_t(1)$  |      | $P_\mu(1)$ |         |         |         |                |
|-----------|------|------------|---------|---------|---------|----------------|
|           |      | 0.0858     | -0.0392 | -0.1642 | -0.2892 | -0.4142        |
| $\eta(1)$ | 0.5  | 59.1290    | 59.2822 | 59.3825 | 59.4315 | <b>59.4309</b> |
|           | 0.75 | 59.0644    | 59.3155 | 59.4860 | 59.5774 | 59.5914        |
|           | 1    | 58.9998    | 59.3488 | 59.5894 | 59.7233 | 59.7519        |
|           | 1.25 | 58.9352    | 59.3821 | 59.6929 | 59.8691 | 59.9125        |
|           | 1.5  | 58.8705    | 59.4154 | 59.7963 | 60.0150 | 60.0730        |



**APPENDIX D: DISTRIBUTED OPTIMIZATION STABILITY  
ANALYSIS**

To analyze the system, it is required to express the gradient term in (3.6) in terms of the system states,  $\alpha_{q_i}$ . Therefore, lets linearize the gradient term of (3.14),  $g_i$ , around the optimal operating point,  $V_i^*$  and  $\alpha_{q_i}^*$ :

$$g_i(V_i, \alpha_{q_i}) \simeq g_i^* + e_i(V_i - V_i^*) + f_i(\alpha_{q_i} - \alpha_{q_i}^*), \quad (\text{D.1})$$

where  $g_i^* = g_i(V_i^*, \alpha_{q_i}^*)$  and utilizing (3.14):

$$\begin{aligned} e_i &= \left. \frac{\partial g_i(V_i, \alpha_{q_i})}{\partial V_i} \right|_{V_i^* \& \alpha_{q_i}^*} \\ &= -\bar{Q}_i \frac{(1 - 2V_i)(\alpha_{q_i} \bar{Q}_i - V_i^2 B_{ii}) + 2(V_i - V_i^2) V_i B_{ii}}{(\alpha_{q_i} \bar{Q}_i - V_i^2 B_{ii})^2} \Big|_{V_i^* \& \alpha_{q_i}^*} \\ &= -\bar{Q}_i \frac{\alpha_{q_i} \bar{Q}_i (1 - 2V_i) + V_i^2 B_{ii}}{(\alpha_{q_i} \bar{Q}_i - V_i^2 B_{ii})^2} \Big|_{V_i^* \& \alpha_{q_i}^*} \end{aligned} \quad (\text{D.2})$$

and,

$$\begin{aligned} f_i &= \left. \frac{\partial g_i(V_i, \alpha_{q_i})}{\partial \alpha_{q_i}} \right|_{V_i^* \& \alpha_{q_i}^*} \\ &= \bar{Q}_i^2 \frac{V_i(1 - V_i)}{(\alpha_{q_i} \bar{Q}_i - V_i^2 B_{ii})^2} \Big|_{V_i^* \& \alpha_{q_i}^*} \end{aligned} \quad (\text{D.3})$$

Also, linearizing the system power flow equations (3.10) around the optimal operating points, provides:

$$\begin{bmatrix} P - P^* \\ \alpha_q - \alpha_q^* \end{bmatrix} = H \begin{bmatrix} V - V^* \\ \delta - \delta^* \end{bmatrix}, \quad (\text{D.4})$$

where  $P = [P_1, \dots, P_N]^T$ ,  $V = [V_1, \dots, V_N]^T$ ,  $\alpha_q = [\alpha_{q_1}, \dots, \alpha_{q_N}]^T$ ,  $\delta = [\delta_1, \dots, \delta_N]^T$  and  $H$  is the Jacobian matrix. Then it follows that:

$$\begin{bmatrix} V - V^* \\ \delta - \delta^* \end{bmatrix} = \begin{bmatrix} H_{11} & | & H_{12} \\ - & \cdot & - \\ H_{21} & | & H_{22} \end{bmatrix} \begin{bmatrix} P - P^* \\ \alpha_q - \alpha_q^* \end{bmatrix} \quad (\text{D.5})$$

where:

$$\begin{bmatrix} H_{11} & | & H_{12} \\ - & \cdot & - \\ H_{21} & | & H_{22} \end{bmatrix} = H^{-1}$$

Substituting (D.1) in (3.6) yields:

$$\begin{aligned} \alpha_{q_i}(k+1) &= \sum_j d_{ij} \alpha_{q_j}(k) - \beta_i g_i, \\ &= \sum_j d_{ij} \alpha_{q_j}(k) - \beta_i [g_i^* + e_i(V_i - V_i^*) + f_i(\alpha_{q_i} - \alpha_{q_i}^*)] \end{aligned} \quad (\text{D.6})$$

Equation (D.6) may be written in the matrix format as follows:

$$\alpha_q(k+1) = D\alpha_q(k) - \beta[g^* + E(V - V^*) + F(\alpha_q - \alpha_q^*)] \quad (\text{D.7})$$

where  $D = [d_{ij}]$  is a row stochastic matrix. Also  $g^* = [g_1^*, \dots, g_N^*]^T$ ,  $E = \text{diag}(e_i)$ ,  $F = \text{diag}(f_i)$  and the gain  $\beta = \text{diag}[\beta_1, \dots, \beta_N]$ .

The parameter  $g^*$  can be calculated by evaluating (D.7) at the optimal operating point,  $\alpha_q^*$  and  $V^*$ :

$$\alpha_q^* = D\alpha_q^* - \beta g^* \Rightarrow g^* = -\beta^{-1}(I - D)\alpha_q^* \quad (\text{D.8})$$

where  $I$  is a  $N \times N$  unity matrix.

Substituting  $g^*$  and  $V - V^*$  from (D.8) and (D.5) respectively in (D.7) provides:

$$\begin{aligned} \alpha_q(k+1) &= [D - \beta(EH_{12} + F)]\alpha_q(k) \\ &\quad + [(I - D) + \beta(EH_{12} + F)]\alpha^* - \beta EH_{12}(P - P^*). \end{aligned} \quad (\text{D.9})$$

If  $P$  is not constant, then  $N$  extra independent active power states are introduced in (D.9). These

states are independent of the states of interest,  $\alpha_q$ . Hence, the stability and the dynamic response of the proposed optimization method is absolutely independent of these active power states. As such, for the simplicity and without loss of the generality, the active power flow,  $P$ , is assumed to be constant at  $P^*$ . Therefore, (D.9) may be reformatted as follows:

$$\alpha_q(k+1) - \alpha_q^* = [D - \beta(EH_{12} + F)](\alpha_q(k) - \alpha_q^*) \quad (\text{D.10})$$

The stability and the convergence rate of the system depend on the state matrix,  $D - \beta(EH_{12} + F)$ , and are based on the following lemmas and theorem:

**Lemma 2.** *If the eigenvalues of the row-stochastic and connected matrix  $D$  are denoted as  $\lambda_i$  with  $\lambda_1 = 1 > \lambda_2 \geq |\lambda_j|$  for  $j = 3, \dots, N$ , then matrix*

$$A' = D - c\mathbf{1}\gamma^T \quad (\text{D.11})$$

*with scalar  $c \in (0, 2]$  has eigenvalues of  $(1 - c)$  and  $\lambda_i$  for  $i = 2, \dots, N$ . Quantity  $\gamma$  is the left eigenvector of  $D$ , corresponding to the left eigenvalue of 1 ( $\gamma^T \mathbf{1} = 1$ ).*

*Proof.* Let  $\xi_i$  denotes the eigenvector corresponding to  $\lambda_i$  for  $i = 2, \dots, N$ . Therefore:

$$\begin{cases} \gamma^T D \xi_i = \gamma^T (D \xi_i) = \lambda_i \gamma^T \xi_i \\ \gamma^T D \xi_i = (\gamma^T D) \xi_i = \gamma^T \xi_i \end{cases} \Rightarrow \gamma^T \xi_i = 0$$

It follows that

$$A' \mathbf{1} = D \mathbf{1} - c \mathbf{1} \gamma^T \mathbf{1} = (1 - c) \mathbf{1}$$

and:

$$A' \xi_i = D \xi_i - c \mathbf{1} \gamma^T \xi_i = \lambda_i \xi_i,$$

which completes the proof.  $\square$

**Lemma 3.**  $EH_{12} + F$  is a positive matrix.

*Proof.* Using the approximation of  $V_i^* \simeq 1$ , (D.2) may be simplified as follows:

$$e_i \simeq -\bar{Q}_i \frac{-\alpha_{q_i} \bar{Q}_i + B_{ii}}{(\alpha_{q_i} \bar{Q}_i - B_{ii})^2} \Big|_{V_i^* \& \alpha_{q_i}^*} \quad (\text{D.12})$$

In (D.12),  $-1 < \alpha_{q_i} < 1$  and  $0 < \bar{Q}_i < 1$ , as all the calculations are in the per unit. This implies that  $-1 < \alpha_{q_i} \bar{Q}_i < 1$ . Furthermore, in power systems usually line impedances, especially when expressed in the per unit, are very small values. As such, the conductances are rather large numbers. This implies that  $B_{ii}$  is rather a negative large in magnitude number. As a reminder,  $B_{ii}$  is the sum of the imaginary parts of the line conductances, connecting node  $i$  to the neighboring nodes. As such,  $\alpha_{q_i} \bar{Q}_i$  is negligible compared to the  $B_{ii}$ . Therefore,  $e_i$  is a positive quantity.

The equation (D.5) implies that  $H_{12} = [h_{12_{ij}}]$  and:

$$h_{12_{ij}} = \frac{\partial V_i}{\partial \alpha_{q_j}}.$$

It is a known fact in the power systems that injecting more reactive power, increases the line voltages and decreasing the reactive power, reduces the voltages. As such, the change of  $V$  and  $\alpha_{q_j}$  are on the same direction and hence  $h_{12_{ij}} > 0$ . This implies that  $H_2$  is a square positive matrix.

In most cases  $V_i^* < 1$  and as such,  $f_i$  in (D.3) are positive. In cases that  $V_i^*$  is greater than unity, yet  $1 - V_i^*$  is a small value, in the range of few percents and not larger than  $0.05P.U$  in magnitude. This small value divided by a rather large denominator makes  $f_i$  to be small enough not to affect the polarity of  $EH_{12}$ . As such,  $EH_{12} + F$  is a positive matrix.  $\square$

**Theorem 4.** It follows from Lemma 2 and Lemma 3 that the system of (D.10) is asymptotically

stable, when  $\beta$  is chosen in such a way that:

$$\beta(EH_{12} + F) = cI\gamma^T + W, \quad (\text{D.13})$$

where

$$0 \leq \|W\| < \sqrt{\|A'\|^2 + \frac{1}{\|P\|}} - \|A'\| \quad (\text{D.14})$$

where  $A'$  is defined by (D.11) and  $P$  is the solution to the following Lyapunov equation:

$$PA' + A'^T P = -I$$

*Proof.* Assuming  $y_k = \alpha_q(k) - \alpha_q^*$ , it follows from (D.10), (D.11) and (D.13) that  $y_{k+1} = (A' - W)y_k$ . Applying the Lyapunov argument with a Lyapunov function of  $V_k = y_k^T P y_k$  yields:

$$\begin{aligned} V_{k+1} - V_k &= y_k^T [(A' - W)^T P (A' - W) - P] y_k \\ &= y_k^T \{ [(A')^T P A' - P] - W^T P A' - (A')^T P W + W^T P W \} y_k \\ &= y_k^T (-I - W^T P A' - (A')^T P W + W^T P W) y_k \\ &\leq (-1 + 2\|P\|\|A'\|\|W\| + \|W\|\|P\|) \|y_k\|^2. \end{aligned}$$

□

Since  $V_{k+1} - V_k$  is negative definite for all  $W$  satisfying (D.14), system (D.10) is stable.

## **APPENDIX E: PUBLICATIONS FROM THE DOCTORAL RESEARCH**

1. A. Maknouninejad, Wei Lin, Z. Qu, "Optimum Design and Analysis of the Cooperative Control, Applied to the Distributed Generators Control in Smart Grids", IEEE PES Innovative Smart Grid Technologies, Feb. 2013
2. A. Maknouninejad, W. Lin, H. G. Harno, Z. Qu, M. A. Simaan, "Cooperative Control for Self-Organizing Microgrids and Game Strategies for Optimal Dispatch of Distributed Renewable Generations", Energy Systems, Vol. 3, No. 1, pp 23-60, 2012
3. A. Maknouninejad, Z. Qu, J. Enslin, N. Kutkut, "Clustering and Cooperative Control of Distributed Generators for Maintaining Microgrid Unified Voltage Profile and Complex Power Control", IEEE PES Transmission and Distribution Conference, pp 1-8, May 2012
4. H. Xin, Z. Qu, J. Seuss, A. Maknouninejad, "A Self Organizing Strategy for Power Flow Control of Photovoltaic Generators in a Distribution Network", IEEE Transactions on Power Systems, vol. 26, pp 1462-1473, 2011
5. A. Maknouninejad, N. Kutkut, I. Batarseh, Z. Qu, "Detailed analysis of generator emulation control impedance network of microgrid inverters", IEEE Industry Applications Society Annual Meeting (IAS) 2011, pp 1-5
6. A. Maknouninejad, N. Kutkut, I. Batarseh, Z. Qu, "Analysis and Control of PV Inverters Operating in VAR Mode at Night", IEEE ISGT 2011, pp 1-5
7. A. Maknouninejad, N. Kutkut, E. Shoubaki, I. Batarseh, Z. Qu, "Detailed Analysis of Inverter Linear Control Loops Design", IEEE APEC 2011, pp 1188-1193
8. A. Maknouninejad, M. Godoy Simoes, M. Zolot, "Single Phase and Three Phase P+Resonant Based Grid Connected Inverters with Reactive Power and Harmonic Compensation Capabilities", IEMDC 09, 3-6 May 2009, pp 385-391



Submitted:

1. A. Maknouninejad, Z. Qu, "Realizing Unified Microgrid Voltage Profile and Loss Minimization: a Cooperative Distributed Optimization and Control Approach", IEEE Tran. on Smart Grid, Apr. 2013

## LIST OF REFERENCES

- [1] “What caused the power blackout to spread so widely and so fast?” Genscape, 15 Oct. 2003.
- [2] H. Pidd, “India blackouts leave 700 million without power,” *The Guardian*, 31 July 2012.
- [3] “Millions could face cold weekend from sandy’s power outages,” CNN, Nov. 2 2012.
- [4] “A vision for the modern grid,” National Energy Technology Laboratory, United States Department of Energy, Tech. Rep., 07 2007.
- [5] National Energy Technology Laboratory US Department of Energy Office of Electricity Delivery and Energy Reliability, *A Vision for the Modern Grid*, March 2007.
- [6] R. H. Lasseter, “Microgrids,” *Power Engineering Society Winter Meeting*, vol. 1, 2002.
- [7] S. Ganguly, N. C. Sahoo, and D. Das, “A novel multi-objective pso for electrical distribution system planning incorporating distributed generation,” *Energy Systems*, vol. 1, no. 3, pp. 291–337, 2010.
- [8] D. Amato, A. Tonielli, and A. Tilli, “An improved sequential hysteresis current controller for three-phase inverter: design and hardware implementation,” in *Proceedings of the IEEE International Conference on Control Applications*, 2001, pp. 294–300.
- [9] M. Davari, I. Salabeigi, G. Gharehpetian, S. Fathi, and J. Milimonfared, “Multifunction current controller for inverter-based distributed generation using combined pi-sliding mode controller via sigma-delta modulation,” in *IEEE International Symposium on Industrial Electronics*, 2009, pp. 1803–1808.

- [10] N. Pogaku, M. Prodanovic, and T. C. Green, "Modeling, analysis and testing of autonomous operation of an inverter-based microgrid," *IEEE Transactions on Power Electronics*, vol. 22, no. 2, pp. 613–625, 2007.
- [11] F. Blaabjerg, R. Teodorescu, M. Liserre, and A. V. Timbus, "Overview of control and grid synchronization for distributed power generation systems," *IEEE Transactions on Industrial Electronics*, vol. 53, no. 5, pp. 1398–1409, Oct. 2006.
- [12] M. Dai, M. Marwali, J. Jung, and A. Keyhani, "Power flow control of a single distributed generation unit," *IEEE Transactions on Power Electronics*, vol. 23, no. 1, pp. 343–352, Jan. 2008.
- [13] Y. Abdel-Rady, I. Mohamed, and E. F. El-Saadany, "Adaptive decentralized droop controller to preserve power sharing stability of paralleled inverters in distributed generation microgrids," *IEEE Transactions on Power Electronics*, vol. 23, no. 6, pp. 2806–2816, Nov. 2008.
- [14] H. F. Bilgin and M. Ermis, "Design and implementation of a current-source converter for use in industry applications of d-statcom," *IEEE Transactions on Power Electronics*, vol. 25, no. 8, pp. 1943–1957, 2010.
- [15] D. N. Zmood and D. G. Holmes, "Improved voltage regulation for current-source inverters," *IEEE Transactions on Industry Applications*, vol. 37, no. 4, pp. 1028–1036, 2001.
- [16] F. Katiraei, M. Iravani, and P. Lehn, "Small-signal dynamics model of a micro-grid including conventional and electronically interfaced distributed resources," *IET Generation, Transmission, and Distribution*, vol. 1, no. 3, pp. 369–378, 2007.
- [17] F. Katiraei, R. Iravani, N. Hatziargyriou, and A. Dimeas, "Microgrids management," *IEEE Power and Energy Magazine*, vol. 6, no. 3, pp. 54–65, 2008.

- [18] H. Alatrash, A. Mensah, E. Mark, G. Haddad, and J. Enslin, "Generator emulation controls for photovoltaic inverters," *IEEE Transactions on Smart Grid*, vol. 3, no. 2, pp. 996–1011, 2012.
- [19] P. M. S. Carvalho, P. F. Correia, and L. A. F. M. Ferreira, "Distributed reactive power generation control for voltage rise mitigation in distribution networks," *IEEE Transactions on Power Systems*, vol. 23, no. 2, pp. 766–772, 2008.
- [20] J. Lopes, N. Hatziargyriou, and J. Mutale, "Integrating distributed generation into electric power systems: A review of drivers, challenges and opportunities," *Elect. Power Syst.*, vol. 77, no. 9, pp. 1189–1203, 2007.
- [21] M. E. Baran and I. M. El-Markabi, "A multiagent-based dispatching scheme for distributed generators for voltage support on distribution feeders," *IEEE Transactions on Power Systems*, vol. 22, no. 1, pp. 52–59, 2007.
- [22] T. Nguyen and M. Pai, "A sensitivity-based approach for studying stability impact of distributed generation," *Int. J. Elect. Power Energy Syst.*, vol. 30, no. 8, pp. 442–446, 2008.
- [23] H. Hedayati, S. Nabaviniaki, and A. Akbarimajd, "A method for placement of dg units in distribution networks," *IEEE Transactions on Power Delivery*, vol. 23, no. 3, pp. 1620–1628, 2008.
- [24] K. D. Brabandere, B. Bolsens, J. V. den Keybus, A. Woyte, J. Driesen, and R. Belmans, "A voltage and frequency droop control method for parallel inverters," *IEEE Transactions on Power Electronics*, vol. 22, no. 4, pp. 1107–1115, 2007.
- [25] M. Chandorkar and D. Divan, "Decentralized operation of distributed ups systems," in *Proc. IEEE PEDES*, 1996, pp. 565–571.

- [26] M. Prodanovic and T. Green, "High-quality power generation through distributed control of a power park microgrid," *IEEE Transactions on Power Delivery*, vol. 53, no. 5, pp. 1471–1482, 2006.
- [27] M. N. Marwali, J.-W. Jung, and A. Keyhani, "Control of distributed generation systems part ii: load sharing control," *IEEE Transactions on Power Electronics*, vol. 19, no. 6, pp. 1551–1561, 2004.
- [28] F. Katiraei and M. Iravani, "Power management strategies for a microgrid with multiple distributed generation units," *IEEE Transactions on Power Systems*, vol. 21, no. 4, pp. 1821–1831, 2006.
- [29] A. Mehrizi-Sani and R. Iravani, "Potential function based control of a microgrid in islanded and grid-connected modes," *IEEE Transactions on Power Systems*, vol. 25, no. 4, pp. 1883–1891, 2010.
- [30] J. M. Guerrero, L. G. Vicuna, J. Matas, M. Castilla, and J. Miret, "Output impedance design of parallel-connected ups inverters with wireless load-sharing control," *IEEE Transactions on Industrial Electronics*, vol. 52, no. 4, pp. 1126–1135, 2005.
- [31] X. Yu, A. Khambadkone, H. Wang, and S. Terence, "Control of parallel-connected power converters for low-voltage microgrid part i: a hybrid control architecture," *IEEE Transactions on Power Electronics*, vol. 25, no. 12, pp. 2962–2970, 2010.
- [32] J. Guerrero, J. Matas, L. de Vicua, M. Castilla, and J. Miret, "Decentralized control for parallel operation of distributed generation inverters using resistive output impedance," *IEEE Transactions on Industrial Electronics*, vol. 54, no. 2, pp. 994–1004, 2007.
- [33] J. M. Guerrero, M. Chandorkar, and T.-L. Lee, "Advanced control architectures for intelligent microgrids part i: Decentralized and hierarchical control," *IEEE Transactions on Industrial Electronics*, vol. 60, no. 4, pp. 1254–1262, 2013.

- [34] Y. W. Lee and C.-N. Kao, "An accurate power control strategy for power-electronics-interfaced distributed generation units operating in a low-voltage multibus microgrid," *IEEE Transactions on Power Electronics*, vol. 24, no. 12, pp. 2977–2988, 2009.
- [35] A. Maknouninejad, Z. Qu, J. Enslin, and N. Kutkut, "Clustering and cooperative control of distributed generators for maintaining microgrid unified voltage profile and complex power control," in *IEEE PES Transmission and Distribution Conference*, Orlando, FL, USA, May 2012, pp. 1–8.
- [36] P. Pardalos, D. Grundel, R. A. Murphey, and O. Prokopyev, *Cooperative Networks: Control and Optimization*. Edward Elgar Publishing, 2008.
- [37] W. Ren and R. W. Beard, *Distributed consensus in multi-vehicle cooperative control: theory and applications*. London, UK: Springer, 2009.
- [38] Z. Qu, *Cooperative Control of Dynamical Systems, Applications to Autonomous Vehicles*. London, UK: Springer, 2009.
- [39] C. Schauder and H. Mehta, "Vector analysis and control of the advanced static VAR compensators," *IEE Proceedings C - Generation, Transmission, and Distribution*, vol. 140, no. 4, pp. 299–306, 1993.
- [40] H. Xin, Z. Qu, J. Seuss, and A. Maknouninejad, "A self-organizing strategy for power flow control of photovoltaic generators in a distribution network," *IEEE Transactions on Power Systems*, vol. 26, no. 3, pp. 1462–1473, 2011.
- [41] Z. Qu, J. Wang, and R. A. Hull, "Cooperative control of dynamical systems with application to autonomous vehicles," *IEEE Transactions on Automatic Control*, vol. 53, no. 4, pp. 894–911, 2008.

- [42] A. Maknouninejad, W. Lin, H. G. Harno, Z. Qu, and M. A. Simaan, “Cooperative control for self-organizing microgrids and game strategies for optimal dispatch of distributed renewable generations,” *Energy Systems*, vol. 3, no. 1, pp. 23–60, 2012.
- [43] C. L. Phillips and H. T. Nagle, *Digital Control System Analysis and Design (3rd Edition)*. Prentice Hall, 1994.
- [44] “www.zigbee.org.”
- [45] H. K. Khalil, *Nonlinear Systems*, 3rd ed. Upper Saddle River, NJ, USA: Prentice-Hall Inc., 2002.
- [46] M. Holmes, *Introduction to perturbation methods*. Springer, 1995.
- [47] A. Nedic and A. Ozdaglar, “Distributed subgradient methods for multi-agent optimization,” *IEEE Transactions on Automatic Control*, vol. 54, no. 1, pp. 48–61, 2009.
- [48] K. S. Narendra and A. M. Annaswamy, *Stable Adaptive Systems*. Mineola, New York: Dover publications, INC., 2005.
- [49] A. Chinchuluun, P. Pardalos, A. Migdalas, and L. Pitsoulis, *Pareto Optimality, Game Theory and Equilibria*. Springer, 2008.
- [50] E. Hasan and F. Galiana, “Fast computation of pure strategy nash equilibria in electricity markets cleared by merit order,” *IEEE Transactions on Power Systems*, vol. 25, no. 2, pp. 722 – 728, 2010.
- [51] P. Jong-Bae, B. Kim, K. Jin-Ho, J. Man-Ho, and Jong-Keun, “A continuous strategy game for power transactions analysis in competitive electricity markets,” *IEEE Transactions on Power Systems*, vol. 16, no. 4, pp. 847 – 855, 2001.

- [52] A. Kannan, U. V. Shanbhag, and H. M. Kim, “Strategic behavior in power markets under uncertainty,” *Energy Systems*, vol. 2, no. 2, pp. 115–141, 2010.
- [53] J. Molina, J. Zolezzi, J. Contreras, H. Rudnick, and J. Reveco, “Nash-Cournot equilibria in hydrothermal electricity markets,” *IEEE Transactions on Power Systems*, vol. 26, no. 3, pp. 1089 – 1101, 2011.
- [54] D. Pozo and J. Contreras, “Finding multiple nash equilibria in pool-based markets: A stochastic epec approach,” *IEEE Transactions on Power Systems*, vol. 26, no. 3, pp. 1744 – 1752, 2011.
- [55] M. Bjorndal, V. Gribkovskaia, and K. Jornsten, “Market power in a power market with transmission constraints,” in *The Proceedings of the 7th International Conference on the European Energy Market*, Madrid, Spain, 23-25 June 2010, pp. 1–6.
- [56] M. Latorre and S. Granville, “The Stackelberg equilibrium applied to AC power systems — A non-interior point algorithm,” *IEEE Transactions on Power Systems*, vol. 18, no. 2, pp. 611–618, 2003.
- [57] P. Luh, Y. Ho, and R. Muralidharan, “Load adaptive pricing: An emerging tool for electric utilities,” *IEEE Transactions on Automatic Control*, vol. 27, no. 2, pp. 320–329, 1982.
- [58] J. Zhao, B. Brereton, and M. Montalvo, “Gaming-based reserve constraint penalty factor analysis,” *IEEE Transactions on Power Systems*, vol. 26, no. 2, pp. 616–626, 2011.
- [59] A. Mohsenian-Rad, V. Wong, J. Jatskevich, R. Schober, and A. Leon-Garcia, “Autonomous demand-side management based on game-theoretic energy consumption scheduling for the future smart grid,” *IEEE Transactions on Smart Grid*, vol. 1, no. 3, pp. 320–331, 2010.



- [60] Z. Vale, H. Morais, and H. Khodr, “Intelligent multi-player smart grid management considering distributed energy resources and demand response,” in *Proceedings of the IEEE Power and Energy Society General Meeting*, Porto, Portugal, 2010, pp. 1–7.
- [61] S. K. Khaitan, J. D. McCalley, and M. Raju, “Numerical methods for on-line power system load flow analysis,” *Energy Systems*, vol. 1, no. 3, pp. 273–289, 2010.
- [62] K. Purchala, L. Meeus, D. V. Dommelen, and R. Belmans, “Usefulness of DC power flow for active power flow analysis,” in *The Proceedings of the IEEE 2005 Power Engineering Society General Meeting*, San Francisco, CA, USA, 12-16 June 2005, pp. 454–459.
- [63] T. Basar and G. J. Olsder, *Dynamic Noncooperative Game Theory*, 2nd ed. Philadelphia, PA, USA: SIAM, 1999.
- [64] R. Myerson, *Game theory: Analysis of Conflict*. USA: Harvard University Press, 1997.
- [65] J. Nash, “Equilibrium points in  $n$ -person games,” *Proceedings of the National Academy of Science of the United States of America*, vol. 36, no. 1, pp. 48–49, 1950.
- [66] ———, “Non-cooperative games,” *The Annals of Mathematics*, vol. 54, no. 2, pp. 286–295, 1951.
- [67] H. F. V. Stackelberg, *The Theory of the Market Economy*. London, UK: William Hodge, 1952.
- [68] M. Simaan and J. Cruz, “Additional aspects of the stackelberg strategy in nonzero-sum games,” *Journal of Optimization Theory and Applications*, vol. 11, no. 6, pp. 613–626, 1973.
- [69] ———, “On the Stackelberg strategy in nonzero-sum games,” *Journal of Optimization Theory and Applications*, vol. 11, no. 5, pp. 533–555, 1973.